UNIVERSITÀ DEGLI STUDI DI
MODENA E REGGIO EMILIA

Dottorato di ricerca in Neuroscienze

in convenzione con l'Università degli Studi di Parma

Ciclo XXXIV

AN *IN VIVO* Ca^{2+} IMAGING STUDY OF iMSN INVOLVEMENT IN THE STRIATAL ENCODING OF MOUSE LOCOMOTOR ACTIVITY

STUDIO IN VIVO DEL RUOLO DEGLI iMSN NELLA CODIFICA DELL'ATTIVITÀ MOTORIA IN MODELLI MURINI MEDIANTE CALCIUM IMAGING

Candidato Miriam Cavagnini

Relatore (Tutor): Prof. Michele Zoli

Correlatore (Co-Tutor): Dott. Paolo Pozzi
Correlatore (Co-Tutor): Prof. Alban De Kerchove d'Exaerde

Coordinatore del Corso di Dottorato: Prof. Michele Zoli

Summary

Abstract

Striatum is the main input nucleus of the basal ganglia and 95% of its neurons are GABAergic Medium Spiny Neurons (MSNs). MSNs are subdivided into neurons of the direct and indirect pathway. The direct pathway consists of MSNs (direct MSNs, dMSNs) mainly expressing dopamine D1 receptors (D1R), whereas MSNs of the indirect pathway (iMSNs) express dopamine D2 receptor (D2R) and adenosine A2A receptor (A2AR) (Gerfen 1992a, Gong et al 2003). According to the classical model, these two pathways exert an opposite effect on movement regulation: the direct pathway promotes activity of the cortex that codes a motor plan, and therefore movement initiation, while the indirect pathway inhibits cortical activity and movement (Albin et al 1989, Alexander & Crutcher 1990, DeLong 1990). Recent studies have challenged this interpretation and demonstrated that both pathways are co-activated during movement initiation but with differential activities (Bonnavion et al 2019, Tecuapetla et al 2016). Yet, while the role of these two pathways is globally understood, cell-specific mechanisms and their interaction in relation to movement control are only partially known. Modern technological advances such as calcium (Ca^{2+}) imaging techniques can be applied to directly observe the neuronal activity in these two pathways. During periods of heightened neural activity, Ca^{2+} flows into the dendritic branches and cell bodies of neurons, increasing its intracellular concentrations. These activity-dependent fluctuations in intracellular Ca^{2+} can be monitored by expressing a Ca^{2+} indicator, such as GCaMP, into the neuronal population of interest. The aim of this study was to investigate the role of murine striatum in locomotion, and in particular the involvement of iMSNs, using recent *in vivo* Ca^{2+} imaging technologies.

Locomotor activity was tested by behavioural experiments and the GABAergic iMSN activity was stimulated by a psychostimulant drug, d-Amphetamine, at different doses. In this study, *in vivo* calcium imaging was used to visualize striatal neural circuit dynamics of the indirect pathway during mouse behaviour with head-mounted microscopes and chronically implanted endoscopes. A2AGCaMP6s mice expressing GCaMP in iMSNs were used as an animal model. Behavioural analysis showed that acute intraperitoneal injection of d-Amphetamine at 3 mg/kg dose markedly increases locomotor activity with a peak 15 minutes after injection, while a dose of d-Amphetamine at 1 mg/kg modestly decreases locomotor activity, possibly due to the induction of stereotyped behaviour. Traces of iMSN calcium activity were extracted from the imaging data and analysed with custom developed software. The results showed a significant decrease in the average number of active iMSNs and a significant increase in the average spike duration after d-Amphetamine 3 mg/kg

injection. At 1mg/kg dose, there was a trend for a significant decrease in the average number of active cells and a significant increase in the average spike duration. Analysis of the acquired datasets showed how iMSNs contribute to the encoding of movement, confirming previous results reported by Parker and colleagues (Parker et al 2018). In detail, the analysis revealed that iMSN activity rises around 0.5-0.3 seconds before motion onset and falls around 0.5 seconds before motion offset, suggesting that increased firing of iMSNs contributes to the encoding of locomotion. However, it is not clear whether movement or rest are encoded by changes in the activity of randomly distributed iMSNs or specific sub-sets of iMSNs change their activity during rest or movement.
This study allows us to better understand the complexity of MSN activity, challenging the classical view where the direct and indirect pathway show an opposite pattern of activity during movement.

Key words: iMSN, striatum, amphetamine, *in-vivo* Ca^{2+}imaging, behavioural study

Abbreviations

5-HT: 5-hydroxytryptamine
A2AR: adenosine A2A receptor
AC: adenylyl cyclase
Ac: anterior commissure
Ach: acetylcholine
AChE: enzyme acetylcholinesterase
ACSF: artificial cerebrospinal fluid
AM: acetoxymethyl ester
AMPAR: α-amino-3-hydroxy-5-methylisoxazole-4-propionate receptor
AMPH: amphetamine
Arc: activity-regulated cytoskeleton-associated protein
BAC: bacterial artificial chromosome
BAPTA: 1,2-bis(o-aminophenoxy) ethane-N,N,N',N'-tetraacetic acid
BG: basal ganglia
CaM: calmodulin
CaMKII: calcium/calmodulin-dependent protein kinase type II
cAMP: cyclic adenosine monophosphate
Cav1 L-type: calcium channel voltage-dependent L type
CBGTC: cortico-basal ganglia-thalamo-cortical loops
CCD: charged couple device
CM/Pf: centromedian/parafascicular nuclei
CMOS: complementary metal-oxide-semiconductor
CN: caudate nucleus
CNMF: constrained non-negative matrix factorization
CNMF_E: CNMF for endoscopy data
CpEGFP: circularly permutated enhanced green fluorescent protein
CPu: caudate-putamen complex
CREB: cAMP responsive element binding protein
CTZ: cyclothiazide
D1R dopamine D1 receptor
D2R: dopamine D2 receptor
DA: dopamine
DAG: diacylglycerol
DAQ: data acquisition device
DARPP-32: 32-kDa dopamine and cAMP-regulated phosphoprotein
DAT: dopamine transporter
DLS: dorsolateral striatum
DMS: dorsomedial striatum
dMSN: direct medium spiny neuron
E: epinephrine
EPSP: excitatory post-synaptic potential
ER: endoplasmic reticulum
ERK: extracellular signal-regulated kinase
FOV: field of view
FSI: fast spiking interneuron

GABA: acid gamma-aminobutyric
GECI: genetically encoded calcium indicator
GIRK: G protein-coupled inwardly-rectifying potassium channel
GP: globus pallidus
GPe: globus pallidus external
GPi: globus pallidus internal
GPIO: general-purpose input/output
HFS: high frequency stimulation
HVA: high voltage activated
i.p: intraperitoneally
IEG: immediate early gene
iMSN: indirect medium spiny neuron
IP_3: inositol 1,4,5-trisphosphate
IP_3R: inositol 1,4,5-trisphosphate receptor
IT-type: intratelencephalic neuron
LSTM: long and short-term memory
LTD: long term depression
LTP: long term potentiation
LTS: low threshold spiking
LVA: low voltage activated
mAChR: muscarinic acetylcholine receptor
MAO: monoamine oxidase
MAO-A: monoamine oxidase type A
MAO-B: monoamine oxidase type B
MEK: mitogen-activated protein kinase
mGluR: metabotropic glutamate receptor
MSN: medium spiny neuron
NAc: nucleus accumbens
NAcc: nucleus accumbens core
nAChR: nicotinic acetylcholine receptor
NAcs: nucleus accumbens shell
Nav1.1: sodium channel voltage-gated type I
NCX: Na^+/Ca^{2+} exchanger
NE: norepinephrine
NET: norepinephrine transporter
NMDAR: N-methyl-D-aspartate receptor
NO: nitric oxide
OF: open field
OFT: open field test
OT: olfactory tubercle
PCA-ICA: principal component analysis and independent component
P-DARPP-32: phosphorylated dopamine- and cAMP-regulated phosphoprotein 32 kDa
PF: parafascicular
PKA: protein kinase A
PKC: protein kinase C
PLC: phospholipase C
PMCA: plasma membrane calcium ATPase
PMT: photomultiplier tube

PP1: protein phosphatase 1
PP2B: protein phosphate 2B
PPF: paired-pulse facilitation
PPTg: peduncolopontine tegmental nucleus
PT-type: pyramidal tract neuron
Put: putament
RMS: root mean square
RNN: recurrent neural network
ROC: receptor-operated calcium channel
ROI: regions of interest
RyR: ryanodine receptor
SERCA: sarco/-endoplasmatic reticulum calcium ATPase
SERT: serotonin transporter
SN: substantia nigra
SNc: substantia nigra pars compacta
SNr: substantia nigra pars reticulata
SOC: store operated channel
STIM: stromal interaction molecule
STN: subthalamic nucleus
TNF: tonically active neuron
TRPC: transient receptor potential type C channels
Ts-ori: temperature-sensitive origin of replication
TTL: transistor–transistor logic
TTX: tetrodotoxin
VDCC: voltage dependent calcium channel
VGCC: voltage-gated calcium channel
VMAT-2: vesicular monoamine transporter type-2
VP: ventral pallidum
VSCC: voltage sensitive calcium channel
VTA: ventral tegmental area

Introduction

Basal Ganglia

Neuroanatomy of the Basal Ganglia

During the 20th century the understanding of the structural and functional organization of the Basal Ganglia (BG) has been strongly improved by clinical observations and by physiological and anatomical findings. The BG are a group of bilateral subcortical nuclei involved mainly in motor control and a variety of other functions (Alexander et al 1986, Graybiel et al 1994), including attention and time estimation, implicit learning and habit formation, reward-related behaviour and emotions. Anatomically, the BG consist of the striatum, globus pallidus (GP), subthalamic nucleus (STN) and substantia nigra (SN). Each structure is constituted by different subregions: the striatum includes the caudate nucleus (CN), putament (Put) and nucleus accumbens (NAc); the globus pallidus is divided into internal (GPi) and external (GPe) part while the SN is divided into pars compacta (SNc) and pars reticulata (SNr) (Obeso et al 2002). The ventral tegmental area (VTA) and peduncolopontine tegmental nucleus (PPTg) can also be considered part of the BG. All these nuclei are generally classified in input, output and intrinsic nuclei (Lanciego et al 2012). The input nuclei include the CN, Put and NAc, which receive incoming information from cortex, thalamus and SN. On the other hand, output nuclei involve the GPi and SNr projecting to the thalamus, in particular to the ventral nuclei. The intrinsic nuclei are formed by STN, GPe, SNc, and VTA located between the input and output nuclei. Considering the input and output structures of the BG, it is evident that the BG are part of complex neuronal circuits, defined as cortico-basal ganglia-thalamo-cortical (CBGTC) loops. Five loops have been defined (motor, oculomotor, associative, limbic and orbitofrontal), that are interconnected. For example, it has been demonstrated that subregions of the BG circuit project to the motor cortex and receive input from cortical limbic areas (Kelly & Strick 2004). In addition, the BG are connected with brain stem nuclei such as the locus coeruleus, the raphe nuclei and the reticular formation (Obeso et al 2002).

Motor circuit

Intentional movements are initiated by the motor cortex, directly or indirectly projecting to the brain stem or spinal motoneurons, which in turn project to the muscles. Before arriving to the motoneurons, the motor information is elaborated by several structures, such as the BG (Groenewegen 2003). In the motor CBGTC loop, the motor areas (area 4, supplementary motor area,

arcuate premotor area) and somatosensory area send somatotopically glutamatergic (excitatory) projections to the basolateral Put (Alexander et al 1986). Thus, the somatotopic features of somatosensory and motor areas projections to the Put are in register (Alexander & DeLong 1985, Alexander et al 1986, Crutcher & DeLong 1984, Liles 1985). The Put sends gamma-aminobutyric acidergic (GABAergic) topographical information to the ventrolateral parts of both internal and external segments of the GP (Cowan & Powell 1966, DeVito et al 1980, Johnson & Rosvold 1971, Nauta & Mehler 1966, Parent et al 1984, Szabo 1967) and to the caudolateral portion of the SNr (Hedreen & DeLong 1991, Nauta & Mehler 1966, Szabo 1967).

There are two main striato-GPi/SNr circuits: the direct and indirect pathways (reported in **Figure 1**). Striatal neurons of the **direct pathway** send directly their GABAergic projections to the GPi and the SNr that contain GABA neurons, hence GABAergic efferent projections reach the anterior ventral and lateral ventral thalamic nuclei, connected to the frontal cortex via excitatory glutamatergic projections. On the other hand, striatal neurons of the **indirect pathway** send their GABAergic axons to the GPe, which contains GABA neurons that project to the STN. The STN sends an excitatory projection to the SNr, GPi and PPTg by using glutamic acid as neurotransmitter (Gerfen & Wilson 1996, Parent & Hazrati 1995). Thus, the output from the direct pathway leads to an inhibition on the GPi and SNr, disinhibiting the output thalamic nuclei (ventrolateral nuclei). Instead, the output from the indirect pathway increases the inhibition from the GPi and SNr onto their projection nucleus.

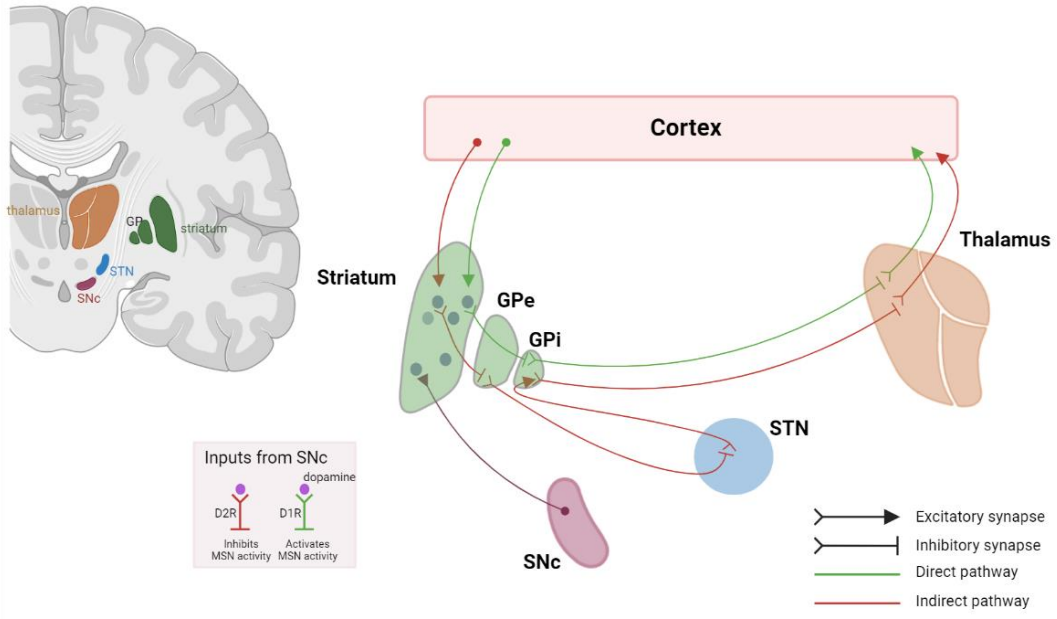

Figure 1 Schematic representation of the **direct** (green) **and indirect** (red) **pathways**. The direct pathway disinhibits the output thalamic nuclei, whereas the indirect pathway increases the inhibition from the output thalamic nuclei. Abbreviations: globus pallidus external (GPe), globus pallidus internal (GPi), substantia nigra pars compacta (SNc), subthalamic nucleus (STN). Created with BioRender.com

So, according to the classical model these two pathways exert an opposite effect on movement regulation: the direct pathway promotes the activity of the cortex and therefore the motor activity, whereas the indirect pathway inhibits its activation (Alexander & Crutcher 1990, DeLong 1990). The model also proposes that dopamine (DA) released by the neurons of the SNc and VTA that project to the striatum modulates the cortico-striatal output by exerting a dual effect on striatal neurons.

The motor loop also has several inner circuits, that modulate the BG network (Obeso et al 2000, Parent 1990). The centromedian/parafascicular (CM/Pf)-thalamic nuclei-striatum-GPi-CM/Pf loop increases the neuronal activity of the CM/Pf neurons and thus is considered as a positive feedback loop, while the CM/Pf-STN-GPi-CM/Pf circuit reduces the neuronal activity of CM/Pf neurons. Conversely, the STN-GPe-STN loop is a self-inhibitory loop, with autoregulation characteristics, while the STN-GPe/GPi circuit may induce excitation and inhibition of the same GPi output neurons. Another inner loop comprises the primary motor cortex (area 4)-STN-GPi-motor thalamus-area 4 loop (so-called hyperdirect pathway), sending inhibitory feedback signalling to the cortex, probably relevant for movement termination (Obeso et al 2002). In light of the complexity of the circuits described here, the question about what BG specifically contribute to the execution of movement and behavioural acts remains open.

Striatum

Neuroanatomy of striatum

The structure of striatum is highly conserved between primates and rodents, thus mice are considered to be a good animal model for humans (Soares-Cunha et al 2016). However, there are some structural and functional differences. The human dorsal striatum is divided into CN and Put by the internal capsule (Graybiel & Ragsdale 1978), while the ventral striatum is composed of the NAc and the olfactory tubercle (OT). Prefrontal and orbitofrontal cortices, and sensorimotor cortex project to the CN and the Put, respectively (Graybiel & Rauch 2000, Krack et al 2010). The prefrontal and limbic cortical regions project to the NAc. Thalamostriatal circuits involve different parts of the striatum; Put receives input from central medial nucleus and dorsolateral parafascicular (PF) of the intralaminar complex, CN is innervated by caudal PF (McFarland & Haber 2000, Smith et al 2004) and ventral striatum receives projections from rostral PF but also from midline group of nuclei (Gimenez-Amaya et al 1995).

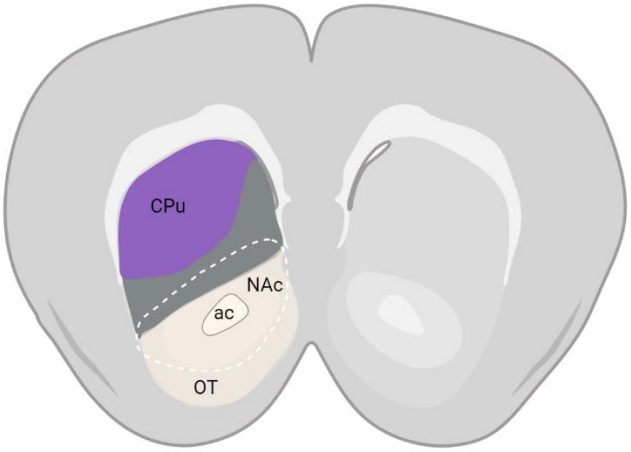

Figure 2. **Structure of striatum**, coronal mouse brain section. Dorsal striatum is identified as the region above the white dashed line, but this border has no clear foundation. While, the ventral striatum is the area below the border between grey and white zones. Functionally, the limbic-innervate striatum is equal to the ventral striatum, the sensorimotor striatum to the dorsal striatum (purple zone). Abbreviations: anterior commissure (ac), Caudate-Putamen complex (CPu), Nucleus Accumbens (NAc), striatal element of olfactory tubercle (OT). Created with BioRender.com

The rodent striatum (**Figure 2**) has partially different subdivisions (Voorn et al 2004). In the classical vision, adopted also by Allen Brain Atlas, the striatum consists of the caudate-putamen complex (CPu), the NAc and the striatal element of the OT. Other interpretations, more detailed, distinguish two macro areas, the dorsal and ventral striatum; the first one is subdivided into dorsomedial (DMS) and dorsolateral (DLS) parts, while the second one is subdivided into NAc core (NAcc) and shell (NAcs) (Zahm & Brog 1992, Zahm & Heimer 1990). The DMS is involved in spatial learning and inhibitory control of behaviour (Devan & White 1999) but also in reversal learning, strategy shifting, execution and maintenance of new strategies (Ragozzino 2007) and receives inputs from ventral region of prefrontal cortex and from medial PF complex. The DLS mediates procedural or stimulus-response learning (Packard & Knowlton 2002, White & McDonald 2002) and receives information from motor cortex and dorsolateral PF nucleus. The ventral striatum is involved in reinforcement learning and also in spatial learning and inhibitory control of behaviour, probably for different aspects from those of the DMS (Christakou et al 2004, Eagle & Robbins 2003); it receives projections from thalamic midline nuclear group, prelimbic and infralimbic cortex and also ventromedial PF (Lanciego et al 2004, Russo & Nestler 2013, Voorn et al 2004, Yin & Knowlton 2006).

Another way to classify striatum is into functional subdivisions based on excitatory input, thus defining associative, sensorimotor and limbic domains (Chuhma et al 2017, Haber & McFarland 1999, Voorn et al 2004)}. The sensorimotor region receives inputs from primary motor and premotor cortices and corresponds to the DLS (Joel & Weiner 2000, Smith et al 2004). The associative area receives input from associative regions of the cortex such as the dorsolateral prefrontal cortex and correspond to the DMS (Berendse et al 1992, Groenewegen et al 1990). The limbic domain consists of NAcc, NAcs and OT, and receives inputs from the hippocampus and amygdala and from the orbitofrontal and anterior cingulate cortices (Floresco 2015, Ikemoto 2007, Voorn et al 2004).

A further striatal classification method is based on neurochemical features. It is possible to identify two components: striosomes and matrix (Graybiel & Ragsdale 1978, Herkenham & Pert 1981, Olson et al 1972). Staining for the enzyme acetylcholinesterase (AChE) reveals a mosaic of striatal areas with low AChE activity, called striosomes (Graybiel & Ragsdale 1978). Striosomes represent 10% of striatal volume and are enriched with μ opioid receptors, characterized by strong immunoreactivity against enkephalin, substance P, GABA and neurotensin (Gerfen 1984, Graybiel et al 1981). Striosomes are immersed in a strong background with intense AChE staining, that represents the matrix. The matrix has a relatively low concentration of μ opioid receptors (Desban et al 1995, Pert et al 1976) and it is enriched with parvalbumin and calbindin immunoreactivities (Lanciego et al 2012, Prensa et al 1999, Soares-Cunha et al 2016, Voorn et al 2004).

Striatal neuronal populations

Medium spiny neurons

95% of striatal neurons are GABAergic medium spiny neurons (MSNs), named for their high density of dendritic spines, while the remaining 5% are interneurons with smooth dendrites (Graveland et al 1985).

According to the axonal target, **dorsal striatal MSNs** can be subdivided into direct MSNs (dMSNs), also called striatonigral MSNs and indirect MSNs (iMSNs), also named striatopallidal MSNs. The first group of striatal neurons project directly to GPi and SNr and VTA, while the second neuronal group, before reaching the output nuclei, projects to GPe. These two MSN populations express different molecules: dMSNs express dopamine D1 receptor (D1R), substance P, dynorphin and muscarinic acetylcholine receptors type 4 (M4), while iMSNs express dopamine D2 receptor (D2R), adenosine A2A receptor (A2AR), enkephalin and neurotensin (Gerfen 1992b, Heiman et al 2008, Lobo et al 2006). However, it has been proposed that 5–15% of dorsal striatal MSNs can express both D1R and D2R (Bertran-Gonzalez et al 2008, Perreault et al 2010, Perreault et al 2011, Perreault et al 2014).

In the **ventral striatum** the separation of D1-MSNs and D2-MSNs into direct and indirect pathways is not precise. Direct NAc innervation of the SNr and VTA is entirely mediated by D1-MSNs, while indirect pathway from NAc and ventral pallidum (VP) has a contribution of both D1 and D2 MSNs. This suggests that NAc MSNs can both inhibit and disinhibit the mediodorsal thalamic nuclei (Kupchik et al 2015, Lu et al 1998, Zahm & Heimer 1990).

D1 and D2 MSNs also have a topographical distribution inside striatum; the anterodorsal portion presents a random distribution, but the most caudal portion of the dorsal striatum is comprised almost exclusively of D1-MSNs. In the NAcc, D1 and D2-MSNs are evenly distributed but D2 in NAcs are less represented (Gangarossa et al 2013, Soares-Cunha et al 2016). Several studies (Cepeda et al 2008, Gerfen 1985, Gertler et al 2008) demonstrate unique electrophysiological properties for each subtype and support the idea that these different populations elaborate different cortical inputs.

MSN activity

In striatum, glutamate binds three receptor types: α-amino-3-hydroxy-5-methylisoxazole-4-propionate receptors (AMPARs), N-methyl-D-aspartate receptors (NMDARs) and metabotropic glutamate receptors (mGluRs), in turn divided into group I (mGluR1 and 5), group II (mGluR2 and 3) and group III (mGluR4, 5, 6, 7 and 8). AMPARs and NMDARs are ionotropic receptors, formed by several subunits, and mediate fast transmission (Kawaguchi 1992, Mori et al 1994). The combination of different subunits determines sub-type-specific functional properties, such as ion permeability, gating and Mg^{2+} sensitivity (Gotz et al 1997). On the other hand, mGluRs are involved in long-term changes of synaptic efficacy (Calabresi et al 1992a, Calabresi et al 1992b). These three receptor types are involved in specific aspect of MSN activity and plasticity including long term potentiation (LTP) and long term depression (LTD), two forms of synaptic plasticity (Calabresi et al 2000a, Calabresi et al 2000b, Gotz et al 1997, Kerr & Wickens 2001, Kombian & Malenka 1994, Mori et al 1994, Reynolds et al 2001, Shen et al 2008).

As regards MSN **electrophysiological properties**, *in vitro* preparations showed that MSNs are generally at hyperpolarized membrane potentials (around -85 mV), and, when recorded intracellularly, have tonic action potentials with amplitude around 100 mV, lasting 1.1-1.3 milliseconds (Calabresi et al 1992b, Cepeda et al 1994, Stern et al 1998, Wilson & Groves 1980). After corticostriatal stimulation, MSNs show excitatory post-synaptic potentials (EPSPs), recorded by patch clamp or intracellular recordings. These EPSPs are inhibited by antagonists of AMPAR and NMDAR (CNQX and AP-V, respectively), leading to the hypothesis of them being dependent on glutamatergic stimulations. EPSPs in MSNs are mainly mediated by AMPARs because NMDARs are inactivated by Mg^{2+} due to MSN spontaneous hyperpolarized potentials. However, the situation is more complex than that, since the activation of MSNs is mediated by several neurotransmitters, such as DA and acetylcholine (Ach), affecting the glutamate system (Brown & Arbuthnott 1983,

Calabresi et al 2000c, Centonze et al 2001a, Cepeda et al 1993, Garcia-Munoz et al 1991, Kerkerian et al 1987, Kulagina et al 2001, Mitchell & Doggett 1980, Nishi et al 1990, Rowlands & Roberts 1980, Yan et al 1997). *In vitro* studies demonstrate that MSNs shift between two membrane potential states: the down-state, where the MSN membrane is hyperpolarized and cannot generate action potentials and the up-state, where the membrane is relatively depolarized and close to the threshold for spiking generation (Calabresi et al 2000a, O'Donnell & Grace 1993, Wilson 1993).

In vivo, MSNs fire in a slow irregular pattern with large spontaneous shifts of membrane potential lasting several seconds (Stern et al 1998, Wilson & Groves 1980). This oscillation of membrane potential is not the result of prominent activation of voltage-dependent inward currents but can be caused by synaptic activation of cortical inputs (Calabresi et al 1990a, Calabresi et al 1990b, Cowan & Wilson 1994, Stern et al 1998, Wilson & Groves 1980). In fact, cortical stimulation generates early fast EPSPs and, in some case, delayed slow depolarization (Calabresi et al 2000a). The phasic release of glutamate from cortical terminals could be the cause of the continuous fluctuation of membrane potentials of MSNs between up- and down-states. Confirming this hypothesis, Cowan and Wilson (Cowan & Wilson 1994) demonstrated that corticostriatal neurons possess spontaneous depolarization and phases of firing activity similar to those of MSNs. More evidence for two-state membrane potential transitions of MSNs was provided by electrical stimulation in the cortex of awake monkeys followed by the analysis of spike latency histogram (Gubellini et al 2004, Kitano et al 2002).

To identify the electrophysiological properties of the MSN sub-population, Cepeda and colleagues (Cepeda et al 2008) used green fluorescent protein as a reporter gene to compare different properties of MSNs. In this study, whole cell patch clamp experiments showed that passive membrane properties of D1 and D2 MSNs were similar. However, D2 MSNs could produce action potentials from more hyperpolarized membrane potentials, indicating that they are probably more ready to transfer information than D1 MSNs, a property which could be explained by differences in subunit composition of Kir2 potassium channels (Shen et al 2007). Furthermore, in voltage clamp experiments with normal artificial cerebrospinal fluid (ACSF), D2 MSNs have higher frequencies of spontaneous synaptic inward current than D1 MSNs, probably due to more inputs and glutamate release on D2 MSNs (Cepeda et al 2008). In fact, electrical stimulation of corticostriatal pathway evokes EPSCs at lower intensities in D2 than in D1 MSNs (Cepeda et al 2008). In the presence of tetrodotoxin (TTX) this difference was reduced, suggesting that Na^+ conductances contribute to

spontaneous EPSCs in D2 MSNs (Cepeda et al 2008). D2 MSNs also display large amplitude synaptic events (> 100 pA) never seen in D1 MSNs, indicating that D1 and D2 inputs are different, possibly due to a different synaptic surface area (Lei et al 2004). Interestingly, cortical pyramidal neurons innervating D2 MSNs, also receive more excitatory inputs from their enlarged dendritic trees in layer I compared to neurons that project to the D1 MSNs (Morishima & Kawaguchi 2006). The idea that D2 MSNs receive more glutamatergic inputs is reinforced by the evidence that pharmacological blockade of $GABA_A$ receptors induce large spontaneous membrane depolarizations and complex responses to cortical stimuli (Cepeda et al 2008). These depolarizations reflect a tighter synaptic interaction between cortical pyramidal neurons and MSNs.

Another aspect emerged through the analysis of the paired-pulse facilitation (PPF), a short-term synaptic plasticity phenomenon. Studies showed difficulty in distinguishing D1 from D2 MSNs, since both express PPF. For Cepeda and colleagues, D2 MSNs display more PPF, while for Kreitzer and colleagues (Kreitzer & Malenka 2008) D2 MSNs have lower PPF compared to D2 negative cells. Moreover, application of AMPA or cyclothiazide (CTZ) evokes larger inward currents in D1 than in D2 MSNs. The reason could be that in D2 MSNs there are fewer AMPARs with different subunit composition (Deng et al 2007, Lanciego et al 2012, Soares-Cunha et al 2016).

Regarding MSN **synaptic plasticity**, LTP and LTD have been studied both *in vitro* (Calabresi et al 1992a, Calabresi et al 1992b, Lovinger et al 2003, Lovinger & Tyler 1996, Lovinger et al 1993, Partridge et al 2000, Walsh 1993, Wickens et al 1996) } and *in vivo* (Charpier & Deniau 1997, Charpier et al 1999, Mahon et al 2004, Reynolds & Wickens 2000). *In vitro* LTD was induced with high frequency stimulations (HFS) of corticostriatal fibers in the presence of physiological Mg^{2+} concentration (1.2 mM), while LTP is obtained by HFS with perfusing solution free of Mg^{2+}, suggesting that the induction of LTP requires the activation of NMDARs (Gubellini et al 2004). However, besides the presence or absence of Mg^{2+} other factors, such as the age of the animal used, can influence the induction of LTP or LTD, as showed in the Patridge experiments (Partridge et al 2000). In addition, different forms of LTD and LTP have been demonstrated (Garcia-Munoz et al 1996), in which glutamate acts on pre-synaptic autoreceptors, inducing Ca^{2+} activation of second messenger cascade.

In detail, there are several mechanisms to generate striatal **LTD**. HFS of corticostriatal fibers promotes the activation of AMPARs and consequent depolarization of neuronal membrane. This event leads to the activation of voltage dependent Ca^{2+} channels (VDCCs), increasing the

intracellular calcium concentration at the post-synaptic level. Calcium ion plays a critical role in several forms of post-synaptic plasticity (Calabresi et al 1994), by activating Ca^{2+}-dependent enzymes and kinases (such as protein kinase C, PKC) involved in different cellular functions (Clapham 1995). The release of DA, acting on D1-like and D2-like DA receptors and the 32-kDa dopamine and cAMP-regulated phosphoprotein (DARPP-32) pathway, with a strict dependence on the balanced activation of DA receptors (Calabresi et al 2000c, Calabresi et al 1992a, Centonze et al 2001a, Choi & Lovinger 1997), is crucial for the induction of LTD. Another neuromodulator for LTD induction is nitric oxide (NO), produced by GABAergic interneurons (Calabresi et al 1999c, Centonze et al 2003b, Centonze et al 2001b). Gerdeman and colleagues (Gerdeman & Lovinger 2001) showed another form of LTD in which the activation of CB1 cannabinoid receptor is essential. Finally, the LTD obtained by HFS can also be induced by focal application of glutamate at corticostriatal synapses (Calabresi et al 1999b). Also mGluRs are involved in the induction of corticostriatal LTD *in vitro*. Some scientists showed that mGluRs have a critical role for the induction but not the maintenance of LTD, as it is suggested by blockade of mGluR group I after the induction of LTD (Gubellini et al 2001, Sung et al 2001). This role of mGluRs in LTD is presumably dependent on the regulation of intracellular Ca^{2+} concentration. On the other hand, group II and III of mGluRs do not seem to be involved in corticostriatal LTD induction, but exert an inhibitory action on glutamate release from presynaptic neurons (Sung et al 2001). For Lovinger and colleagues (Lovinger & McCool 1995), the induction of LTD required both types of group I mGluRs. This idea was confirmed by Sung and Kahn, using murine brain slices they reported that agonists of both types of group I mGluRs induce LTD of evoked synaptic responses in the striatum (Kahn et al 2001, Sung et al 2001). However, this form of LTD seems to be different from the one induced by HFS, because it is independent from synaptic activity and insensitive to antagonists of D1 and D2 DA receptors. It seems to be due to a presynaptic glutamate release inhibition from group II mGluR activation.

Other mechanisms are necessary for the induction of **LTP.** The most important is mediated by NMDARs, whose activation combined with VDCCs leads to massive increase of intracellular Ca^{2+} concentration. At post-synaptic level, Ca^{2+} increases as a consequence of NMDAR activation, while, at extra-synaptic sites, L-type voltage sensitive calcium channels (VSCCs) produce an increase of this ion (Artola & Singer 1993, Berridge 1998, Calabresi et al 1992b, Calabresi et al 1996, Clapham 1995). *In vitro*, LTP is inducible by applying different protocols, such as using a perfusion solution with (Partridge et al 2000) or without Mg^{2+} ion (Gubellini et al 2004), whereas it can be induced *in vivo* in the presence of Mg^{2+} ion (Charpier & Deniau 1997). For the induction of LTP, DA plays a crucial role.

LTP induction can be blocked by antagonists of D1-like DA receptors (Kerr & Wickens 2001), whereas LTP can be amplified by antagonists of D2-like DA receptors (Calabresi et al 1997, Centonze et al 2001a). Ach is another important neuromodulator involved in the LTP induction. Ach acts activating MSN M1-like receptors, which lead to an increase of striatal NMDAR responses through PKC-mediated mechanism (Calabresi et al 1999a, Calabresi et al 1998). The release of Ach from cholinergic interneurons is stimulated by activation of D1-like DA receptors, highlighting the important role of DA in the induction of LTP (Aosaki et al 1998, Centonze et al 2003a, Centonze et al 2002). *In vivo*, Charpier and colleagues (Charpier & Deniau 1997) observed that a couple of HFS and current injection in the recorded neurons was necessary for the induction of LTP, as HFS of the facial motor cortex alone can induce only short term changes in synaptic plasticity. The same group also induced LTP by mimicking the spontaneous large-amplitude oscillation applying a low frequency protocol at 5 Hz. Co-activation of mGluR1 and 5 plays a critical role also in the induction of LTP, since application of antagonists of these two receptor types blocks this kind of plasticity. However, co-activation of group I of mGluRs plays a critical role only for the induction of LTP and not for its maintenance, similarly to LTD (Gubellini et al 2003). Whereas Dos Santos Villar (Dos Santos Villar & Walsh 1999) obtained contrasting results, a support to Gubellini hypothesis came from experiments using mGluR1 and 5 -/- mice that evidenced the necessity of co-activation of these receptors for LTP induction (Chiamulera et al 2001, Conquet et al 1994). These receptors have a key role in augmenting intracellular Ca^{2+} concentration through direct and second-messenger mediated mechanisms (Clapham 1995, Fagni et al 2000, Stefani et al 1996), in this way participating to LTP induction.

Interneurons

The remaining 5% of striatal neurons are interneurons (Graveland & DiFiglia 1985), and play a critical role by controlling MSN activity (Charara & Grace 2003, Gittis & Kreitzer 2012, Hikida et al 2001, Kaneko et al 2000, Tepper et al 2010, Tritsch & Sabatini 2012). Five groups have been defined by morphological and neurochemical features. The cholinergic neurons use Ach as neurotransmitter, they are also known as tonically active neurons (TNFs) for their constant firing pattern of activity (Aosaki et al 1994, Dautan et al 2014, Morris et al 2004). TNFs are able to modulate the direct and activate the indirect striatal pathways (Cachope et al 2012, Centonze et al 2003a, Hikida et al 2001, Kaneko et al 2000, Maurice et al 2004, Pisani et al 2000, Threlfell et al 2012, Tozzi et al 2011, Witten et al 2010). TNFs also express D2 and D5 dopamine receptors (Surmeier et al 2007). In addition, there are different GABAergic interneurons. One class of these interneurons contains parvalbumin,

is characterized by fast spiking; therefore, they are called fast spiking interneurons (FSIs). FSIs send their inhibitory synapses to D1 and D2-MSNs, providing a feed-forward inhibition (Bennett & Bolam 1994, Gittis et al 2010, Kreitzer & Malenka 2008, Lapper et al 1992, Planert et al 2010, Sidibe & Smith 1999, Tepper et al 2010). Like for MSNs, the activity of both TNFs and FSIs is under dopaminergic control. Another GABAergic class is formed by GABAergic interneurons that express somatostatin and neuropeptide Y and use NO as neurotransmitter. They are characterized by low threshold spiking (LTS) and are involved in long-term plasticity (English et al 2011, Ibanez-Sandoval et al 2010, Ibanez-Sandoval et al 2015, Kreitzer 2009, Vuillet et al 1989). Also present but less studied are the GABA-tyrosine hydroxylase and the GABA-calretinin interneurons, characterized by sparse connections with MSNs (Lanciego et al 2012, Soares-Cunha et al 2016).

Main striatal neuromodulators

Glutamate (Glut). The entire cerebral cortex projects to the striatum, connecting cortical glutamatergic neurons to the dendritic spines of striatal MSNs. In detail, pyramidal neurons from layers III and Va innervate the matrix, whereas inputs from prelimbic cortices, originating from pyramidal neurons of the layer V, reach the striosomal compartment (Donoghue & Herkenham 1986, Gerfen 1984). According to this, two different types of cortical pyramidal neurons innervate the striatum: pyramidal tract neurons (PT-type), and intratelencephalic neurons (IT-type). PT-type neurons innervate ipsilateral striatum, preferentially iMSNs, whereas IT-type neurons innervate the striatum bilaterally, mainly dMSNs (Reiner et al 2010, Reiner et al 2003). In addition to corticostriatal input, the thalamostriatal projections contribute a glutamatergic input to the striatum (Cowan & Powell 1956), including MSNs and interneurons. It has been hypothesized that CM/Pf thalamic nuclei target dendritic shafts of striatal neurons, while inputs from other thalamic nuclei contact dendritic spines (Raju et al 2006). Midline and intralaminar thalamic nuclei are often considered as the main source of the thalamostriatal circuit, but also the ventral thalamic motor nuclei contribute to this pathway (Berendse & Groenewegen 1990, Groenewegen & Berendse 1994). Other sources of glutamatergic inputs to the striatum are from the amygdaloid complex, reaching the striosomes (Lanciego et al 2012, Ragsdale & Graybiel 1988).

Dopamine (DA). While glutamatergic terminal inputs serve as a trigger, making synapses with the head of striatal dendritic spines, the DA projections serve as a modulator, making contact with the neck of the dendritic spines. The main input of dopaminergic system to striatum arises from SNc (A9 group (Dahlstrom & Fuxe 1964)), but the retrorubral field (A8) and VTA (A10) also participate to

mesolimbic and mesostriatal projections (Lanciego et al 2012). Neurons in the dorsal tier of SN project mainly to the limbic and associative striatum while neurons from the ventral tier of SN project to the sensorimotor striatum (Gerfen 1992a). VTA DA neurons project to the Nac, medial prefrontal cortex and amygdala, implicated in reward processing and drug addiction (Beier et al 2015). Nigrostriatal axons synapse with both types of striatal MSNs. DA excites or inhibits MSNs activating different G-protein coupled dopamine receptors, D1 and D2, respectively, by modulating the gating of voltage-dependent and ligand-gated (ionotropic) ion channels, located in the cell membrane (Missale et al 1998, Surmeier et al 2007). Regulation of these neurons by DA has a critical role in psychomotor function, such as habit learning and control of movement (Albin et al 1989, Schultz 2006).

In detail, DA interacts with the seven transmembrane domain **receptor D1**, being able to activate the heterotrimeric protein type Gs/olf (Herve et al 1995), which are coupled to adenylyl cyclase (AC) and stimulate the production of cytosolic second messenger cyclic adenosine monophosphate (cAMP) and, subsequently, the activation of protein kinase A (PKA). Activation of PKA leads to the phosphorylation of intracellular targets such as Ca^{2+} (Cav1 L-type), K^+ and Na^+ voltage gated channels, ionotropic glutamate receptors (AMPAR, NMDAR), GABA receptors and several transcription factors. One of the major PKA targets is DARPP-32. When DARPP-32 is phosphorylated, the protein phosphatase 1 (PP1) is inhibited (Svenningsson et al 2004) and the PKA signalling is amplified. PKA activation promotes phosphorylation of Nav1.1 Na^+ channels entering into inactivated state (Carr et al 2003, Scheuer & Catterall 2006), inhibits several K^+ channels, as Kirk2, Kv1 and Kv4 (Hernandez-Lopez et al 2000) and enhances the opening of Ca^{2+} channels (e.g. Cav1.3) (Surmeier et al 1995, Vilchis et al 2000). Stimulation of D1 receptors can also increase Ca^{2+} influx through NMDARs. This leads to the activation of several pathways, including ERK by Ras-Raf-MEK cascade. Thus, PKA can influence directly or indirectly CREB, inducing the transcription of target genes. CREB activity is also influenced by the activation of Gq protein coupled D1/D2 receptor heteromers (Lee et al 2004, Rashid et al 2007). This regulates the phospholipase C (PLC) increasing intracellular Ca^{2+} concentration, the activation of Ca^{2+}/calmodulin-dependent protein kinase II (CaMKII) and its translocations to the nucleus (as reported in **Figure 3**). In summary, D1 signalling increases the responsiveness of striatonigral neurons to glutamate, by enhancing expression of its receptors and modulating ion channels function to promote the MSN up-state (Soares-Cunha et al 2016, Surmeier et al 2007).

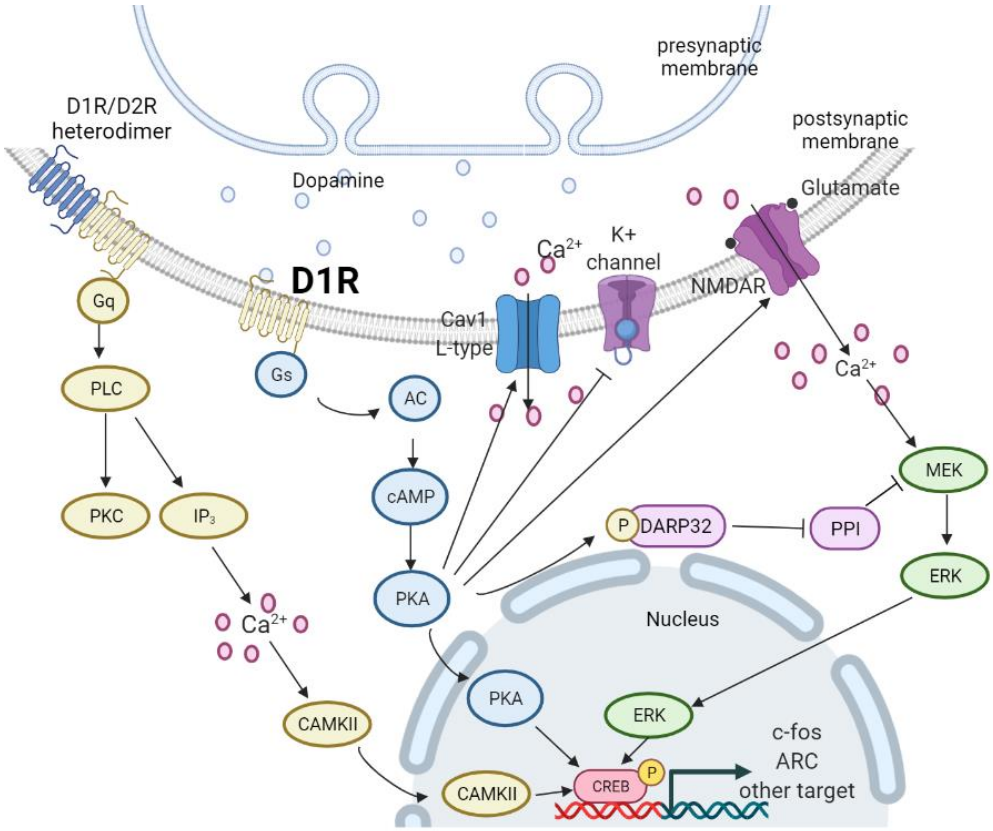

Figure 3. D1R signalling. D1R activation enhances the responsiveness of striatonigral neurons to glutamate through the increase of its receptors. Abbreviations: adenylyl cyclase (AC), cyclic adenosine monophosphate (cAMP), protein kinase A (PKA), activity-regulated cytoskeleton-associated protein (Arc), calcium/calmodulin-dependent protein kinase type II (CaMKII), cAMP responsive element binding protein (CREB), extracellular signal-regulated kinases (ERK), inositol 1,4,5-trisphosphate (IP_3), mitogen-activated protein kinase (MEK), Calcium channel voltage-dependent L type (Cav1 L-type), phospholipase C (PLC), protein kinase C (PKC), phosphorylated dopamine- and cAMP-regulated phosphoprotein 32 kDa (P-DARPP-32), protein phosphatase 1 (PP1), N- methyl-D-aspartate glutamate receptor (NMDAR), phospholipase C (PLC), inositol (1,4,5)-trisphosphate (IP_3), dopamine receptor 1 (D1R). Created with BioRender.com

D2 receptors are coupled to Gi/o proteins, leading to inhibition of AC and limiting PKA activity (Stoof & Kebabian 1984). In parallel, release of Gβγ subunits reduce Cav2 Ca^{2+} channels opening and stimulating PLC to generate diacylglycerol (DAG) and PKC activation as well as inositol (1,4,5)-triphosphate (IP_3) and mobilization of intracellular calcium stores. Inhibition of PKA is also mediated by dephosphorylation of DARPP-32 by calmodulin-dependent protein phosphate 2B (PP2B). Similar to D1, D2 receptor alters glutamate receptor function in dorsal striatum. At the opposite, D2 receptor signalling facilitates the removal of AMPARs from the plasma membrane due its dephosphorylation (Hakansson et al 2006). By activation of calcineurin-dependent mechanism, D2 receptor mediates negative modulation of Cav1.3 Ca^{2+} channels (Hernandez-Lopez et al 2000, Olson et al 2005). Nav1.1 Na^{+} channels are also negatively modulated, presumably by a PKC-mediated enhancement of slow inactivation that reduces their opening, (Surmeier et al 1992). Moreover, D2 receptor enhances the opening of K^{+} channels (Kir3), which causes a transient decrease in neuronal excitability (Greif et al 1995, Hernandez-Lopez et al 2000). There are also D2 receptor-A2A receptor

heterodimers, with an antagonistic allosteric interaction, that modulate AC activity (Fuxe et al 2010), as shown in **Figure 4** below. This coordinated modulation of ion channels reduces MSN responsiveness.

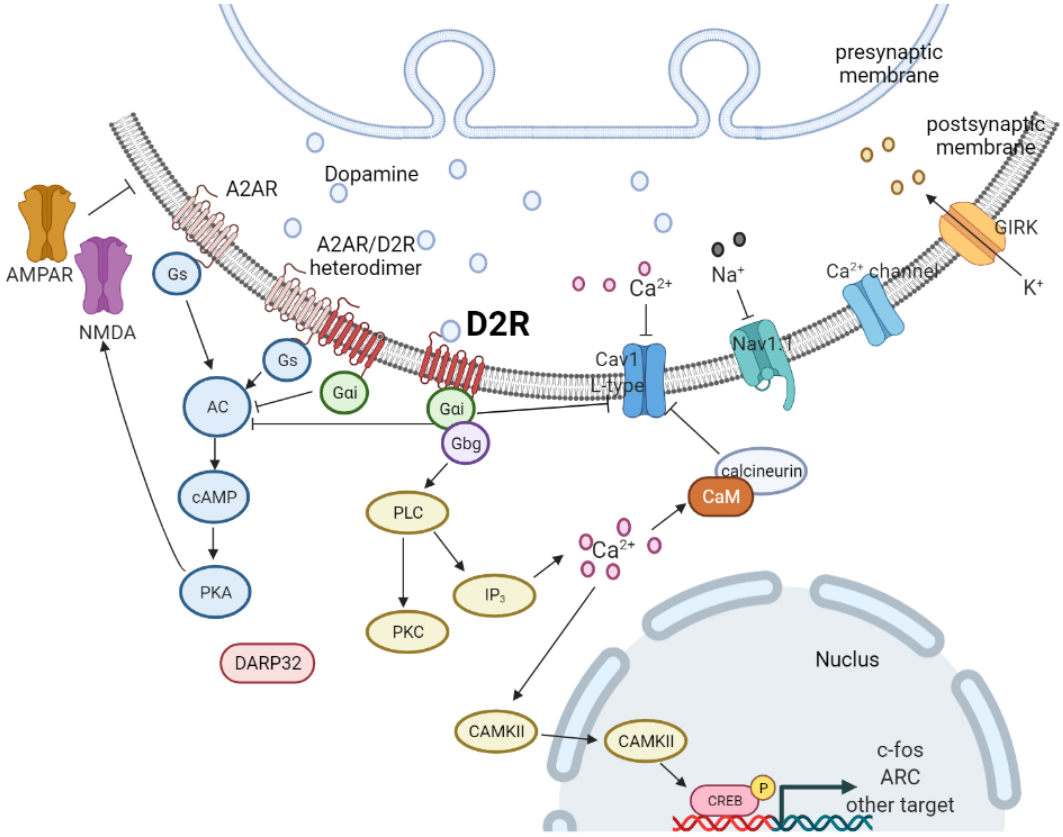

Figure 4. D2R signalling. D2R reduces MSN responsiveness by reducing the opening of its channels. Abbreviations: adenylyl cyclase (AC), cyclic adenosine monophosphate (cAMP), protein kinase A (PKA), α-amino-3-hydroxy-5-methyl-4-isoxazolepropionic acid glutamate receptor (AMPAR), activity-regulated cytoskeleton-associated protein (Arc), calcium/calmodulin-dependent protein kinase type II (CaMKII), cAMP responsive element binding protein (CREB), G protein-coupled inwardly-rectifying potassium channels (GIRK), inositol 1,4,5-trisphosphate (IP_3), sodium channel voltage-gated type I (Nav1.1), Calcium channel voltage-dependent L type (Cav1 L-type), phospholipase C (PLC), protein kinase C (PKC), dopamine- and cAMP-regulated phosphoprotein 32 kDa (DARPP-32), N- methyl-D-aspartate glutamate receptor (NMDAR), phospholipase C (PLC), inositol (1,4,5)-trisphosphate (IP_3), dopamine receptor 2 (D2R), adenosine receptor 2a (A2AR). Created with BioRender.com

Some striatal **interneurons** also express dopamine receptors. Among these, cholinergic interneurons express D2 receptors. D2 receptor signalling in interneurons reduces the excitability and responsiveness to glutamate by reducing autonomous interneurons spiking and inhibiting calcium entry necessary for exocytosis of Ach (Soares-Cunha et al 2016).

Adenosine. Adenosine is another important striatal glutamatergic modulator through its action on adenosine receptors (Fredholm et al 2001). Differently from DA, adenosine can be considered as an intrinsic signal, as it is locally produced depending on striatal activity. Two main sources of adenosine have been discovered. The first, a hormone-like formation of adenosine, can be found when adenosine increases as a function of general circuit activity. Intracellular adenosine

concentration (which at the basal level is in the nanomolar range) increases when ATP is dephosphorylated as a result of increased workload. This is translated into increased extracellular adenosine concentration through bidirectional and non-concentrative nucleoside transporters. The second source of extracellular adenosine derives from the action of ecto-nucleotidases on ATP released from synaptic vesicles upon nerve stimulation (Cunha 2001, Zimmermann 2000). As mentioned above, adenosine A2A receptors are expressed by iMSNs and affect striatal functions. A2A receptors might play a role in long-term plasticity of glutamatergic cortico-striatal synapses such as LTD and LTP (Cunha et al 1996, Wieraszko et al 1989), but it is unclear if they regulate the plasticity pre- or post-synaptically or both. Studies of chronic cocaine adaptation (Baldo et al 1999) or sensitization to amphetamine (Bastia et al 2005) or L_DOPA treatment (Fredduzzi et al 2002) suggest a regulation of LTP induction by A2A receptors. Moreover, adenosine receptors may play a role in excitotoxicity once over-stimulated (Popoli et al 2002, Schiffmann et al 2007).

Acetylcholine (Ach). Interneurons are the main intrinsic source of striatal Ach (English et al 2011, Kitai & Surmeier 1993, Pisani et al 2007). At the cellular level, Ach acts through the activation of two receptor families: muscarinic (mAChR) and nicotinic (nAChR). mAChRs are divided into group I (M_1, M_3, M_5) and group II (M_2 and M_4). Group I receptors are found in striatal d- and i-MSNs, located postsynaptically and extrasynaptically (Yan et al 2001), they are coupled with $G_{q/11}$ and, when bound to Ach, the α subunit activates PKC and PLC, leading the production of DAG and IP_3 and consequently increasing the intracellular calcium concentration. Group II receptors are found mostly extrasynaptically and act as autoreceptors on cholinergic interneurons and as inhibitory heteroreceptors on striatal neuropeptide Y-somatostatin expressing GABAergic interneurons and on corticostriatal glutamatergic terminals (Bernard et al 1998). Group II receptors are coupled to $G_{i/o}$ proteins and, when activated, AC is inhibited and the Cav2 channels are close while Kir3 are open (Caulfield 1993, Eglen 2006, Haga 2013, Nathanson 2000). Nicotinic receptors are pentameric ligand-gated ion channels that consist of both heteromeric subunit combinations of α and β subunits (Exley & Cragg 2008, Gotti et al 2009). The most common types of nAChRs in the striatum are the homomeric α7 subunit and α4β2. The α4β2 subtype acts as autoreceptor in cholinergic interneurons, as a postsynaptic heteroreceptor in GABAergic interneurons and as a presynaptic heteroreceptor in GABA, serotonin, and dopamine axon terminals (Abudukeyoumu et al 2019, Eskow Jaunarajs et al 2015).

Striatal encoding of movement

As depicted above, the dorsal striatum contains a majority of intermingled MSNs, organized into the direct (dMSNs) and indirect (iMSNs) projection pathways; these neurons are the main protagonists in motor planning and learning processes (Balleine et al 2009, Graybiel 1998, Hilario et al 2012, Jin & Costa 2015, Marsden & Obeso 1994, Yin & Knowlton 2006).

The classical view sees direct and indirect pathways with functional opposite effects by either increasing or reducing thalamo-cortical activation to promote or inhibit motor action (Albin et al 1989, DeLong 1990). The classical view of BG function has been largely supported by the development of optogenetic and genetic approaches and the progress of bacterial artificial chromosome (BAC) transgenic mice. Kravitz and colleagues (Kravitz et al 2010), were able to optogenetically activate BG circuits, demonstrating that activation of dMSNs facilitates movements while activation of iMSNs inhibits it. Also in agreement with the classical model, the first genetic inactivation by Bateup and colleagues (Bateup et al 2010) and other experiments with selective lesions (Durieux et al 2009) showed that lesion or loss of function of dMSNs reduce movements while movements increase when iMSNs are targeted. However, other scientists suggested that a coordinated activity of both pathways is crucial for the timing and synchrony of BG signalling during movement (Brown 2007, Chan et al 2005) and a more versatile role of d-and iMSNs has been proposed (Bonnavion et al 2019).

In vivo fluorescence recordings using genetically-encoded fluorescent calcium indicators (GCaMP) to monitor cell activity in the direct and indirect pathways, highlighted the concurrent activation of both pathways at the movement onset with similar kinetics (Barbera et al 2016, Cui et al 2013). The authors observed a transient increase in neural activity of dMSNs and iMSNs when the animal initiates the actions but not when it is inactive. Optogenetic activation (Tecuapetla et al 2016) showed a complementary role of direct and indirect pathways, confirming previous studies. These data suggested that the balanced activity between these two pathways may be crucial for appropriate action sequence initiation. Related to the action sequences, Jin and colleagues (Jin et al 2014) investigated the subtypes of MSNs, by using photostimulation assisted cell identification, and showed that both types of cells have concomitant activity during action initiation, but distinctively encode action sequences during the execution. Other scientists highlighted the important role of DLS to combine motor sequences in spontaneous motor behaviours (Markowitz et al 2018). Having identified in naturalistic behaviour a set of sub-second behavioural motifs through the use of an

unsupervised machine learning technique, they demonstrated that the striatum encodes each behavioural motif identified on the basis of kinematic information and the rules to combine them into sequences forming the naturalistic behaviour. In addition, they showed that activity in d- and iMSNs is de-correlated at sub-second time scale but correlated at longer time-scales suggesting that contrasting theories about opposition or complementarity of MSN functions could be reconciled. All these recent findings support the model suggested by Hikosaka and Mink, which hypothesized that the activation of both pathways is fundamental for action selection, permitting the facilitation of desired movements and suppression of unwanted ones (Mink 2003:Hikosaka, 2000 #165). It seems evident that the contribution of d- and i-MSNs needs further investigation. Other scientists (Oldenburg & Sabatini 2015), more recently, confirmed the antagonistic activity of d- and iMSNs on cortical activity, but these effects are heterogeneous with cortical neurons excited biphasically by iMSN stimulation. In 2018, Parker and colleagues (Parker et al 2018) challenged the suppression-selection models, in which the iMSNs suppress competitive actions. The authors demonstrated that direct and indirect pathways participate together in movement selection via synchronized activation. In detail, to track d- and iMSN activity they used transgenic Drd1a^{cre} and Adora2a^{cre} mice, respectively, with virus causing expression of GCaMP in Cre-dependent manner. During mouse movement, they found that calcium event rates rise in both MSN populations with similar dependency on locomotion. This means that d- and iMSN activities have indistinguishable kinetics at motion onset and offset, rising approximately 1 second before motion onset and decreasing approximately 1 second before motion offset. Moreover, the ensemble activity in both MSN populations that encode specific behavioural types seems to be organized in comparable clusters, supporting the study from Klaus and colleagues (Klaus et al 2017). On the other hand, in 2020, Shin and colleagues (Shin et al 2020) suggested the broad and learning-dependent spatial organization of functional clusters of dorsal striatum neurons in direct and indirect pathways. With endoscopic calcium imaging of DMS, they found that both pathways formed functional spatial cluster for different variables in a partially overlapping manner. In conclusion, the situation is more complex than what is suggested by the classical view of BG function.

Amphetamine

Reward, locomotion and response to conditioned reinforcement are influenced by psychostimulant drugs, such as amphetamine (AMPH), acting mainly through the ventral striatum (Amalric & Koob 1993, Cardinal et al 2002, McBride et al 1999). However, these effects can also arise from the dorsal stratum (Baker et al 1998, Dickson et al 1994, Kelley & Delfs 1991, Voorn et al 2004). The chemical structure of AMPH, characterized by an aromatic ring and a nitrogen on the aryl side-chain, reminds most monoamine neurotransmitters including catecholamines (DA, norepinephrine, NE, epinephrine, E) and indoleamines (serotonin, 5-HT, tryptamine and other trace amines) (Heal et al 2013). Because of this high chemical similarity, AMPH acts as a competitive substrate for the reuptake through monoamine transporters, including norepinephrine transporter (NET), DA transporter (DAT) and 5-HT transporter (SERT) (Fleckenstein et al 2007, Rothman & Baumann 2003, Sitte & Freissmuth 2015). The targets of AMPH are the monoamine-containing neurons, with widespread innervation into limbic, motor and isocortical areas, thus explaining the behavioural, motor and vegetative effects of this psychostimulant drug (Bucci et al 2017). In physiological conditions the amount of catecholamines and indoleamines in the synaptic space is determined by exocytotic release followed by uptake and possible degradation.

At the subcellular level, the targets of AMPH are the cell body and the axon terminal, with the latter as the primary target. Here, NET, DAT and SERT normally work by taking monoamines from the extracellular fluid to the axoplasma (Aggarwal & Mortensen 2017, Axelrod & Kopin 1969, Coyle & Axelrod 1971, Iversen et al 1965). Once bound to the plasma membrane, AMPH enters into the axoplasma and reverses the transport direction of NET, DAT and SERT (Sulzer et al 1993), promoting an increase of NE, DA and 5-HT in the synaptic cleft. In detail, AMPH in the axoplasma encounters a vesicular monoamine transporter type-2 (VMAT-2) and enters into a monoamine vesicle. Once in the synaptic vesicle, AMPH increases H^+ ion concentration in the vesicle up to 1000-fold, altering pH from 4 to 7 (Sulzer et al 1995, Sulzer et al 1993, Sulzer & Rayport 1990). Neutralization of vesicle pH value induces charge loss of monoamines, which are weak base. Indeed, at neutral pH, the monoamines lose their charge allowing them to diffuse through the vesicle membrane and into the axoplasma (Brown et al 2000, Brown et al 2002, Pothos et al 2000). The monoamines, once in the axoplasma, are transported to the extracellular space passively or through reverted plasma membrane transporters (Sulzer et al 1995, Sulzer et al 2005). The last AMPH target is the mitochondrial-bound enzyme monoamine oxidase (MAO), which oxidatively deaminates DA, NE and

5-HT. AMPH competitively inhibits MAO-A/-B iso-enzymes with different affinity, with MAO-A inhibition 10-fold higher than MAO-B. MAO-A is in DA and NE terminals, while MAO-B is only operating in 5-HT terminals and non-catecholamine neurons. All these differences explain the higher AMPH effects on the NE and DA transmissions (shown in **Figure 5**) (Bortolato et al 2008, Ferrucci et al 2019, Gesi et al 2001, Robinson et al 1977, Sourkes 1983, Youdim 1980, Youdim et al 2006).

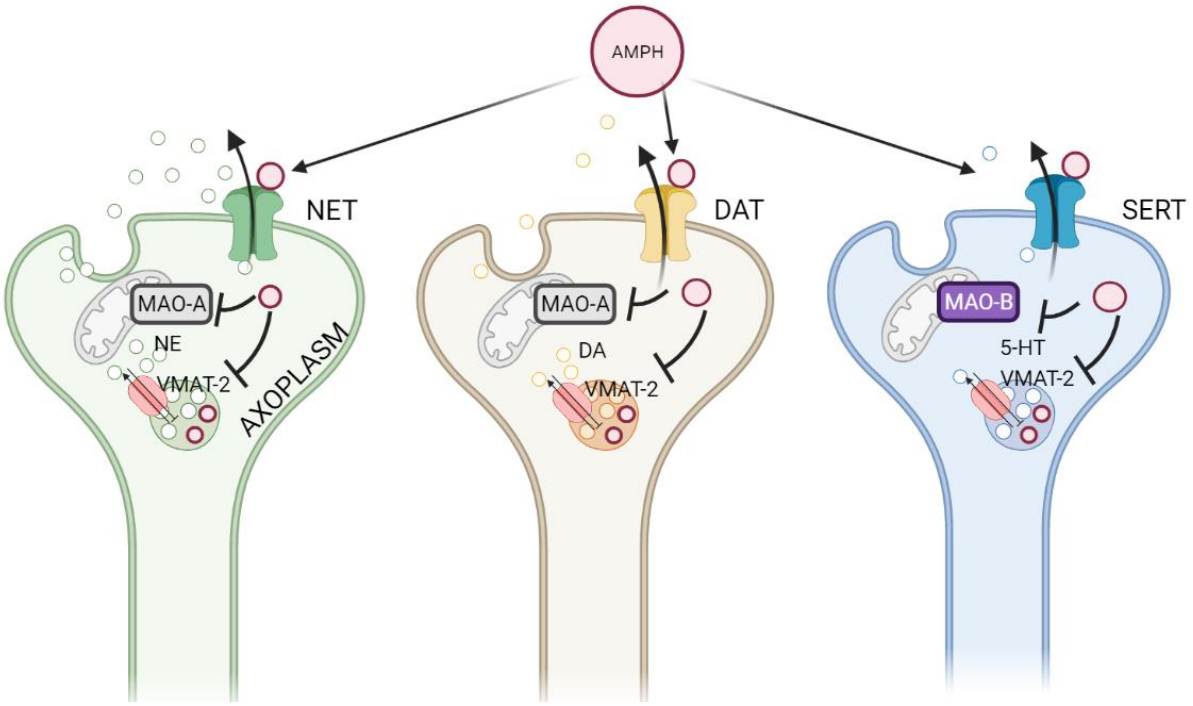

Figure 5. Subcellular effects of amphetamine. AMPH promotes the increase of NE, DA and 5-HT in the synaptic cleft. Abbreviations: amphetamine (AMPH), dopamine (DA), dopamine transporter (DAT), monoamine oxidase (MAO) type A (MAO-A) or type B (MAO-B), norepinephrine (NE), norepinephrine transporter (NET), 5-hydroxytryptamine (5-HT), serotonin transporter (SERT), vesicular monoamine transporter type-2 (VMAT-2). Created with BioRender.com

At the behavioural level, for the implication of DA, NE and 5-HT systems, AMPH has several effects involving physiological and behavioural processes: motor activity (Randrup & Munkvad 1966, Scheel-Kruger 1971, Smith 1963, Thornburg & Moore 1972), oral behaviour (Hoebel 1977, Holtzman & Jewett 1971, Stark & Tooty 1967), sleep (Hartmann 1970, Oswald 1968, Rechtschaffen & Maron 1964), attention (Barondes & Cohen 1968, Evans & Smith 1964), aggression (Consolo et al 1965, Miczek & Gold 1983, Welch & Welch 1966), sexual behaviour (Bignami 1966), learning and memory (Bohdanecky & Jarvik 1967, Carr & White 1984, Doty & Doty 1966, Rech 1966), classical conditioning (Evangelista et al 1970) and operant behaviour (Clark & Steele 1966, Laties & Weiss 1966). In mice, AMPH effects on locomotor activities show a typical bell-shaped dose-response curve. Low doses of AMPH cause an increase of different behaviours, such as locomotion and stereotypies, while higher doses favour smaller behavioural sequences so that shorter behaviours, such as stereotypies,

become predominant over longer behaviours, such as locomotion. According to Yates and colleagues (Yates et al 2007), AMPH induced a biphasic effect on locomotion, with an initial peak of locomotor activity followed by its suppression. When AMPH dose was increased, the initial peak became less pronounced while the locomotion suppression was more relevant. While, in general, the total psychomotor activity increases with AMPH dose, locomotion is predominant at lower doses and stereotypy becomes predominant at higher doses. At all doses, AMPH induced the total activity peak between 30 and 60 minutes after injection. Similar to the peak effect, following activity for 2 hours, a general trend for locomotion decrease and stereotypy increase occurs when AMPH dose increases.

Calcium imaging

Behavioural information is encoded in neuronal firing (spike frequency, spike amplitude, spike duration, spike synchrony across different neurons) of specific cell-types within neuronal populations, in our case within striatal MSNs. Before the availability of fluorescent Ca^{2+} indicators, electrophysiological techniques have been used to record neural activity. Intracellular recording such as voltage clamp or current clamp allows to measure the current and the voltage across the membrane of a single cell without any information regarding the collective activity of many cells. On the other hand, extracellular recording detects the collective activity generated by neurons adjacent to the electrode tip, without information about single cells activity within the population. The development of Ca^{2+} indicators such as fluorescence calcium dyes and genetically encoded calcium indicators (GECIs) allows the study of single cell activity without losing spatial information. Ca^{2+} is an essential intracellular messenger in neurons and acts as an indicator of neuronal activity (Inoue 2021).

Neuronal calcium signalling

Calcium ions have a crucial role in the nervous system, including promotion of neurotransmitter release and induction of synaptic plasticity. At rest, most neurons have an intracellular calcium concentration of about 50-100 nM, which can change and increase up to 100-fold during an action potential (Berridge et al 2000). Cytosolic calcium concentration is dependent on the balance between calcium influx and efflux through plasma membrane as well as on its release and uptake from the intracellular stores. In addition, calcium-binding proteins, such as parvalbumin, calbindin-D28k or calretinin, participate to calcium homeostasis by buffering intracellular calcium concentration (Schwaller 2010). There are three major groups of calcium channels in the plasma membrane that interact to regulate calcium ion flux through the membrane: voltage-gated Ca^{2+} channels (VGCCs), receptor operated Ca^{2+} channels (ROCs) and store operated Ca^{2+} channels (SOCs) (Fucile 2004, Higley & Sabatini 2008, Ramsey et al 2006), as reported in **Figure 6**.

VGCCs mainly respond to electrical signals. They are categorized into high (HVA) and low (LVA)-voltage activated channels, based on the threshold of voltage-dependent activation (Catterall 2000). HVA can be further classified as L-, P/Q-, N- and R-type, while T-type are LVA channels. At synaptic endings, HVA channels trigger the release of neurotransmitters, after their activation by action potential. In more detail, the action potential in the presynaptic cell promotes the activation of

VGCCs causing an inward calcium current and release of the neurotransmitter, while, at the cell body and proximal dendrite, L-type channels provide the calcium signal that induces gene activation.

Differently from VGCCs, ROCs are activated by the binding of specific ligands. Among them, glutamate receptors of the NMDAR, AMPAR and mGluR subtypes play a significant role in the calcium influx at the level of dendritic spines in various neuronal cell types (Bloodgood & Sabatini 2007, Koester & Sakmann 1998, Kovalchuk et al 2000, Nevian & Sakmann 2006, Sabatini et al 2002, Yuste et al 1999). The increase in calcium concentration in spines is particularly important for long-term changes in synaptic efficacy (Zucker 1999). However, among the total cation current that passes through NMDARs, only 6%-12% is formed by calcium ions (Burnashev et al 1995, Garaschuk et al 1996, Rogers & Dani 1995, Schneggenburger et al 1993). The NMDAR calcium ion permeability is determined by subunit compositions, by the receptor phosphorylation status and by the membrane potential of the neuron. In more detail, calcium ion permeability is enhanced by increased NMDAR phosphorylation whereas it is decreased by dephosphorylation (Skeberdis et al 2006, Sobczyk & Svoboda 2007). Another factor influencing calcium ion flux through NMDARs is membrane potential, as calcium flux through the channel receptor increases with neuronal depolarization that removes channel block by Mg^{2+}. AMPARs also regulate calcium concentration in the synaptic area. Their subunit composition influences the permeability to Ca^{2+} and Zn^{2+} ions and varies in a synapse-specific manner within individual neurons (Liu & Zukin 2007, Toth & McBain 1998). Thus, calcium ion permeability is a dynamic event contributing to synaptic plasticity mechanisms (Liu

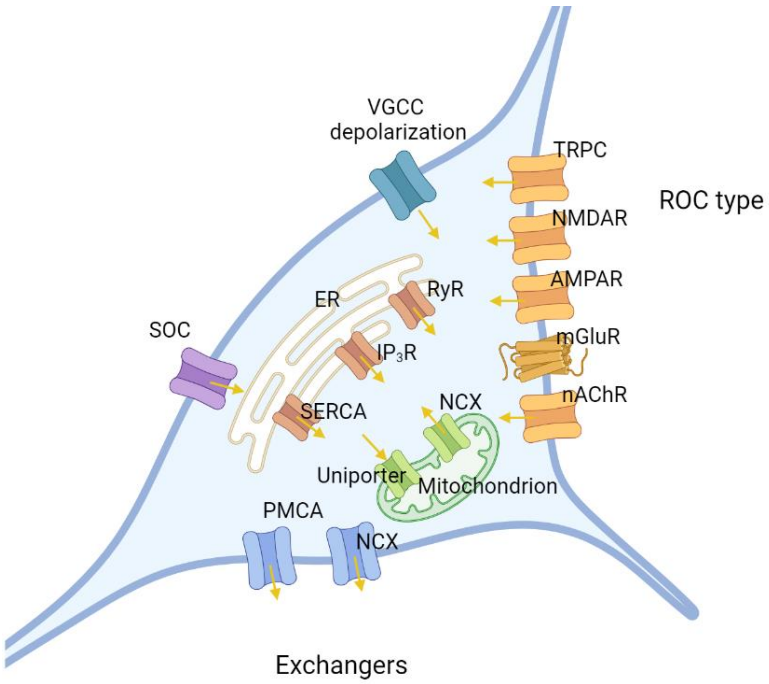

Figure 6. Neuronal calcium flux. Ca^{2+} flux is indicated by yellow arrows. Abbreviations: alpha-amino-3-hydroxy-5-methyl-4-isoxazolepropionic acid receptors (AMPARs), inositol trisphosphate receptors (IP_3Rs), metabotropic glutamate receptors (mGluRs), nicotinic acetylcholine receptors (nAChRs), sodium-calcium exchanger (NCX), N-methyl-D-aspartate glutamate-type receptors (NMDARs), plasma membrane calcium ATPase (PMCA), receptor-operated Ca^{2+} channel (ROC), Ryanodine receptors (RyRs), sarco-/endoplasmic-reticulum calcium ATPase (SERCA), store operated channels (SOCs), transient receptor potential type C (TRPC) channels, Voltage-gated calcium channels (VGCCs). Created with BioRender.com

& Zukin 2007). mGluRs differ in their downstream signalling mechanism; some of them activate PLC, inducing the generation of IP_3 and consequent release of calcium ions from endoplasmic reticulum (ER) stores (Niswender & Conn 2010). Moreover, among ROC types, transient receptor potential type C (TRPC) channels and nicotinic acetylcholine receptors (nAChRs) play a role in neuronal calcium signalling. TRPC channels have varying Ca^{2+} selectivity and probably act as SOC activators or ROC regulators, while nAChRs are non-selective cation channels activated by acetylcholine.

The SOC is a structure activated by stromal interaction molecule (STIM) proteins located at the ER and plasma membrane junctions through the depletion of Ca^{2+} from ER (Prakriya & Lewis 2015). There are also exchanger channels such as plasma membrane Ca^{2+} ATPase (PMCA) and Na^{+}/Ca^{2+} exchanger (NCX) that play roles in cellular calcium export by removing calcium ions from cytosol (Bagur & Hajnoczky 2017, Berridge et al 2003, Grienberger & Konnerth 2012).

Cell storage organelles are the second major source of calcium ions. Intracellular calcium is stored mainly in the ER and its release is mediated by IP_3 receptors (IP_3Rs) and ryanodine receptors (RyRs) (Berridge 1998). Both IP_3Rs and RyRs are regulated by several factors including calcium itself, mediating the process known as calcium-induced calcium release (Berridge 1993). Calcium ions are transported from cytoplasm to the lumen of ER by the sarco/-endoplasmatic reticulum calcium ATPase (SERCA). Mitochondria also participate to calcium homeostasis by taking it from cytosol through calcium uniporter and releasing it through sodium-calcium exchange (Duchen 1999).

Calcium indicators

Calcium imaging allows to study the activity of thousands of neurons *in vitro, ex vivo* and *in vivo* by using fluorescent calcium indicators. Calcium indicators measure changes in the cytosolic free calcium concentration and can be classified into two main classes: chemical or synthetic and GECIs. Fluorescent chemical or synthetic molecules are based on 1,2-bis(o-aminophenoxy) ethane-N,N,N',N'-tetraacetic acid (BAPTA) with high selectivity for calcium ions. Chemicals molecules can be divided into ratiometric and non-ratiometric indicators (Paredes et al 2008). Fura-2 is a combination of calcium chelator and fluorophore and is a representative example of ratiometric indicators. When fura-2 binds calcium ions there is a conformational change leading to a change in the emitted fluorescence and if the molecule is excited at 350 nm its emission light increases, whereas if it is excited at 380 nm its emission light decreases (Grynkiewicz et al 1985, Sohya et al 2007, Tsien 1989). The ratio of the emission at those wavelengths is directly related to the intracellular calcium concentration. On the other hand, an example of non-ratiometric indicator is

the Oregon green dye (Dombeck et al 2010, Ohki et al 2005, Sullivan et al 2005). In more recent times, calcium sensitive fluorescent proteins, known as GECIs, were developed. For calcium imaging, the most widespread calcium reporters belong to the GCaMP GECI (Chalasani et al 2007, Dombeck et al 2010, Fletcher et al 2009, Wang et al 2003). GCaMP is a circularly permutated enhanced green fluorescent protein (cpEGFP) combined at the C-terminus with calcium binding protein calmodulin (CaM) and at N-terminus with calmodulin-binding peptide M13 fragment from myosin light chain kinase (Nakai et al 2001). When calcium binds CaM the fluorescence intensity changes due to a conformational change in cpEGFP, depending on Ca^{2+}-CaM-M13 interaction (Nakai et al 2001, Tian et al 2009).

There are several methods to load dyes into neurons. For synthetic or chemical dyes, the most widely used techniques are single-cell loading and “acute” network loading. In more detail, single cell loading can be performed by a sharp electrode, whole cell patch clamp and single cell electroporation. “Acute” network loading means that many neurons can be marked by acetoxymethyl ester (AM) loading, dextran conjugate loading and bulk electroporation. Single cell calcium imaging allows to study basic mechanisms of calcium signalling at a subcellular scale. At the beginning of calcium imaging *in vitro* and *in vivo*, chemical calcium dyes were injected through sharp microelectrodes (Jaffe et al 1992, Svoboda et al 1997). More recently, calcium dyes have been delivered through whole-cell patch-clamp micropipettes (Eilers & Konnerth 2009, Margrie et al 2002). *In vivo* whole-cell recordings can be performed using two-photon imaging by shadow patching technique, taking advantage of the contrast between the dye in the neuropil and the dark unlabeled cells (Jia et al 2011, Kitamura et al 2008). For this methods, target cells can express fluorescent marker protein through genetical modifications (Margrie et al 2003). Other single cell approaches are the targeted electroporation (Judkewitz et al 2009, Kitamura et al 2008, Nevian & Helmchen 2007) or single cell bolus loading (Helmchen et al 1996). In the electroporation experiments, current pulses with appropriate polarity allow the dye to flow from a micropipette to the target cell. Calcium imaging is also used to study the activity in local population of interconnected neurons, a neuronal network (Aaron & Yuste 2006, Bonifazi et al 2009, Kozloski et al 2001). This requires dye loading into all cells in the neuronal network, which can be achieved through AM calcium dye (Grynkiewicz et al 1985, Stosiek et al 2003). This technique consists of the injection of an AM calcium dye by an air pressure pulse to brain tissue (Connor et al 1999, Garaschuk et al 2006, Stosiek et al 2003). This method can be combined with transgenic mouse lines or virally transduced animals with specific neuronal labels spectrally separated from the calcium indicator

(Runyan et al 2010, Sohya et al 2007, Tamamaki et al 2003). Another type of network loading dyes consists of dextran-conjugated chemical calcium indicators. The calcium dye is injected by pressure to axonal pathways, where through antero- or retrograde transport, it reaches the axon terminals or the cell bodies, respectively (Gelperin & Flores 1997). Finally, electroporation is suitable for staining local neuronal networks (Nagayama et al 2007). This approach uses a micropipette containing dye. A train of electrical current pulse allows the dye to be taken by cell bodies and cellular processes.

Recently, GECIs have become a common tool used in neuroscience (Looger & Griesbeck 2012). The expression of a GECI can be achieved by viral transduction, in utero electroporation and generation of transgenic mice. Among these methods, the viral transduction is the most widespread. Lenti- (Dittgen et al 2004), adeno- (Soudais et al 2004), adeno-associated- (Monahan & Samulski 2000), herpes-simplex (Lilley et al 2001), ΔG rabies (Osakada et al 2011) viral vectors are used to target specific brain regions, through stereotaxic injection (Cetin et al 2006). Cell populations of interest can be targeted, beside viral tropisms, with the use of cell-type-specific promoters (Chhatwal et al 2007, Nathanson et al 2009, Shevtsova et al 2005) or with a combination of mouse lines expressing cell-type-specific Cre recombinase driver with a recombinase-dependent viral vector (Gong et al 2007, Wirth et al 2007, Witten et al 2011). Another method employed for the expression of GECIs is through in utero electroporation of DNA plasmids encoding for GECI (Mank et al 2008). This technique drives negatively charged DNA molecules into the target cells using an electrical field (De Vry et al 2010). Finally, GECIs can be expressed by generating transgenic mouse lines (Grienberger & Konnerth 2012, Heim & Griesbeck 2004, Nagai et al 2004, Pologruto et al 2004, Tsai et al 2003).

GECI parameters

In general, GECI performance is determined by four parameters: dynamic range, calcium sensitivity, response kinetics and response properties. In more detail, the dynamic range is one of the most important aspects of GECIs and is defined as the maximal fluorescence intensity (I_{max}), typically when indicator is saturated, divided by minimal fluorescence intensity (I_{min}), when indicator is free of binding Ca^{2+} ions. Increases in dynamic range value make calcium signal detection easier, however, if I_{min} is too low, the signal detection is possible only when intracellular calcium concentration is saturated. Calcium sensitivity is a GECI feature indicating the ability to detect small changes in calcium concentration associated with a single action potential. Another critical parameter is the responsivity time; GECI needs to respond to a wide range of neuronal firing rates

across multiple orders of magnitude, from sparse to high activity. Calcium sensitivity and response kinetics are inversely linked. GECIs have to be able to follow single spike activity, which results in a rapid rise of intracellular Ca^{2+} concentration within 10 ms with a decay time constant of 50-70 ms. The correlation between fluorescence change and spike count has to be taken under consideration. Increases in this parameter allow to discriminate changes in the number of successive spikes for a wider range. To achieve this, GECIs should show low cooperative calcium binding with a Hill coefficient of 1 (Inoue 2021). All these parameters should be taken under consideration to enable the decoding of neuronal firing.

In vivo GECI imaging

Several imaging methods are used for *in vivo* GECI imaging, represented in **Figure 7**. The first group of techniques involves wide-field microscopy. Among these, calcium imaging can be performed by using a photodiode array (Ross & Werman 1987), a charged couple device (CCD)- based detection unit, and increasingly by complementary metal-oxide-semiconductor (CMOS)- based cameras. In all three cases, the light source was usually a mercury or xenon lamp and excitation wavelengths could be changed with a filter wheel or a regulated monochromatic light sources. Nowadays the light source is generally a monochromatic LED. Within these types of microscope, a dichroic mirror allows to separate the excitation and the emission light (Baker et al 2005, Carlson & Coulter 2008, Smith & Augustine 1988). The classical photodiode arrays are formed by a set of photodiodes (124-1020 elements) and each one is a pixel (Grinvald et al 1981). However, the photodiode arrays are not very common anymore, because despite their high dynamic range and high speed they have a poor spatial resolution. In more recent years, integrated arrays of detectors on silicon, generally CCD or CMOS cameras, have been used for wide-field imaging. Cameras have better spatial and temporal resolution than photodiode arrays but, for some types of cameras, a higher noise level per pixel. The limitation of using wide-field microscopy is related to out of focus fluorescence emission and light scattering, especially when the cells targeted are located deep inside the tissue (Denk & Svoboda 1997).

Deeper regions in the brain are reached by using confocal or two-photon microscopy, that are types of laser scanning microscopy. The specimen is scanned by the focused laser beam and its emitted fluorescence is acquired and generate the image (Lichtman & Conchello 2005). Confocal microscopy usually involves a laser light source, that illuminates the specimen above and below the focal plane. This may generate photodamage throughout the tissue. The emission light is descanned and reaches

the photomultiplier tube (PMT) after passing a pinhole. The pinhole blocks out of focus fluorescence, so that only photons originated from the focal plan reach the PMT. However, on the way through the optical pathway, some photons generated in the focal plan can be scattered or absorbed, an event occurring especially in deep brain regions. The photon loss could be compensated by an increase of excitation light power with the trade-off of an increase of tissue photodamage.

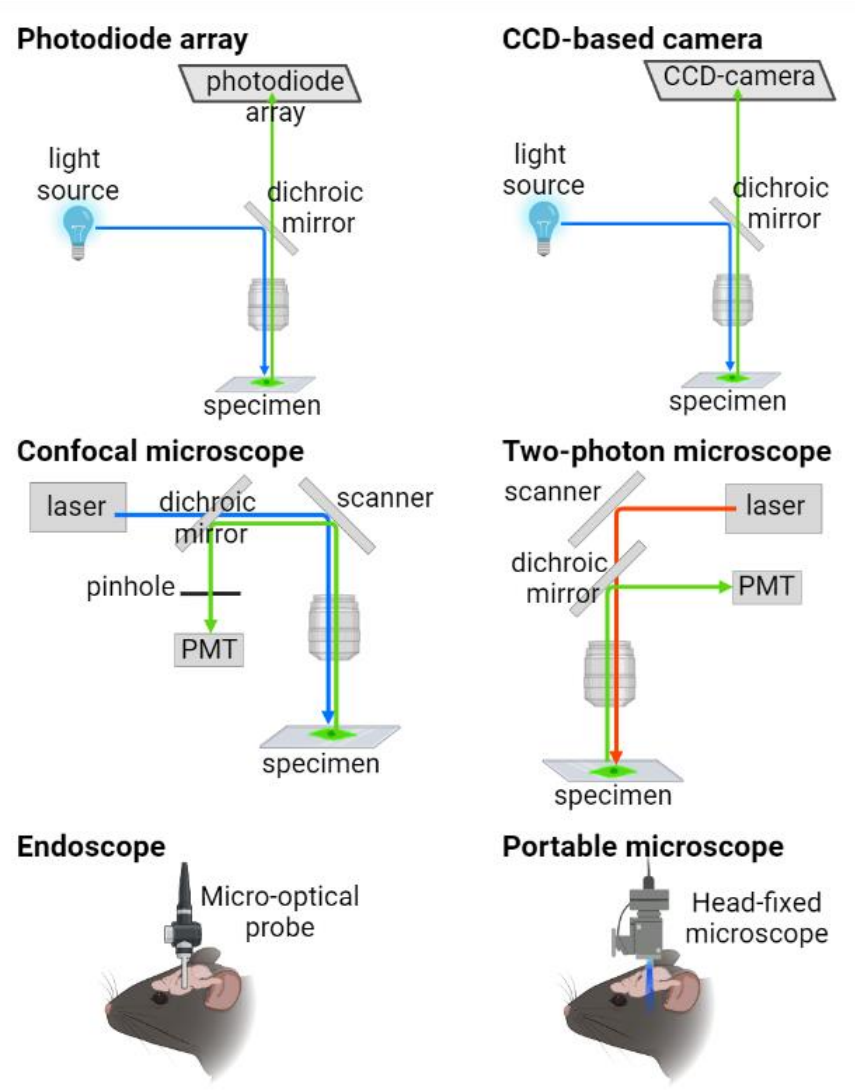

Figure 7. Imaging methods. Schematic representation of imaging methods used for in vivo GECI imaging. Abbreviations: photomultiplier tube (PMT). Created with BioRender.com

Another type of laser scanning imaging method is two-photon microscopy. Two-photon microscopy allows calcium imaging with high resolution and high-sensitivity in deep, highly scattering brain regions (Denk et al 1990). This imaging method uses two near-IR photons to excite the fluorescent molecules from the ground to the excited state. Absorption of two photons with identical or different frequencies is proportional to the excitation power squared, and is therefore a nonlinear process. In order to achieve two-photon excitation a pulsed excitation source with femtosecond-scale pulses needs to be employed and focused in a diffraction-limited focal volume to obtain the shift of molecule state previously mentioned (Svoboda & Yasuda 2006). According to this, out-of-focus excitation and photodamage are strongly reduced. Since the excitation occurs only in the focal spot, no pinhole is necessary, and all fluorescent photons are

detected by the PMT. Using near-IR excitation light allows a better penetration into brain tissue than the visible light used for one photon excitation. In fact, the near-IR laser is absorbed and scattered less by endogenous chromophores in the brain (Oheim et al 2001). Thus, two-photon microscopy allows clearer and more stable images reducing the background signal, signal overlapping and photodamage. Imaging with wide-field and laser scanning microscopy requires to fix the head of an animal restrained in place. This problem can be partially overcome by using virtual reality system. With this imaging method the animal can perform locomotion on a treadmill or walking ball, while images on surround screens simulate movement in a virtual environment. While multiphoton imaging can reach deeper than wide-field or confocal microscopy, even in the most ideal circumstances the maximum imaging depth is limited to around a single millimeter.

In order to perform *in vivo* calcium imaging in deep brain areas, microendoscopes can be used. There are several applications, among these optical fibers; fibre-like gradient refractive index (GRIN) lenses and GRIN-based microendoscopes have been developed (Adelsberger et al 2005, Chia & Levene 2009, Flusberg et al 2005, Grienberger et al 2012, Jung et al 2004, Levene et al 2004, Murayama et al 2007). Microendoscopes can be surgically implanted into mouse brain and allow optical access to deep brain areas for wide-field (Saunter et al 2012, Zhang et al 2020), confocal (Kim et al 2008), or multiphoton imaging (Jung et al 2004).

Recently, the necessity to pair calcium imaging with recordings of freely moving animals, led to the improvement of head-mounted imaging devices (Engelbrecht et al 2008, Flusberg et al 2008, Grienberger et al 2012, Helmchen et al 2001, Sawinski et al 2009). In more detail, an endoscope is implanted into the mouse brain, and a miniature wide-field microscope is mounted on the mouse head, aligned over the endoscope with a baseplate and connected to commutator, that allows cable rotation. A data acquisition device (DAQ hardware) sends digital signals to the computer recording program. Simultaneously, the mouse behaviour is recorded with the behaviour camera through behavioural software. This technique allows to record neuronal population activity through the wide-field microendoscopy focus. However, one-photon devices mounted onto mouse head have all the limitations of wide-field imaging. Among them, the two dimensional imaging does not allow the understanding of neuronal connectivity and the photobleaching problem intensifies with the imaging time and the degree of light power. Indeed, the two-photon version of the miniaturized two-photon microscope has been developed (Helmchen et al 2001, Oh et al 2019, Silva 2017, Zong et al 2017).

Analysis of GECI imaging

GECI analysis at the single cell level has difficulties due to the complexity of neuronal populations; in addition, the analysis can be restricted by the huge size of the video files from GECI images. GECI data undergo three general step process: pre-detection process, cell detection process and post-detection process.

Among pre-detection processes there are motion artefacts deletion, regions of interest (ROI) segmentation and ROI dF/F0 calculations. It is practically impossible, during *in vivo* calcium imaging experiment, to obtain perfectly stable images due to movement or vibration of camera/microscope or of the target. Thus, motion artefact deletion is done generally by correcting motion artefacts by estimating motion vectors with subpixel resolution over a set of overlapping patches within the field of view (FOV). Additionally, it is possible to calculate the maximum cross-correlation between different frames and cross correlation results can be used to align targeted structures. ROI segmentation is a process that discriminates an area of interest in the image. The dF/F0 calculations is important to separate noise from fluorescent signals. F0 can be calculated using the average of ROI from field targeted or by applying algorithms that estimate fluorescence baseline fluctuations.

There are various methods for cell detection processing from principal component analysis and independent component (PCA-ICA) to neural network algorithms, such as constrained non-negative matrix factorization (CNMF) and CNMF for endoscopy data (CNMF_E). However, these methods are less suitable for wide-field data because single-photon data display a large background noise due to fluorescence contributions from neurons outside the focal plane. This large background signal is a combination of local fluctuations from out-of-focus fluorescence, hemodynamic of blood vessels and global fluctuations across the FOV.

PCA-ICA is an automated cell sorting algorithm that performs dimension reduction and noise removal and deconstructs the data set into statistically independent signals composed of a spatial filter as well as the activity traces. The spatial filter indicates the number and coordinates of pixels that contribute to identify the signal, whereas the activity trace shows how the pixel intensity changes over time within this define spatial filter (Mukamel et al 2009). However, there are limitations especially with low intensity signals or noise artefact (Lu et al 2018) and also the process typically fails when the neural components have strong spatial overlaps. There are some open source calcium analysis codes that can resolve this issue. CNMF-E (Zhou et al 2018) is another unsupervised learning algorithm like PCA; it works by simultaneously denoise, deconvolve and

demix data (Pnevmatikakis et al 2016). With CNMF-E the data are represented by a matrix. Each neuron is characterized by a spatial vector, defining cell shape and location, and by a calcium activity time series. Both spatial vector and calcium activity are constrained to be nonnegative because of their physical interpretations. The spatial components should be spatially defined and sparse, since a given neuron covers only a small fraction of the FOV. Thus, spatial locality and sparsity can be constrained. Similarly, the temporal components are highly structured as they represent the neuron fluorescent response to sparse, non-negative trains of action potentials. Moreover, constraints on background activity are also essential to the success of CNMF_E, because for example the extracted neuronal activity could be mixed with background fluctuations leading to artificial signals or high correlation between nearby cells (Zhou et al 2018). Recently, other algorithms were developed such as MIN1PIPE, with Recurrent Neural Networks (RNN) and Long and Short-Term Memory (LSTM) (Lu et al 2018). Additionally, there are some codes as Mosaic (Inscopix), CaImAn (Giovannucci et al 2019) and CAVE (Tegtmeier et al 2018), that can be modified depending on researcher goals.

After detection and modification, the data are further elaborated by a post-detection processing. Before using calcium imaging data, it is preferable to identify and remove baseline noise and sharp noises by dF/F0 (Mao et al 2001), dynamic programming (Greenberg et al 2008), temporal deconvolution (Holekamp et al 2008), machine learning techniques (Sasaki et al 2008) and high pass filter or low pass filter (Balkenius et al 2015). It is also possible, but still under development, to compare separate GECI video data acquired in different days from the same brain area in the same animal, by applying CellReg codes, analyzing the neighboring cells across daily videos (Sheintuch et al 2017).

Aim

The striatum is the main input nucleus of the BG and 95% of its neurons are GABAergic MSNs. Based on their main targets, MSNs are distinguished into neurons of the direct and the indirect pathway. In the classical view, the direct pathway promotes the cortex activity and therefore movement, while the indirect pathway inhibits it. However, recent data support the hypothesis that both direct and indirect striatal pathways participate to action initiation and execution. Dysfunctions of these two pathways are at the base of several movement disorders. For example, loss of modulatory control on MSNs exerted by DA is at the base of Parkinson's Disease. Due to the fine regulation of movement exerted by these two pathways, a study of the single pathway at the cellular level in relation to movement is extremely important, as well as the study of each pathway in relation to the other.

The aim of this study was therefore to investigate the role of striatum in movement regulation at the cellular level, and in particular the changes of iMSN activity during behaviour in the freely moving mouse. The GABAergic activity of iMSNs was stimulated with a psychostimulant drug, d-Amphetamine, at different doses. In order to study iMSN activity, calcium imaging was performed using endoscopic fluorescence imaging.

iMSN activity was analyzed in two conditions:

1. During mouse movement in an open field arena, in order to investigate the involvement of iMSNs during action initiation and arrest.
2. During acute d-Amphetamine treatment at different doses, to analyze the effect of this psychostimulant drug on iMSN activity of a mouse freely moving in an open field.

Materials and methods

Animals

Animal care and housing

All animal procedures were performed according to the guidelines of the Animal Care Committee and approved by the Ethical Committee of the Pôle Santé of the Université Libre de Bruxelles. Mice were housed under standard conditions (12 hour dark-light cycle, lights OFF at 8a.m.; 22 ± 1°C ambient temperature; 40-55% relative humidity; food and water ad libitum). For behavioural experiments, male and female mice older than 3 months were used. Every effort was made to minimize the number of mice used and their suffering.

Mouse lines

During this project, two transgenic mouse lines were used and crossed either with C57Bl6 mice (Jackson lab) or between them to generate double transgenic mice. However, to avoid any genetic drifts, mouse colonies were refreshed twice a year with new commercial C57Bl6 breeders.

The transgenic mouse line used Cre-recombinase as transgene, which catalyzed the recombination at specific sites through Cre-Lox system. This system is based on the ability of Cre-recombinase to recognize short DNA sequences, called LoxP, and catalyze their homologous recombination.

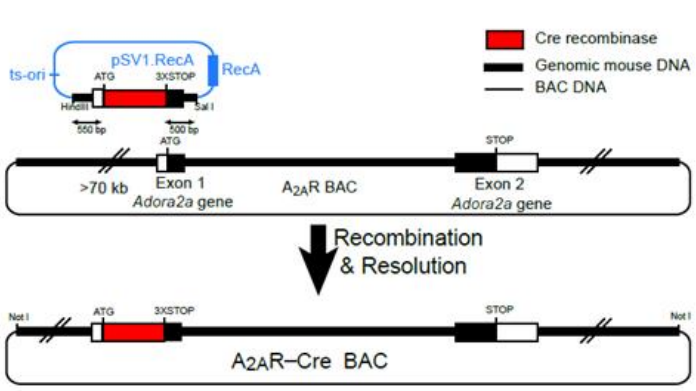

Figure 8. Expression of Cre recombinase in A2AR Cre Bac mice. A2AR-Cre BAC transgenic mouse line is created by targeting a BAC on Adora2a gene (adenosine A2A receptor (A2AR)) with Cre recombinase {Durieux, 2009 #328}.

In De Kerchove d'Exaerde laboratory the specific expression of Cre-recombinase in the striato-pallid neurons of A2Acre BAC mice was obtained by homologous recombination of bacterial artificial chromosome (BAC) and Cre-containing shuttle vectors (pSV1RecA), as shown in **Figure 8**. The resulted new A2AR-Cre BAC was microinjected in B6SJL7F1 zygote which was reimplanted into pseudogestant B6CBA/F1 mice (Durieux et al 2009). In detail, the shuttle vector pSV1RecA carries a temperature-sensitive origin of replication (ts-ori), a Cre-recombinase domain and RecA gene, which provide the enzymatic

machinery needed for the homologous recombination (Cox et al 2002). The A2A BAC was formed by exon 1 and exon 2 of Adora2A gene (adenosine A2AR). The Cre transgene was inserted at the level of the first Adora2A exon at the level of ATG by homologous recombination mediated by RecA protein. The A2AR-Cre BAC construct was isolated, microinjected and reimplanted into pseudogestant mice. Only neurons with A2AR had specific transcription factors allowing the expression of Cre-recombinase. The enzyme Cre-recombinase can target and splicing specifying sequences of DNA thought Cre-LoxP system. Cre protein catalyzes the recombination of DNA flanked by specific sites known as LoxP.

On the other hand, crossing Cre mice with LoxP-Stop-Loxp-GCaMP6s-Lox2272-Stop- Lox2272-Tta2 mice allowed the excision of the stop sequences and the expression of calcium indicator in neurons expressing Cre recombinase. In detail, Daigle and colleagues reported a large set of new transgenic mouse lines. In particular, a reported gene was dependent and cointegrated with Cre and tTA cassette into TIGRE locus. The TIGRE-Lox-Stop-Lox-GCaMP6s-CAG-Lox-Stop-Lox-tTA line was obtained by "Knock in" of the locus ubiquitous TIGRE genomics (Daigle et al 2018, Madisen et al 2015), the mice therefore expressing construction in all cells. This reported line expressing GCaMP6s in a Tet Off / Cre dependent manner was called Ai162(TIT2L-GC6s-ICL-tTA2) and generated at Allen Institute for Brain Science (Madisen et al 2015).

Genotyping procedure

The genotype of each animal was checked by PCR performed on DNA extracted from tail biopsies (about 2mm). Tissue was collected individually and digested by adding 100 µL of digestion Buffer A (below) and incubated at 95° C for 25 min. When the digestion was finished, Buffer B (below) was added to the mix. Subsequently, the solution was vortexed for 5 s and centrifuged at 13000 rpm for 10 min. 3 µL of supernatant from the DNA extraction and 22 µL of PCR solution was added to a PCR microtube.

Digestion Buffer A: 25 mM NaOH (Merck), 0.2 mM EDTA (Merck), pH 12
Digestion Buffer B: 40 mM TrisHCl (Merck), pH 5

PCR mix solution and conditions for each genotype:

Genotype	**PCR mix solution**						**PCR conditions**	
	Buffer 10x (Qiagen)	dNTPs 10mM (Invitrogen)	Taq	Primers 100 µM	H2O	DNA	Annealing temperature	Number of cycles
A2A-Cre	2.5 µL	0.5 µL	1 µL	2x0.125µL	17.75 µL	3 µL	60 °C	36
GCaMP6s	2.5 µL	0.5 µL	1 µL	1 µL	17 µL	3 µL	60 °C	36

Primers used for A2A-Cre genotype:

A2aEx1-301F: 5’ GCC-TGG-AGT-GAG-AAC-GAT-GTA-TCT-T 3’
Cre +50 R: 5’ TTT-TGG-TGT-ACG-GTC-AGT-AAA-TTG-G 3’
Gives an amplicon of 600 bp in the presence of the Cre allele.

Primers used for GCaMP6s genotype:

F: 5’ TAG-GGA-AGC-ACT-GGC-CAA-AGG-AA 3’
R: 5’ ATT-GGC-CGG-CCG-AAA-GAA-GTT 3’
N: 5’ CAT-CCC-AAA-GTT-AGG-TGT-TAT-GGC-AGT 3’
They give an amplicon of 505 bp in the presence of the GCaMP6s allele.

To visualize PCR results, each sample was loaded on a 2% agarose (Sigma) gel made with 1.3 µg/mL ethidium bromide (Sigma). The sample and the DNA ladder (Quickload 1kb Plus DNA Ladder, New England BioLabs, USA) were loaded into the tank filled with TAE buffer 1x solution. The system was run at 120 V for 40 min approximately. The presence of DNA bands was revealed with UV light lamp.

TAE buffer 1x solution: 40 mM Tris-acetate, 1 mM EDTA

Stereotaxic surgery

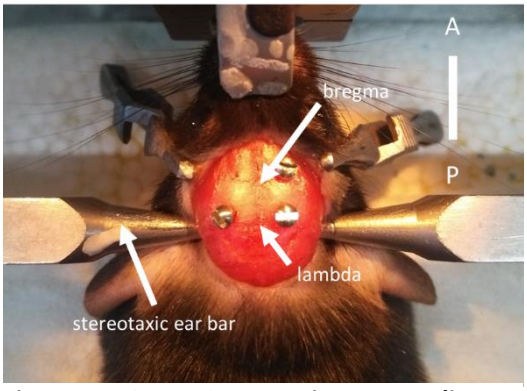

Figure 9. Stereotaxic coordinates. Representative image of skull sutures of deeply anesthetized mouse.

Microendoscope systems for imaging were precisely positioned by stereotaxic surgery. This technique allows targeting of the neuronal population in the brain area of interest. Brain structures were selected using Franklin and Paxinos mouse brain atlas (ed. 2008), which provided the coordinates of each area referring them to anatomical landmark of the skull sutures including bregma (β) and lambda (λ), as shown in **Figure 9**. Deep anesthesia was induced in the animals with avertin (1.25% 2,2,2- Tribromoethanol, Sigma; 0.78% 2-methyl-2-butanol, Sigma) 20 µL/gr and maintained with gaseous isoflurane (0.5L/min). Anesthetized animals were placed in the stereotaxic frame (KOPF Instruments).

Lens implantation

To perform *in vivo* calcium imaging, microendoscopes (Inscopix) were used, with different diameter and length (1 mm diameter, 4.1 mm length, 0.5 NA; 0.5 mm diameter, 6.1 mm length, 0.5 NA). The microendoscope is composed of two GRIN lenses attached onto either side of a lens and is designed

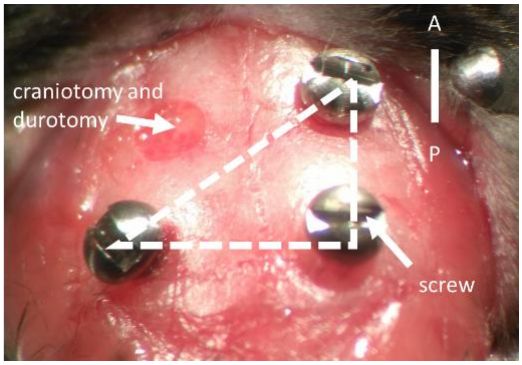

Figure 10. Craniotomy, durotomy and screw placement. Representative image of skull screw arrangement, craniotomy and durotomy of deeply anesthetized mouse.

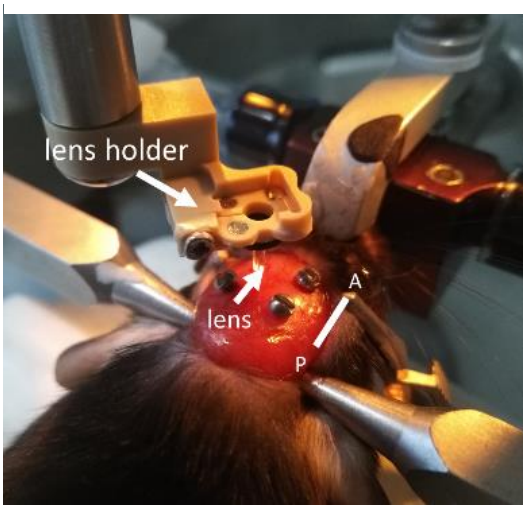

Figure 11. Lens placement at the beginning. Representative image of lens placement in a deeply anesthetized mouse.

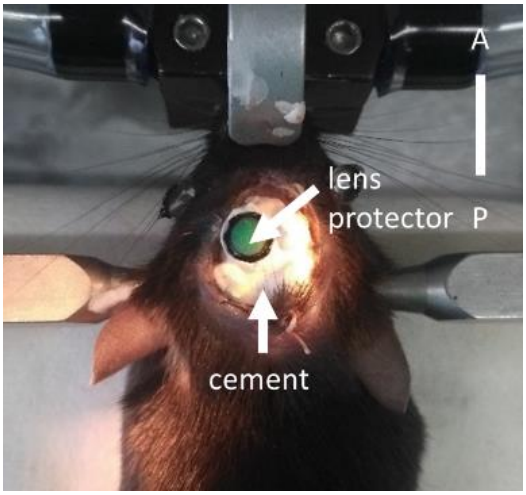

Figure 12. Lens placement at the end. Representative image of cement placement in a deeply anesthetized mouse.

to transmit light below the surface of the brain. Once the animal was anesthetized and fixed with the ear and mouth bars, the skull orientation was adjusted so that β and λ were aligned at the same height. Then, the fur was removed and the skull exposed through a small skin incision (1-2 cm), connective tissue was removed and cold saline was applied to the skull. In order to reduce movement noise artefacts during imaging sessions, three screws were attached to the skull. For maximum stability of the microendoscopic lens, each screw was placed in a triangle shape of around 0.5 cm side (**Figure 10**). Craniotomy and durotomy were performed by using a microdrill to the stereotaxic coordinates (AP 1.2 mm; ML 2.0 mm; DV - 2.8 mm) where the microendoscope was implanted. To facilitate the lens implantation neural tissue was expose and the remaining fragments of dura were removed by using a needle. To reduce tissue overheating the surface of tissue was constantly irrigated with cold saline. The lens was held by bulldog serrefine holder and attached to stereotaxic apparatus (**Figure 11**). The microendoscope was moved to the target coordinates and was lowered at constant velocity (0.5 µm/s). Once the lens reached the final position, metabond cement was applied (Super bond C&B kit). The screws allowed the cement to anchor the lens to the skull. The lens was protected from the dust and scratches by a small amount of silicone (Kwik-Cast) (**Figure 12**). When the cement was completely dried, the microendoscope was removed from the bulldog serrefine and the mouse was placed in a cage to recover on top of a heating pad until it was completely awake.

Baseplate attachment

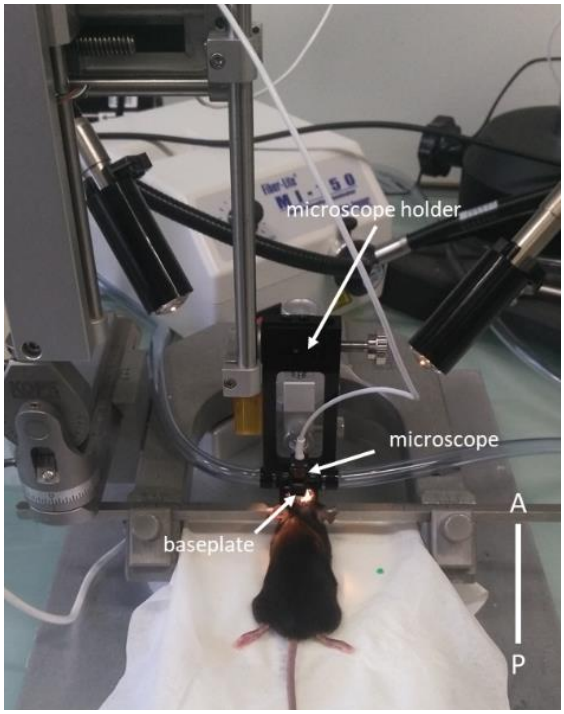

Figure 13. **Stereotaxic apparatus for baseplate attachment.** Representative image of stereotaxic setting for baseplate attachment in deeply anesthetized mouse.

One week after lens implantation, a baseplate (Inscopix) was attached. The miniature epifluorescence microscope (Inscopix) with the baseplate was placed into a holder gripper and attached into the stereotaxic frame. The miniaturized microscope was used to check calcium signals and to correctly place the baseplate, as shown in stereotaxic setting **Figure 13**. The microscope was connected to the acquisition computer by the data acquisition (DAQ) box. The mouse was anesthetized and placed into the stereotaxic frame and the dust Kwik-Cast cap was removed. The microscope objective with the baseplate was aligned over the lens (2mm above) and the focus was adjusted so that it was in the mid-range. The objects under the lens were visualized using the acquisition software. The baseplate was in a correct position when vasculature and fluorescence signals were into focus and fluorescence signals resembled calcium transient activity and neuron morphology. To avoid photodamage the intensity of the LED was set below 20% of its maximum power. The baseplate was attached by forming pillars with dental cement (**figure 14**) from each corner of the baseplate to the cement cap, made during lens implantation. When the pillars were completely dried, the remaining walls were built. After 15 min the microscope was removed and dislodged from the microscope gripper. The plastic dust cap was placed above the baseplate to protect the lens and it was locked with the set screw on the baseplate (**figure 15**). The mouse was placed in a cage on top of a heating pad until it was completely awake and recovered.

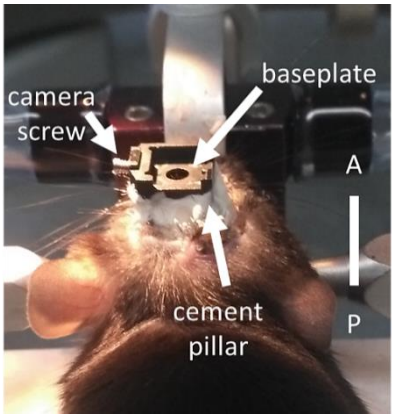

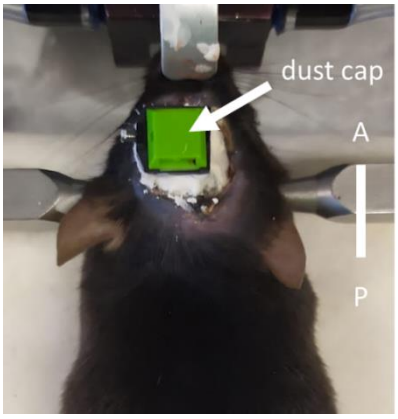

Figure 14 (on the left). Baseplate attachment. Representative image of baseplate attachment with cement pillars in deeply anesthetized mouse.

Figure 15 (on the right). **Baseplate dust protector.** Representative image of baseplate dust protector (green cap).

Behavioural test

All behavioural tests were performed in the animal house with inverted 12h dark-light cycle, lights OFF at 8a.m. in order to study the mice during their active phase.

Open field

Figure 16. **OFT.** Image of mouse during open field test connected with the miniaturized microscope.

The open field test (OFT) is a common test for exploratory behaviour and general activity in rodents, an example is represented in **Figure 16**. Many features of locomotor activity can be analyzed such as distance moved, time spent moving and at rest, rearing, grooming, freezing and other stereotypic behaviours. OFT can be used to assess general activity level as "control" and compare it to activity resulting by administration of stimulant compound (such as amphetamine). Generally, the open field (OF) is a square or rectangular arena where the animal can freely move. The first 10 min of the OFT can be considered as time spent for exploration and response to novelty, rather than baseline activity.

For these experiments a squared arena was used (40 cm x 40 cm x 40 cm). Mouse behaviour was recorded with an infrared video camera above the arena by a video tracking system at frequency of 40 Hz (Ethovision XT14, Noldus Information Technology). Behavioural recording was composed of 30 min baseline followed by 45 min post-injection. The injection was made i.p. and as quickly as possible.

Data analysis for locomotor acts

From behavioural data several parameters were extracted, including:

. The **position** in x and y of the body center, nose and tail into time bins of 0.025 s.
. The **distance moved,** that is the travelled distance by mouse center, nose or tail-base point between two samples. The total distance travelled was divided into time bins of 5 min.
. The mouse **area** and the change in mouse area between two samples.
. The body **elongation** calculates the mouse shape and is expressed in percentage, from 0% when the mouse shape is perfectly circular to 100% when the mouse shape is a line.
. Head **direction**, that is the angle formed by the head direction line of the current sample relative to a line parallel to the x axis in the coordinate system.

. The **speed,** that is obtained by dividing distance moved by the time difference between two samples.

In order to estimate whether calcium signals are correlated with movement, motion onsets and arrests needed to be determined with sub-second precision, which was not achievable with Ethovision's software. Therefore, Ethovision was used for movement speed, and a custom Python script was developed to determine **motion onsets and offsets** precisely. Onset of locomotion was identified by finding all movement bouts longer than 2 s that occur 2 s after the prior movement bout and offset of locomotion was identified by finding all movement bouts that preceded the next movement bout by more than 2 s. In more detail, locomotion speed traces were downsampled from 20 Hz frame rate to 5 Hz frame rate. According to the parameters reported in Parker and colleagues (2018) (Parker et al 2018), each 200 ms time bin was classified as one in which the mouse was either moving or not moving according to the downsampling speed trace. 0.5 cm/s was used as the threshold to separate moving state (≥0.5 cm/s) from non-moving state (<0.5cm/s). State changes of less than two bins were ignored.

An open source software, DeepLabCut (Mathis et al 2018), was applied to extract each body part position during all videos with a 0.025 s bin. This method gives a markerless pose estimation based on transfer learning with deep neural network. The output from DeepLabCut was further processed by SimBA, a software able to classify different mouse behaviours.

Calcium imaging

Data acquisition

One week after baseplate attachment the mouse was placed in the arena. The microscope was fixed onto the mouse head and connected to a rotatory joint, placed over the OF, following the mouse during its behaviour. The calcium images were sent to the computer recording program, which applied spatial downsample by a factor of four for efficient data processing. Through Inscopix software the exposure time was set to 50 ms, gain on 2, led power was 0.3% of the maximum allowed and the lens focus was adjusted in each animal. Simultaneously, the mouse behaviour is recorded with the infrared camera previously described (**Figure 17**).

To synchronize calcium imaging acquisition (nVista, Inscopix) in a millisecond-time resolution with behavioural video tracking, a transistor–transistor logic (TTL) synchronization was used. The TTL

pulse comes from the Sync port of the DAQ box and was used to trigger certain frames through the general-purpose input/output (GPIO) pins on the camera.

The integrated microscope is composed of an excitation light source (475 nm, 0.2-0.6 mW/mm^2), excitation filter, lenses for guiding and focusing light and a fluorescence sensor to detect emission light (535 nm). One-photon imaging of intracellular calcium activity was acquired at frequency of 20 Hz. To avoid photodamage, blue LED excitation and calcium recording started every 5 min and lasted 3 min.

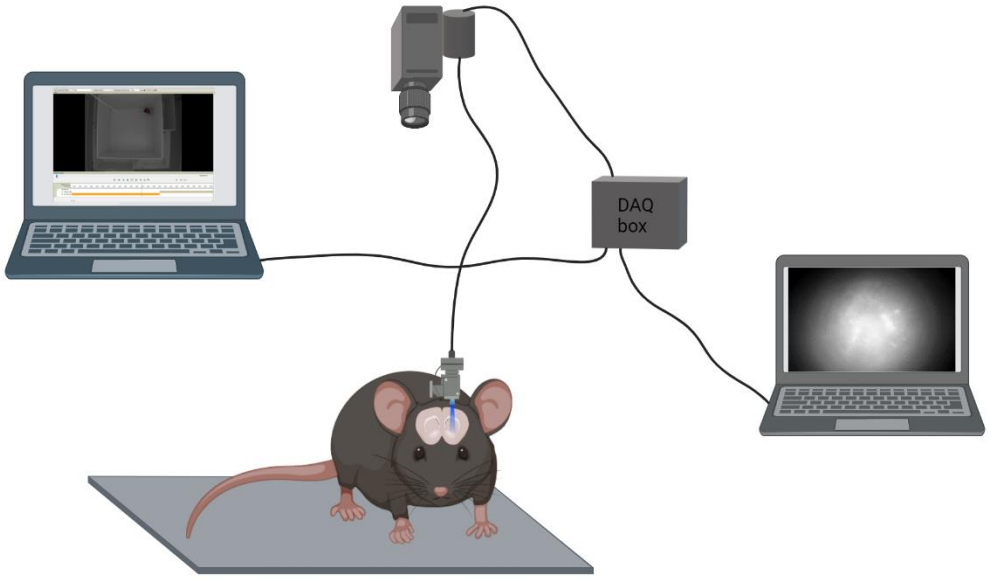

Figure 17. *In-vivo* recording system. Calcium imaging acquisition and behavioural acquisition were paired by using a data acquisition device box during open field test. Created with BioRender.com

Behavioural and calcium recording combined with pharmacology approach

In order to study the neuronal effects of amphetamine, mice were injected with d-Amphetamine at the dose of 1 mg/kg or 3 mg/kg intraperitoneally (i.p.). Drug was diluted in saline solution (NaCl 0.9%) and injected at the volume of 10 µL/g. For control condition, before the OFT started, mice were injected with saline solution (NaCl 0.9%), 10 µL/g.

Timeline for behavioural and *in vivo* calcium imaging

At least 1 week after baseplate attachment, mice were place in the arena. Although the microscope is extremely lightweight (2 g), some mice take time to get used to implant and initially have difficulties to explore the environment with the head mounted microscope. To avoid or reduce possible behavioural alterations, mice were habituated for 5 days to the arena and the apparatus carrying a dummy scope with similar properties as the microscope, except first and last day when the epifluorescence microscope was used in order to study the neuronal activity during the

habituation time. Each habituation day was composed of 30 min of baseline (without any injection) followed by 45 min after saline injection. 1 week after, the mouse was placed in the same arena and the experimental procedure was composed of 30 min of baseline (without any injection) followed by 45 min after d-Amphetamine 1mg/kg injection. 1 week later, the mouse was placed in the same arena and the recording procedure was composed of 30 min of baseline (without any injection) followed by 45 min after d-Amphetamine 3mg/kg injection.

Data Analysis for calcium imaging

The in vivo study of the neuronal population activity is a powerful instrument to understand neuronal function and its relations with behaviour. In order to achieve this purpose, new imaging techniques and development of genetic tools permit researchers to better investigate the complexity of brain function. However, development of new computational tools able to analyze a huge amount of data is also necessary. Calcium imaging data need automatic analysis to extract the relevant information from recorded videos. The pipeline of CaImAn identifies neurons in the imaged field of view and extracts their activity as peak of fluorescence (spikes) from the background fluorescence. To reach this goal, the pipeline goes through several steps:

. **motion correction**, where for each data frame the FOV are registered against a template, to correct the normal brain movements,
. **source extraction**, where neurons are identified and their signals are unmixed from each other and from the background signals,
. **deconvolution**, where the neuronal activity is identified as peak traces from fluctuation of signals for a specific neuron (Giovannucci et al 2019).

Calcium raw data were collected and processed by customized Python scripts. Due to the design of freely behaving *in vivo* calcium imaging experiments, the possible movement of neural tissue under the field of view was taken into consideration and corrected through motion-correction algorithm. The correction was made by comparing all video frames with the first one. Due to few consistent motion artefacts the first frame was chosen as reference, in order to avoid to introduce errors during motion correction. The second image processing was cropping of motion correction. Following movement correction, the frame series were cropped to avoid edge artefacts. In presence of large shift values the frame was cancelled.

CNMF-E (for further details see “Analysis of GECI imaging” paragraph) was applied as algorithm for source extraction and deconvolution of one photon microendoscopic data (Pnevmatikakis et al 2016, Zhou et al 2018). Single cell images and signal intensity fluorescence per frame were obtain

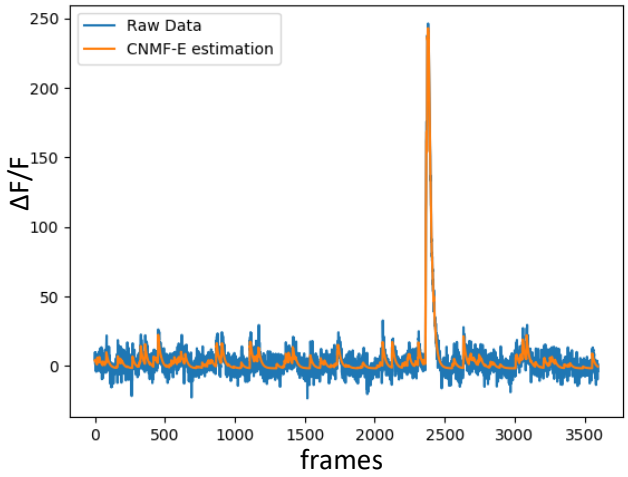

Figure 18. Example **of CNMF-E estimation** (orange peaks) and row data (blue peaks) plotted from our customized Python script.

applying several parameters for source extraction and deconvolution. These parameters were chosen to fit with the experimental design. As reported in the **Figure 18**, the software fits the calcium raw signal (blue line) as a series of Ca^{2+} spikes with exponential rise and decay kinetics, and provides as output only the fitted line, here represented in orange. CNMF-E fits a high amount of low peaks, that are in fact noise. For instance, reasonably, only a single calcium peak is present in this trace. We, therefore, used a custom Python script to perform our own peak detection on the traces. From CNMF-E results the signals extracted were filtered with high-pass filter determined by Nyquist theorem. In our case, the sampled signal had a frequency of 20 Hz and the signals accepted had a frequency higher than a cut-off frequency of 10 Hz. Peak CNMF-E outputs were further analyzed to identify the correct calcium traces avoiding the background noise, selecting only spikes with a signal higher than at least 4 standard deviation of the background noise and lasting at least a second.

From this processing of data 4 parameters were obtained:

. Number of **active cells** in each video
. Average spike **frequency**
. Average spike **amplitude** (ratio of signal peak to noise Root Mean Square (RMS))
. Average spike **duration**

To avoid photodamage, calcium imaging videos lasted 3 min and were followed by a 2 min period without recording. Thus, it was necessary to identify the same cell during different videos. A given cell was considered active when it had at least one spike. Spike frequency was calculated as the average of total spike frequency of the active cells. Spike amplitude was obtained from the average of total peak amplitudes per number of peaks. Spike duration was the average of total peak durations per number of peaks. In order to follow the same cell over multiple videos, a Python script was developed. The shape and position of each cell in each video were taken and it was checked if the cell had already appeared in a previous video or if it was new.

Behaviour and cell event rate correlation, data analysis

With the purpose of studying whether a given neuron had an activation time locked to motion onsets or offsets or if a given neuron responded after specific drug stimulation, the cell activity was related to movement. Calcium event rates were normalized to number of motion events for each mouse as a function of delay from motion onset and the iMSN activity around motion onset was analyzed. The same analysis was also applied to motion offset.

Histological analysis

Mice were deeply anesthetized using avertin and perfused transcardially with PBS 1x, followed by cold 4% paraformaldehyde (PFA) for tissue fixation. Brains were then removed and post-fixed overnight in 4% PFA at 4°C. 24 hours after tissue extraction PFA solution was change with PBS 1x and brains were cut by using a vibratome (Leica VT1000S). Coronal sections of 40 µm were cut and put into dissection solution (ice-cold PBS 1x). Slices containing the striatum were transferred into the multiwell plate with PBS 1x with sodium azide to prevent bacterial growth and stored at 4°C. After few days, slices were used for immunofluorescence staining.

PBS 1x, (1L): 8 g NaCl (VWR Chemicals), 0.2 g KCl (Merck), 1.78 g Na_2HPO_4 $2H_2O$ (Merck), 0.24g KH_2PO_4 (Merck), pH 7.4

Immunological staining

For immunofluorescence labelling, sections were rinsed in PBS 1x for 10 min and treated with Hoechst 4 µM in PBS-Triton 0.1% (Stock 100x Sigma) for 10 min. Slices were rinsed with PBS 1x for 10 min, two times and mounted on Superfrost slides (ROTH) with cover glass (VWR) using Glycergel Mounting Medium with 2.5%Dabco (DAKO) and stored at 4°C.

Image acquisition

Slices were visualized using Zeiss V16 zoom microscope with Apotome 2 equipped with a Hamamatsu Orca Flash 4.0 V2 camera. Images were taken with PlanNeoFluar Z 2.3x objective (variable total magnification) and automatically stitched by Zen blue.

Statistical analysis

The statistical analysis was performed by means of 1 or 2 way ANOVA, followed by Dunnett, Sidak post-hoc test for multiple comparisons, or paired t-test according to the experimental design and

factors compared. A p-value ≤0.05 was considered as a threshold for significant difference. In graphs, the following symbol code was used: * $p<0.05$, ** $p<0.01$, *** $p<0.001$ and **** $p<0.0001$. GraphPad Prism 7 was used for statistical calculations and graph representation.

Results

Locomotor effects of d-Amphetamine treatment

In order to investigate the activity of iMSNs during locomotor activity in control condition (saline injection) and under the effect of a psychostimulant drug, 9 A2A GCaMP6s mice were treated with different doses of d-Amphetamine (1 mg/kg and 3 mg/kg) or saline injection and tested in an open field.

Mice were tested at the OFT with saline injection for 5 days (habituation), and behaviour was recorded on day 1 (habituation day 1) and day 5 (habituation day 5). One week after habituation, mice were placed in the same arena and the OFT was performed with d-Amphetamine 1 mg/kg injection. One week later, the experiment was repeated with d-Amphetamine 3 mg/kg injection. The OFT session lasted 75 min. The mice were placed in an OFT arena and their behaviour recorded for 30 min (baseline or pre-injection period). At minute 30, the animals were injected i.p. with saline or d-Amphetamine and recorded for 45 min (post-injection period). **Figures 19**, **20** and **21** show the behavioural results during OFT. **Figure 19** shows the distance travelled in OFT with time bins of 5 min. Saline-treated mice progressively decreased locomotor activity in the first 45 min of day one of habituation period (black line). Acute d-Amphetamine at 3 mg/kg dose markedly increased locomotor activity reaching a plateau within 15 min after i.p. injection (orange line) (Repeated measure 2way ANOVA, Interaction $F(48, 448) = 13.75$, $p<0.0001$; Time $F(14, 448) = 6.095$, $p<0.0001$; Experiment type $F(3, 32) = 34.1$, $p< 0.0001$, Dunnett post-hoc test Vs. habituation day 1). **Figure 20** shows the mean speed during the post-injection period of the OFT, for each experimental condition. Acute d-Amphetamine at 3 mg/kg dose significantly increased speed (orange bar) compared to the habituation day 1 (black bar) (1way ANOVA, $F(3, 32) = 58.73$, $p<0.0001$, Dunnett post-hoc test Vs. habituation day 1). **Figure 21** shows the percentage of frames in which the animal was moving during the pre- and post-injection periods for each experimental condition. d-Amphetamine 1 mg/kg group significantly decreased ($p= 0.0001$) the time spent moving, whereas d-Amphetamine 3 mg/kg group had the same time spent moving as the control group (Paired t-test pre-injection Vs post-injection has been performed for each experiment type. Habituation day 1 $t=0.6019$, $df=8$; Habituation day 5 $t=0.2225$, $df=8$; d-Amphetamine 1 mg/kg $t=5.242$, $df=8$; d-Amphetamine 3 mg/k $t=0.6543$, $df=8$). Since d-Amphetamine 3 mg/kg group shows an increased distance travelled, this implies that these mice move faster.

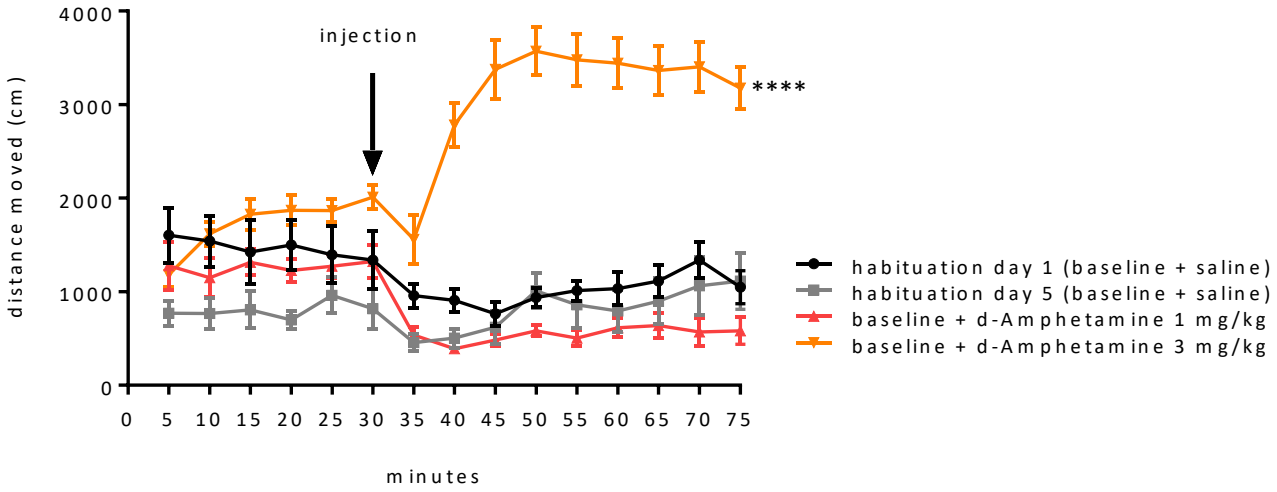

Figure 19. d-Amphetamine 3 mg/kg increases locomotor activity. Distance travelled (in cm) in the open field arena (y axis) per time bins of 5 min (x axis) for different treatments. Repeated measure 2way ANOVA (Time*Treatment) has been performed. Error bars represent SEM. ****p=0.0001.

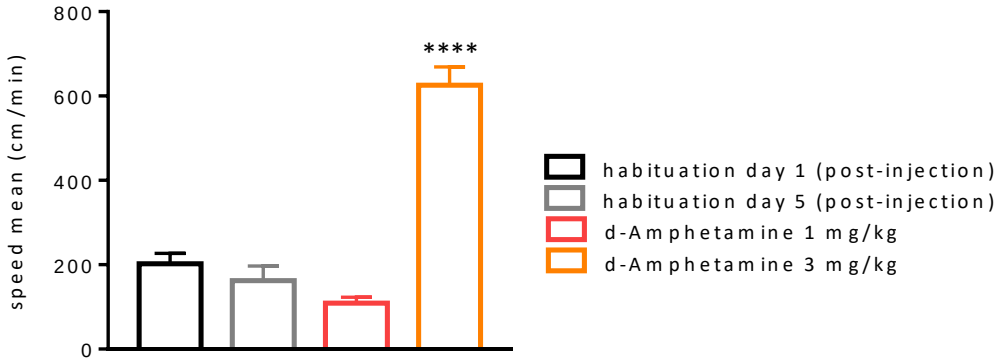

Figure 20. d-Amphetamine 3 mg/kg increases speed. Axis y represents the speed mean (cm/min) in the open field arena during the 45 min of the post-injection period for different treatment. 1way ANOVA has been performed. Error bars represent SEM. ****p=0.0001.

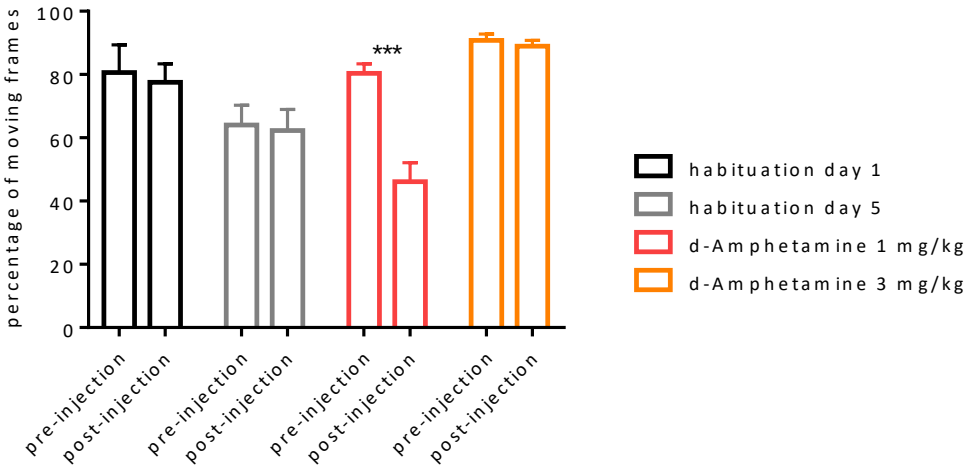

Figure 21. d-Amphetamine 3 mg/kg does not change time spent moving. Ratio between moving and non-moving frames in the different mouse group. Paired t-test has been performed, pre-injection vs post-injection for each experiment type. Error bars represent SEM. ***p=0.0001.

Analysis of iMSN cell activity during an open field test

22a

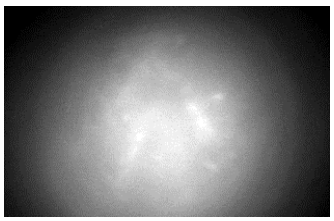

22b

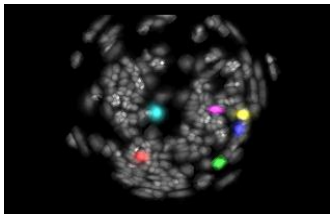

22c

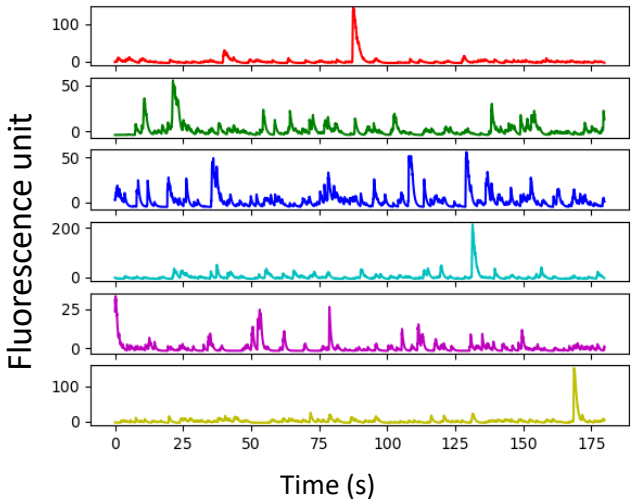

Figure 22. Calcium activities. Panel 22a. A representative image of raw data video. **Panel 22b.** Maximum intensity projection of optically detected cells. **Panel 22c.** Traces of cells outlined in the corresponding spatial map 22b.

The activation of iMSN population was studied in freely moving mice at the OFT. The images above (**Figure 22**) show representative examples of *in vivo* Ca^{2+} imaging data collected from striatum of mice, as they actively engage with their environment. **Panel 22a** reports an image of a representative video that shows raw data acquired from the camera. Neurons appear when their intracellular calcium concentration increases, causing GCaMP fluorescence to show up as brighter flashes over the background. CNMF-E allows to extract the positions, shapes and calcium signal intensity of iMSNs from the video. **Panel 22b** represents the maximum intensity projection of optically detected GCaMP6s expressing cells with the spatial shape and location. **Panel 22c** shows the activity traces (variation of fluorescent signal over time) of cells outlined in the corresponding spatial map (**Panel 22b**). These traces obtained with CNMF-E were used for the custom peak analysis described in the methods section.

iMSN peak analysis

The output from peak analysis is represented in **Table 1**, showing raw data of iMSN parameters:

. **average number of active cells**, takes into account all cells having at least one spike divided by the number of videos;
. **average spike frequency**, is the number of detected peaks divided by the number of active cells;
. **average spike amplitude,** is the sum of all peak amplitudes divided by the number of peaks;
. **average spike duration**, is the sum of peak widths divided by the number of peaks.

Each iMSN parameter was considered for each mouse and experimental condition, divided into pre-injection and post-injection periods. As reported in **Figure 23**, the statistical analysis (1way ANOVA, for each iMSN parameters. Cell number: Treatment F (3, 32) = 9.9, p<0.0001. Peak frequency: Treatment F (3, 32) = 4.571; p=0.0090; Peak amplitude: Treatment F (3, 32) = 2.339, p=0.0920; Duration: Treatment F (3, 32) = 21.56, p<0.0001. Dunnett post-hoc test Vs. habituation day 1) shows a significant decrease in the average number of active cells (p=0.0001) and of spike frequency (p=0.0056) and a significant increase in the average spike duration (p=0.0001) after d-Amphetamine 3 mg/kg injection (orange bars) with respect to habituation day 1. In addition, there was a significant decrease in the average number of active cells (p=0.041), peak frequency (p=0.017) and increase of peak duration (p=0.0049) after d-Amphetamine 1 mg/kg injection (red bars) with respect to habituation day 1.

average number of active cells								
mouse (date of birth) yy-mm-dd	**habituation day 1**		**habituation day 5**		**d-Amphetamine 1 mg/kg**		**d-Amphetamine 3 mg/kg**	
	pre-injection	post-injection	pre-injection	post-injection	pre-injection	post-injection	pre-injection	post-injection
mouse3 (19-02-21)	307.5±6.05	301.22±6.23	264.83±7.99	274.44±19.77	282.17±54.81	279.56±37.67	259.33±7.35	250.33±10.2
mouse4 (19-04-10)	89.5±8.29	102.11±8.56	77.83±7.96	74.5±6.13	85.67±4.59	61.78±5.38	48±3.76	18±1.52
mouse3 (19-07-18)	186.2±20.34	167.11±15.66	178.5±3.36	188.56±4.26	158.83±6.78	138.44±4.9	133.17±3.12	119.22±5.85
mouse1 (19-07-18)	228.17±4.57	209.89±9.32	199.17±5.36	204.11±8.07	196.17±6.63	160.11±7.9	185.83±6.36	90.78±2.22
mouse2 (19-04-10)	76.5±3.14	82.38±3.01	90.17±3.48	82.56±3.71	75.67±5.75	77.89±4.1	109.33±6.23	65.78±3.25
mouse9 (19-04-10)	216.5±4.82	231.33±7.82	185.17±3.84	211.11±4.6	163.17±5.29	131.67±4.98	225.33±6.36	157.89±4.37
mouse7 (19-04-10)	214.17±4.21	212±7.85	214.83±8.21	212.89±3.41	235.17±9.62	243.78±8.23	257±12.26	232.44±4.44
mouse2 (19-05-22)	310.5±27.38	383.11±10.8	371.5±10.59	299.22±14.64	354.33±24.35	304.78±17.06	343.67±5.58	266.44±4.48
mouse3 (19-05-22)	80.83±1.94	86.22±1.86	117.67±4.18	112.33±2.93	151.67±6.12	103.89±6.6	170.83±4.21	116.67±2.87
average peak frequency (Hz)								
mouse (date of birth) yy-mm-dd	**habituation day 1**		**habituation day 5**		**d-Amphetamine 1 mg/kg**		**d-Amphetamine 3 mg/kg**	
	pre-injection	post-injection	pre-injection	post-injection	pre-injection	post-injection	pre-injection	post-injection
mouse3 (19-02-21)	0.02±0.00084	0.02±0.00084	0.02±0.0013	0.02±0.00169	0.02±0.00109	0.02±0.00078	0.03±0.00078	0.02±0.00051
mouse4 (19-04-10)	0.01±0.0006	0.01±0.00104	0.01±0.0003	0.01±0.00056	0.01±0.0006	0.01±0.00054	0.01±0.0004	0.01±0.00069
mouse3 (19-07-18)	0.01±0.0016	0.02±0.00051	0.02±0.0006	0.02±0.00067	0.02±0.0005	0.02±0.0004	0.02±0.0004	0.02±0.00048
mouse1 (19-07-18)	0.02±0.0007	0.02±0.00163	0.02±0.0003	0.02±0.00048	0.02±0.0003	0.02±0.00036	0.02±0.0008	0.02±0.00056
mouse2 (19-04-10)	0.02±0.0006	0.02±0.00045	0.02±0.001	0.02±0.00091	0.01±0.0005	0.01±0.00045	0.02±0.0003	0.01±0.00053
mouse9 (19-04-10)	0.02±0.0008	0.02±0.00063	0.02±0.0005	0.02±0.00078	0.02±0.0007	0.01±0.00045	0.02±0.0004	0.02±0.00036
mouse7 (19-04-10)	0.03±0.0004	0.03±0.00068	0.02±0.0007	0.02±0.00053	0.02±0.0003	0.02±0.00055	0.02±0.0004	0.02±0.00032
mouse2 (19-05-22)	0.02±0.0005	0.02±0.00063	0.02±0.0012	0.02±0.00068	0.02±0.0012	0.02±0.00058	0.02±0.0004	0.02±0.00033
mouse3 (19-05-22)	0.02±0.0008	0.02±0.00052	0.02±0.0014	0.02±0.00033	0.02±0.0009	0.01±0.0006	0.02±0.0007	0.02±0.00039
average peak amplitude								
mouse (date of birth) yy-mm-dd	**habituation day 1**		**habituation day 5**		**d-Amphetamine 1 mg/kg**		**d-Amphetamine 3 mg/kg**	
	pre-injection	post-injection	pre-injection	post-injection	pre-injection	post-injection	pre-injection	post-injection
mouse3 (19-02-21)	254.07±3.85	228.62±2.23	323.54±27.46	248.9±6.07	113.93±1.16	109.34±0.88	97.57±0.76	99.5±0.98
mouse4 (19-04-10)	129.34±5.03	118.63±2.23	89.33±1.25	88.01±1.33	47.13±0.82	46.01±1.15	48.17±1.4	40.12±0.95
mouse3 (19-07-18)	100.7±2.07	105.72±2.34	90.54±1.02	89.12±0.84	45.86±0.52	45.98±0.46	74.59±1	96.82±1.34
mouse1 (19-07-18)	115.03±1.1	114.17±0.92	109.35±1.15	103.39±0.87	53.15±0.49	52.67±0.47	89.64±0.92	68.75±0.71

mouse2 (19-04-10)	102.8±1.74	97.99±1.34	85.35±1.36	84.46±1.15	103.4±1.91	100.38±1.53	88.61±1.18	94.08±1.68
mouse9 (19-04-10)	113.9±1.02	105.79±0.83	107.91±1.09	96.77±0.75	134.54±1.37	132.6±1.5	114.04±1.09	113.2±1.13
mouse7 (19-04-10)	142.72±1.36	128.52±1	134.93±1.4	85.38±0.59	126.82±1.25	122.77±0.94	126.45±1.16	137.32±1.13
mouse2 (19-05-22)	138.56±1.19	125.2±0.76	125.96±0.83	90.77±0.51	119.65±0.74	113.8±0.7	106.73±0.64	107.66±0.64
mouse3 (19-05-22)	112.72±1.5	104.7±1.1	108.19±1.17	99.99±1.04	121.09±1.27	114.51±1.69	125.38±1.16	112.25±1.19
average peak duration (s)								
mouse (date of birth) yy-mm-dd	**habituation day 1**		**habituation day 5**		**d-Amphetamine 1 mg/kg**		**d-Amphetamine 3 mg/kg**	
	pre-injection	post-injection	pre-injection	post-injection	pre-injection	post-injection	pre-injection	post-injection
mouse3 (19-02-21)	1.15±0.005	1.17±0.005	1.12±0.006	1.15±0.005	1.15±0.006	1.19±0.005	1.13±0.005	1.3±0.005
mouse4 (19-04-10)	1.11±0.015	0.96±0.011	1.17±0.013	1.11±0.013	1.04±0.015	1.19±0.014	1.19±0.018	1.53±0.024
mouse3 (19-07-18)	1.07±0.013	1.09±0.009	1.2±0.008	1.19±0.007	1.2±0.009	1.23±0.008	1.21±0.01	1.3±0.009
mouse1 (19-07-18)	1.13±0.007	1.07±0.006	1.11±0.008	1.11±0.006	1.14±0.007	1.24±0.007	1.21±0.007	1.55±0.01
mouse2 (19-04-10)	1.17±0.01	1.18±0.008	1.19±0.01	1.24±0.008	1.1±0.01	1.14±0.009	1.13±0.008	1.41±0.015
mouse9 (19-04-10)	1.14±0.006	1.16±0.006	1.14±0.007	1.11±0.005	1.16±0.008	1.1±0.008	1.13±0.006	1.29±0.008
mouse7 (19-04-10)	1.16±0.006	1.14±0.005	1.1±0.006	1.17±0.005	1.11±0.006	1.26±0.005	1.13±0.005	1.34±0.006
mouse2 (19-05-22)	1.07±0.005	1.04±0.004	1.06±0.004	1.09±0.004	1.09±0.004	1.14±0.004	1.1±0.004	1.25±0.005
mouse3 (19-05-22)	1.16±0.01	1.13±0.007	1.15±0.008	1.14±0.007	1.14±0.007	1.36±0.01	1.13±0.006	1.32±0.008

Table 1. iMSN parameters. The table reports the raw data from CNMF-E and customized python peak analysis divided between peak parameters (average number of active cells, average peak frequency, average peak amplitude and average peak duration), different mouse and different experimental condition (habituation day 1, habituation day 5, d-Amphetamine 1 mg/kg and d-Amphetamine 3 mg/kg). Each experimental condition is divided into pre- and post-injection periods), ± SEM.

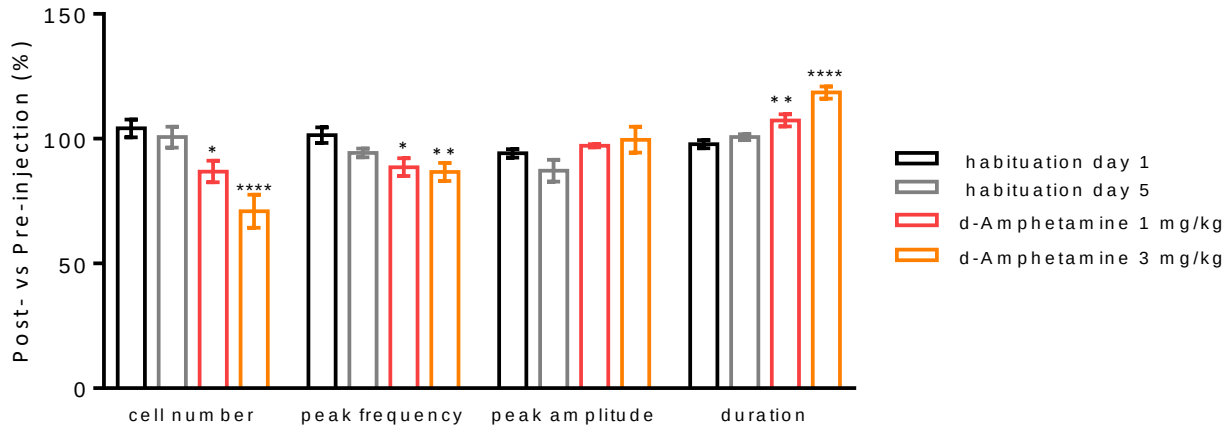

Figure 23 d-Amphetamine-elicited changes in global iMSN parameters. Post-injection values are normalized to pre-injection values (y axis) for each parameter and experimental condition. 2way ANOVA has been performed. Error bars represent SEM. * p<0.05, ** p<0.01, ****p=0.0001.

Analysis of longitudinal cell activity in relation to d-Amphetamine

Each iMSN position and shape was extracted in order to investigate the same iMSN over multiple videos, allowing to identify if a specific cell had already appeared or if it were new. These results allowed to study the longitudinal activity of each iMSN over the different videos; for instance, one neuron could be activated or increase its activity after a specific treatment or only when the mouse was moving or non-moving.

Figure 24 reports an example of cell longitudinal tracking from one mouse during d-Amphetamine 3 mg/kg experiment. Each image shows the maximum fluorescence intensity projection of each cell appeared during the 3 min videos from the beginning of the OFT till the end. During the 75 min of the experiment, calcium imaging videos lasted 3 min and were followed by a 2 min period without recording to avoid tissue photodamage, thus 15 images were taken from 15 videos from each experimental condition and labelled with a sequential order. In the experiment reported in **Figure 24**, 474 iMSNs were visible in total, and 294 were active in the first video of the series. iMSNs that appear for the first time are shown in magenta, while iMSNs that have already appeared in any previous video are shown in green.

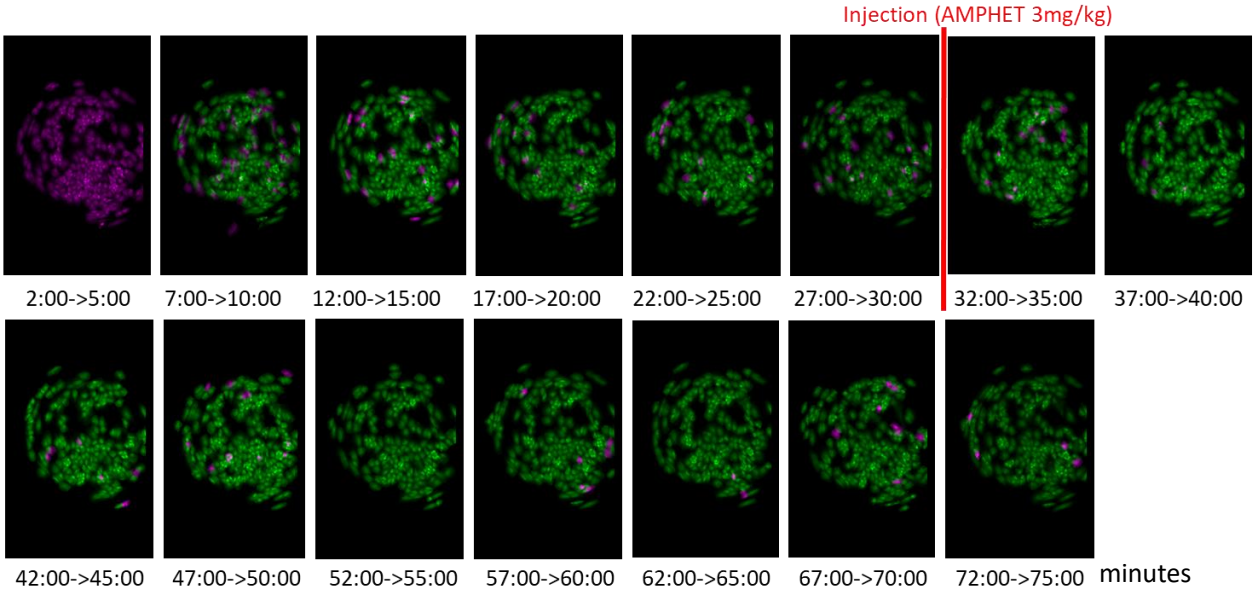

Figure 24. Longitudinal tracking. The images are an example of cell longitudinal tracking taken from one mouse of the d-Amphetamine 3 mg/kg group. The images show maximum intensity projection of active iMSNs (cells that have at least one spike during the experimental session) during baseline (30 min) followed by d-Amphetamine 3 mg/kg injection (45 min) divided into 3 min videos. Injection time is indicated with red vertical line. iMSNs making their first appearance are shown in magenta, whereas cells already appeared in any of the previous videos are shown in green. The 3 min time interval recorded by the video is reported below each image.

Figure 25 shows the proportion of cells making their first appearance in a given video with respect to the cumulative number of cells from any of the previous videos. Roughly the same pattern of new

appearances occurs after all the treatments, without statistical differences between treatments (Repeated measures 2way ANOVA, Videos F (14, 112) = 360.9, p<0.0001; Treatment F (4, 32) = 1.194, p=0.3322; Videos*Treatment F (56, 448) = 0.9979, p=0.4835).

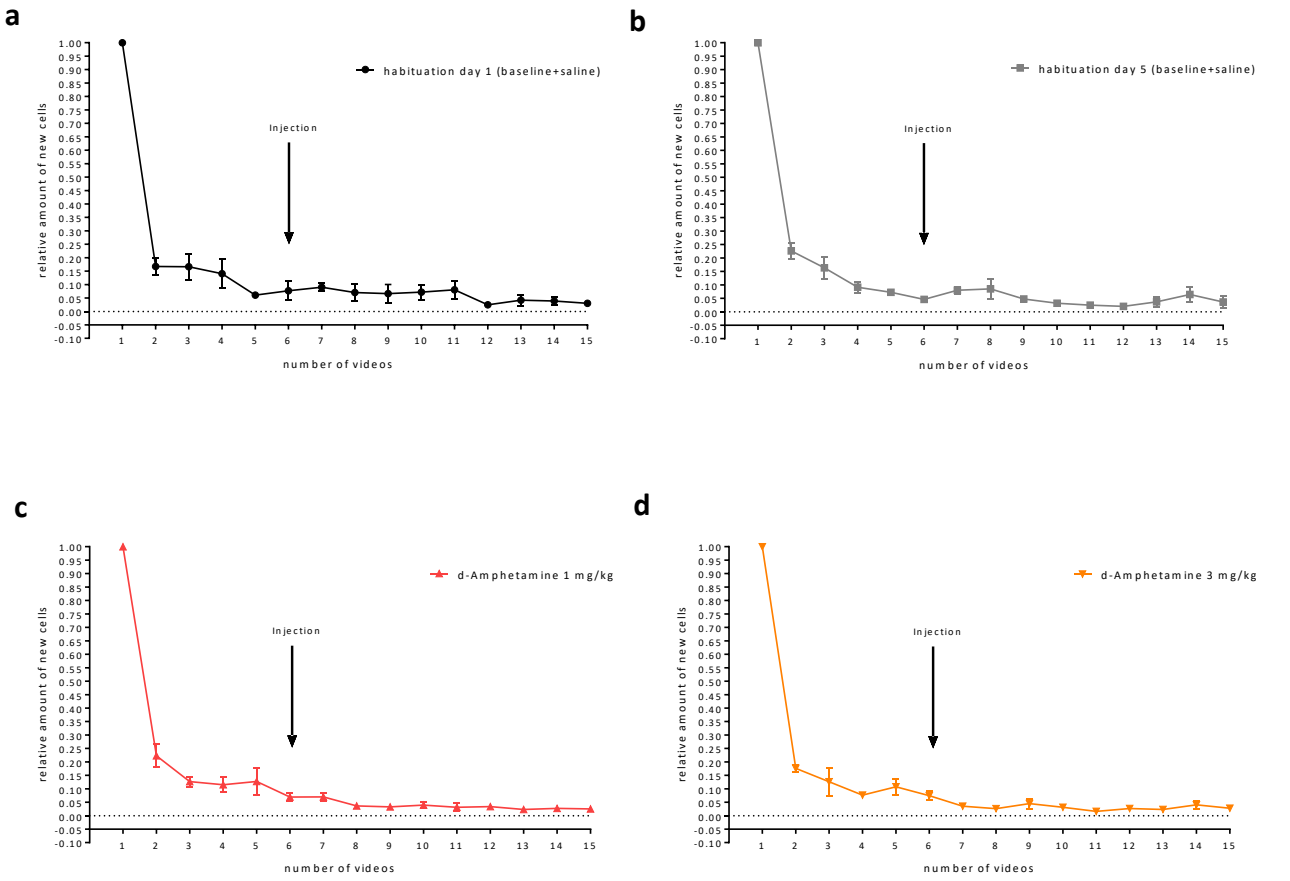

Figure 25. Same pattern of new cell appearance in all treatment groups. Each panel shows the portion of cells making their first appearance in a video with respect to the cumulative number of cells from any of the previous videos. On the x axis the number of the 3 min videos of the experiment is indicated. On the y axis the relative amount of new cells is reported. Panels **a-d** report the data from habituation day 1, habituation day 5, d-Amphetamine 1 mg/kg and d-Amphetamine 3 mg/kg groups, respectively. Arrows indicate the injection time. 2way ANOVA has been performed. Error bars represent the SEM.

Detection of motion events

Due to iMSN kinetics, accurate detection of each motion event with the required sub-second precision is necessary to correlate them with calcium traces. We examined Ethovision results by applying several parameters and we realized the impossibility to detect motion onset and offset with precision. To solve this problem, we decided to use Ethovision only to extract mouse velocity, while we developed a custom Python script in accordance to Parker's parameters (Parker et al 2018) to precisely detect motion events (onsets and offsets). Implementing this new work flow, we were able to pair Ca^{2+} spikes and movement events of each mouse. The next step, that is still ongoing, will be to pair specific behaviours (such as grooming, rearing, jumping) to Ca^{2+} events. Automatically classifying behaviour is fundamental to reach this goal. Therefore, we applied a method for markerless pose estimation based on transfer learning with deep neural networks using an open source software called DeepLabCut . By doing so, we were able to successfully extract each body part position during all videos with a 0.025 s bins as shown as example in **Figure 26.**

Figure 26. Example of qualitative DeepLabCut pose estimation.

Once we extracted all body part coordinates, these data were imported to another software in order to estimate different behavioural events. Using SimBA, a software able to create supervised machine learning predictive classifiers of mouse behaviours (for example grooming or rearing, as shown in **Figure 27**), we tried to extract mouse behaviours and pair them with Ca^{2+} events. However, the behavioural classification did not meet the required set goals, probably due to some limitation of the video features (an insufficient resolution), as the algorithm was not able to predict, with precision, the different behaviours. Further test of these procedures is ongoing.

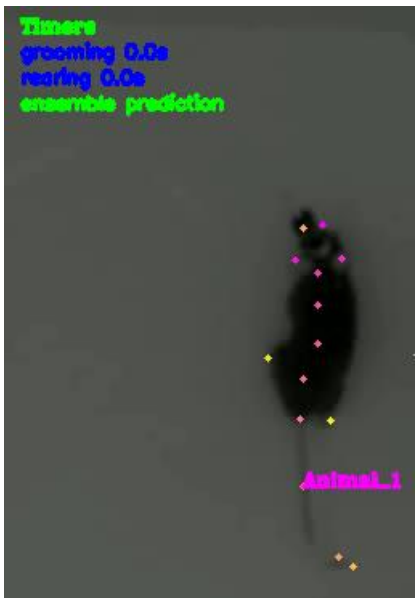

Figure 27. Example of SimBA behaviour estimation.

Analysis of longitudinal cell activity in relation to movement

iMSN activity was analyzed in relation to movement. **Figure 28** reports the average number of iMSN spikes as a function of delay from motion onset (green vertical line) or offset (red vertical line) for the different experimental conditions. A qualitative analysis of **Figure 28** shows that iMSN activity rises around 0.5-0.3 s before the motion onset and falls around 0.5 s before the motion offset, suggesting that increased firing of iMSNs contributes to the encoding of locomotion. A quantitative analysis shows a significant difference between the mean of all cell spike before and after the motion event (onset and offset). 2way ANOVA has been performed, mean of cell spikes before Vs after motion onset and mean of cell spikes before Vs after motion offset (Repeated measure 2way ANOVA, delay to onset F (1, 8) = 21.07, p=0.0018; Treatment F (4, 32) = 1.732, p=0.1672; Delay to onset*Treatment F (4, 32) = 2.174, p=0.0943. Sidak post-hoc test has been performed: mean of cell spikes before Vs after motion onset). In all pre-injection condition p<0.0001, post-injection habituation day 1 p=0.0057, post-injection habituation day 5 p<0.0001, post-injection d-Amphetamine 1 mg/kg p<0.0001, post-injection d-Amphetamine 3 mg/kg p<0.0001. Repeated measure 2way ANOVA, delay to offset F (1, 8) = 24.76, p=0.0011; Treatment F (4, 32) = 1.219, p=0.3223; Delay to onset*Treatment F (4, 32) = 2.142, p=0.0983. Sidak post-hoc test has been performed: mean of cell spikes before Vs after motion offset. In all pre-injection condition p<0.0001, post-injection habituation day 1 p=0.0939, post-injection habituation day 5 p=0.0012, post-injection d-Amphetamine 1 mg/kg p<0.0001, post-injection d-Amphetamine 3 mg/kg p=0.0022.

a

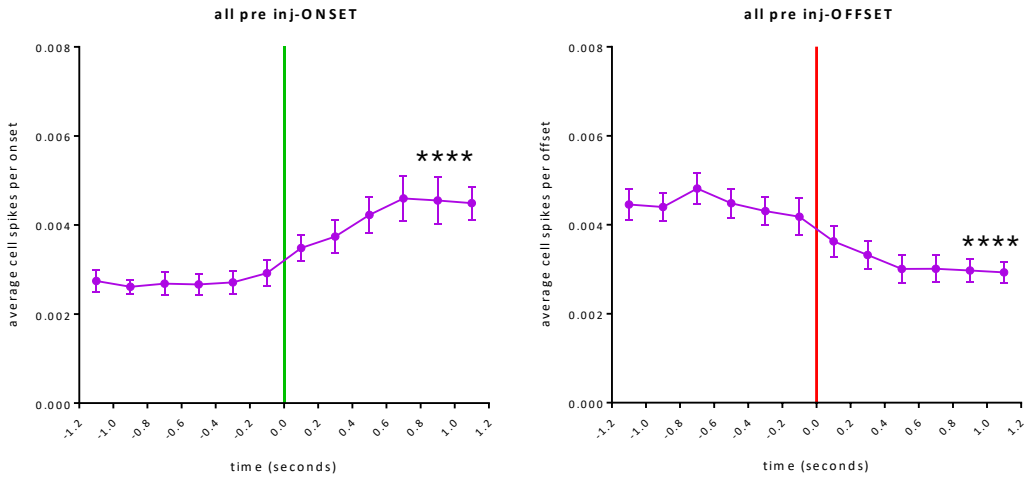

b

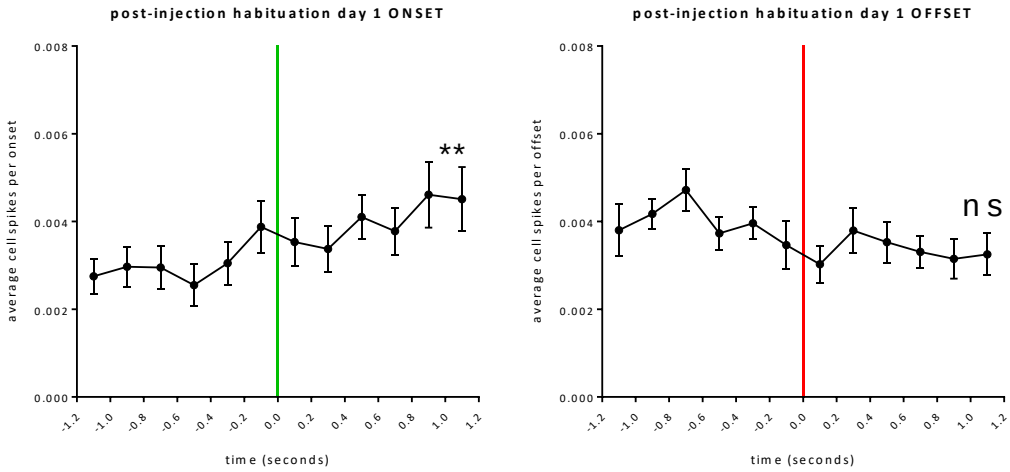
post-injection habituation day 1 ONSET
post-injection habituation day 1 OFFSET
average cell spikes per onset
average cell spikes per offset
time (seconds)
**
n s

c

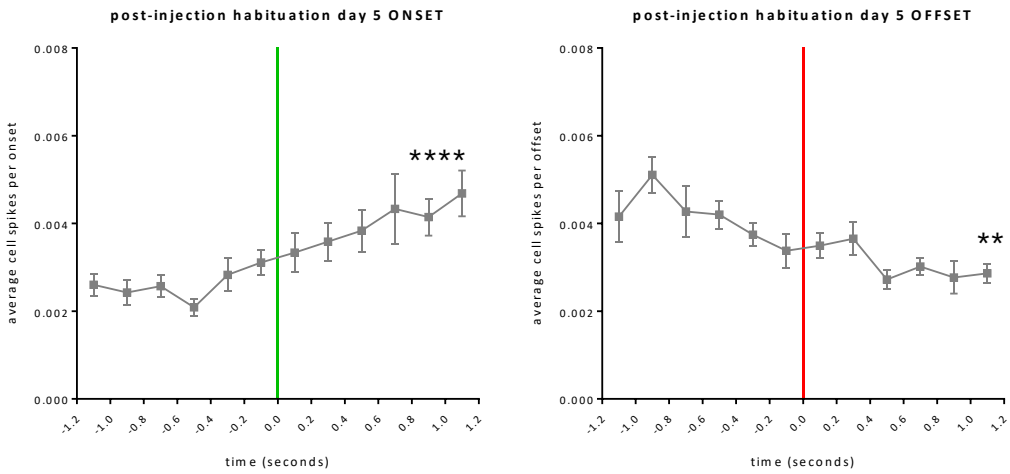
post-injection habituation day 5 ONSET
post-injection habituation day 5 OFFSET
average cell spikes per onset
average cell spikes per offset
time (seconds)
****
**

d

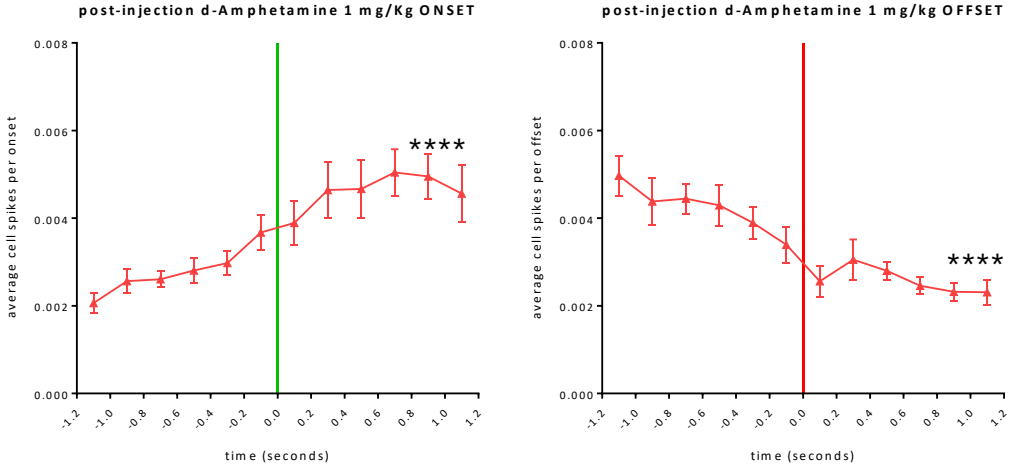
post-injection d-Amphetamine 1 mg/Kg ONSET
post-injection d-Amphetamine 1 mg/kg OFFSET
average cell spikes per onset
average cell spikes per offset
time (seconds)
****
****

e

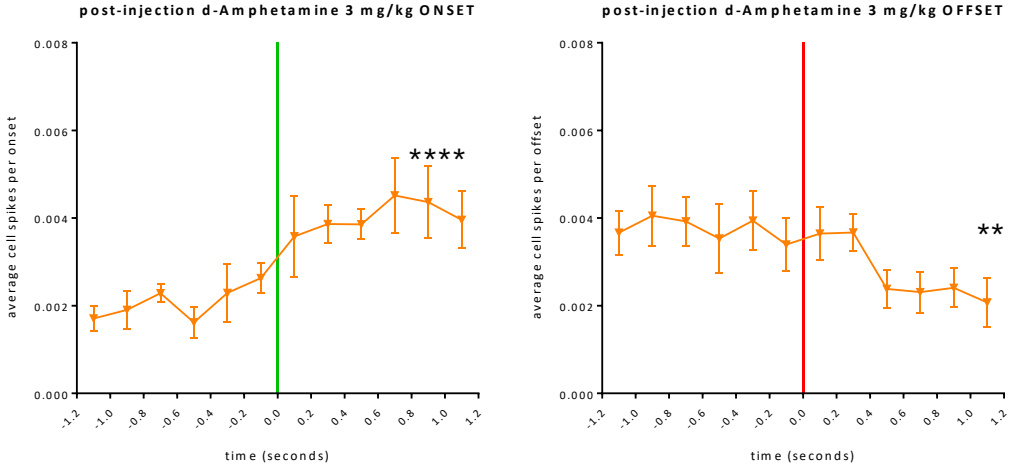
post-injection d-Amphetamine 3 mg/kg ONSET
post-injection d-Amphetamine 3 mg/kg OFFSET
average cell spikes per onset
average cell spikes per offset
time (seconds)
****
**

Figure 28. iMSNs encode movement. Each panel shows the average cell spikes as a function of delay from motion onset (vertical green line, left image) or offset (vertical red line, right image). Y axes represent the average spike number divided per total number of cells and per number of onset or offset, while x axes represent time around motion event (onset or offset, respectively). Panel **a** reports the data from pre-injection periods of all treatments, whereas panels **b-e** report the data from post-injection periods from habituation day 1, habituation day 5, d-Amphetamine 1 mg/kg and d-Amphetamine 3 mg/kg, respectively. 2way ANOVA has been performed, mean of cell spikes before vs after motion onset and mean of cell spikes before vs after motion offset. Error bars represent SEM. ** p<0.01, ****p<0.0001

We first determined whether the different treatments were associated with a change in the baseline spike frequency expressed as average number of spikes/200 ms bin in 4 baseline bins preceding motion event (**Figure 29**). The statistical analysis showed a significant reduction in the baseline number of spikes/200 ms in the d-Amphetamine 3 mg/kg group with respect to any other treatment group (Repeated measures ANOVA, Treatments: F (1,7) = 4.209, p=0.018, followed by paired sample t test, d-Amphetamine 3 mg/kg Vs. habituated day 1: t= 2.524, p=0.040, Vs. habituated day 5: t= 3.978, p=0.005, Vs. d-Amphetamine 1 mg/kg: t= 3.163, p=0.016).

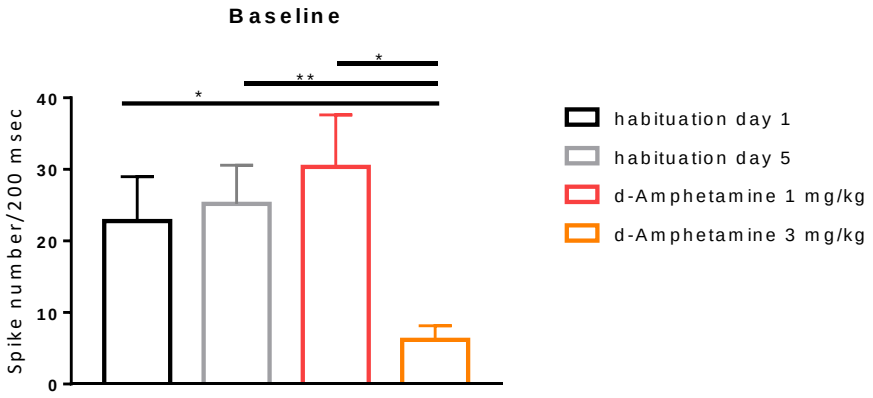

Figure 29. d-Amphetamine treatment change baseline spike frequency. Baseline spike frequency is expressed as average number of spikes/200 ms time bin in 4 baseline bins preceding motion event. Repeated measures ANOVA followed by paired samples t-test has been performed. Error bars represent SEM. * p<0.05, **p<0.01.

Then, in order to compare the time-course of the changes in spike number/time for the different treatments the data were normalized to the baseline and expressed as percent of the average number of spikes/200 ms bin in 4 baseline bins preceding motion event (**Figure 30a**). The statistical analysis showed that normalized spike frequency changes related to motion onset were not significantly different between treatment groups (Repeated measures ANOVA, Time: F (11,28) = 16.182, p<0.001, Treatment: F (3,28) = 1.796, p=0.171, Time*Treatment: F (33,28) = 1.249, p=0.170). However, d-Amphetamine 3 mg/kg induced a significant increase (p=0.014) in the normalized peak number of spikes/200 ms bin after motion onset (1way ANOVA F (3,28) = 4.041, p=0.017, post-hoc Dunnett test, d-Amphetamine 3 mg/kg Vs. habituation day 1) (**Figure 31**). On the other hand, the same analysis carried out on normalized spike frequencies related to motion offset showed a significant difference of amphetamine 3 mg/kg treatment with respect to habituation day 1 group

(p=0.027) (Repeated measures ANOVA, Time: F (11,28) = 11.372, p< 0.001, Treatment: F (3,28) = 3.179, p=0.039, Time*Treatment: F (33,28) = 1.256, p=0.165, Dunnett post-hoc test, Amphetamine 3 mg/kg Vs. Habituation day 1) (**Figure 30b**).

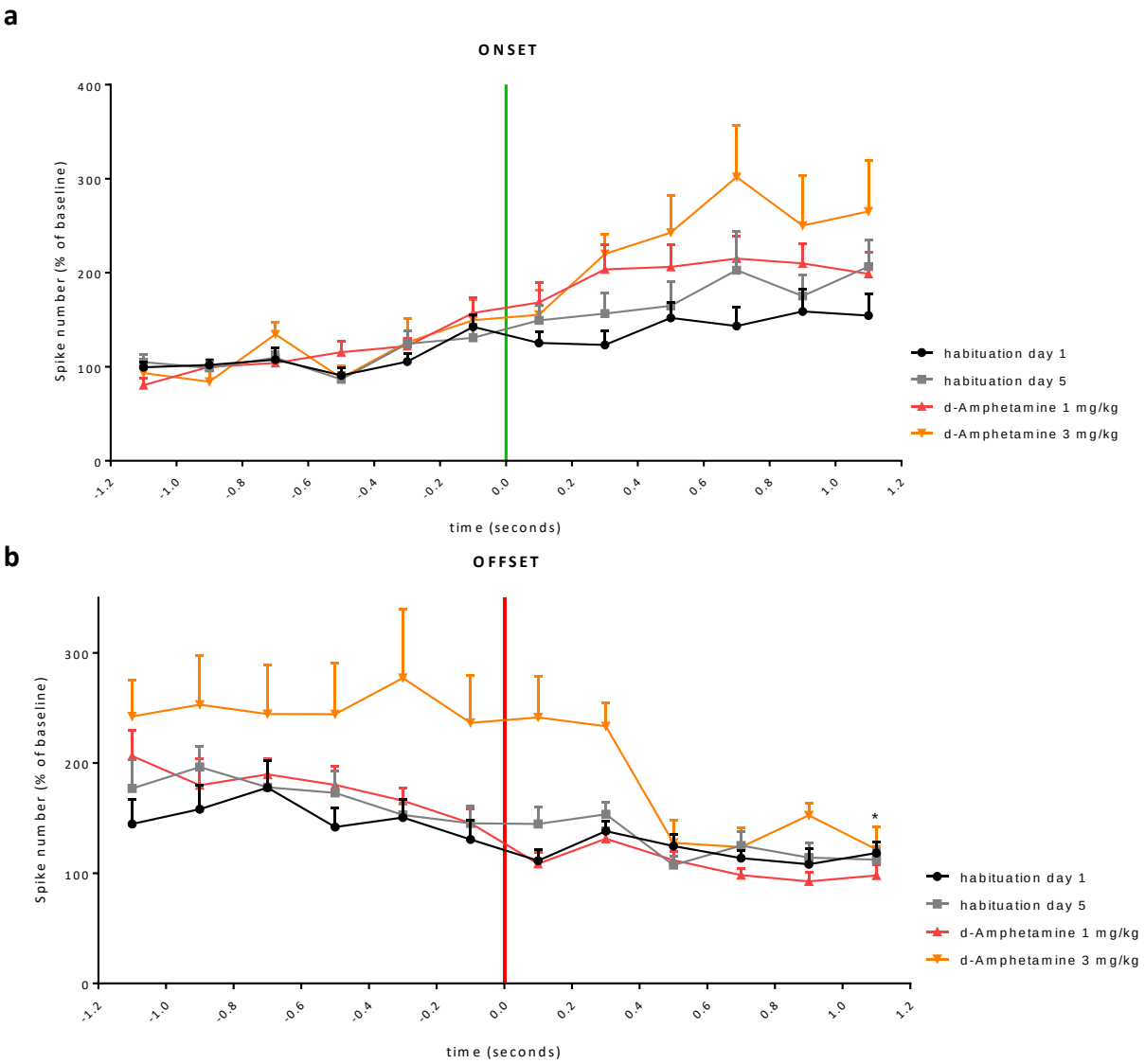

Figure 30. The normalized peak number of spikes/200 ms bin after motion onset does not change between treatment. Data were normalized to the baseline and expressed as percent of the average number of spikes/200 ms bin in 4 baseline bins preceding motion event (onset in Figure 30a and offset in Figure 30b). Repeated measure ANOVA has been performed. Error bars represent SEM.

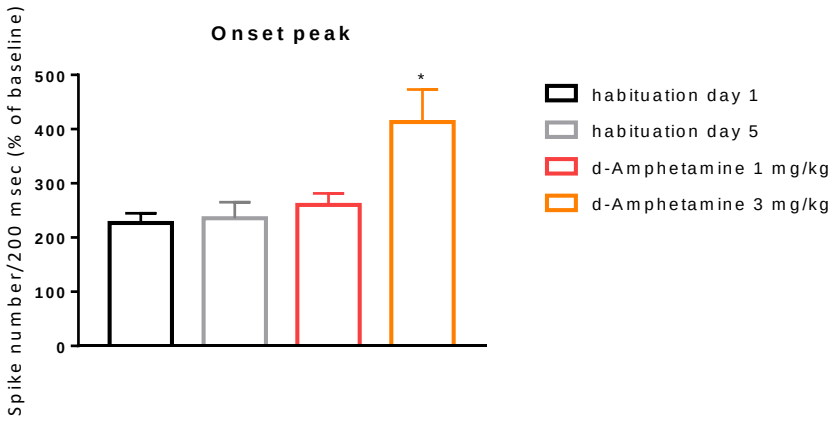

Figure 31. D-Amphetamine 3 mg/kg induced a significant increase in the normalized peak number of spikes/200 ms bin after motion onset. Data were normalized to the baseline and expressed as percent of the average number of spikes/200 ms bin in 4 baseline bins preceding motion onset. 1way ANOVA has been performed. Error bars represent SEM. * p<0.05 Vs habituation day 1.

To further analyze the relation of spike frequency changes and motion events, we performed an analysis of the normalized curves of the different groups using a 4-parameter logistic function. While the time to reach 50% of the upper plateau during motion onset was not significantly different between the different treatments, as reported in **Figure 32** (1way ANOVA, F (3,27) = 0.175, p=0.913) and was around 0.1 to 0.3 s before motion onset, the time to decrease from upper plateau to 50% of its value was significantly retarded in d-Amphetamine 3 mg/kg treatment with respect to habituation day 1 (p=0.009) (1way ANOVA, F (3,28) = 5.421, p=0.005, post-hoc Sidak test d-Amphetamine 3 mg/kg Vs. habituation day 1: p=0.011, Vs. habituation day 5: p=0.017, Vs. d-Amphetamine 1 mg/kg: p=0.052), and was around 0.7 s after motion offset in d-Amphetamine 3 mg/kg treatment and around 0 to 0.25 s before motion offset in all the other groups.

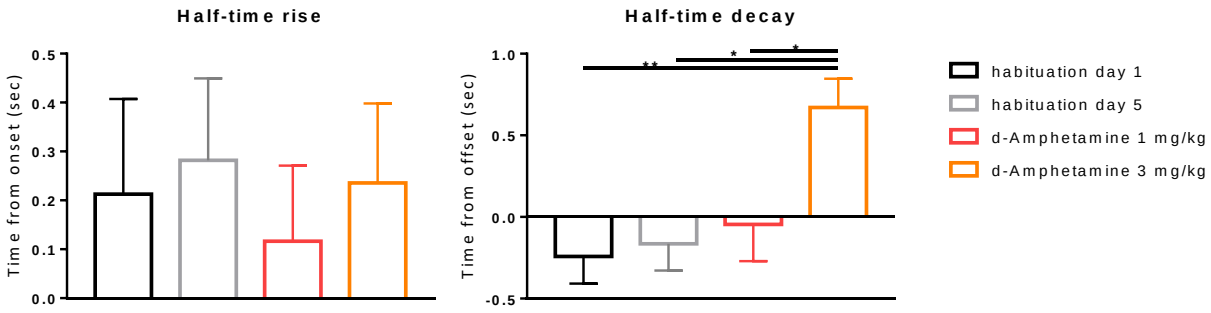

Figure 32 d-Amphetamine retarded the time to decrease from upper plateau to 50% of its value. Normalized curves of the different groups using a 4-parameter logistic function was performed. 1way ANOVA has been performed. Error bars represent SEM. * p<0.05, ** p<0.01, *** p<0.001

Analysis of neuronal activity time locked to movement onset or offset

In order to investigate whether the activation of a specific subpopulation of cells is constantly associated to motion onset or offset, the temporal relation between the firing of each iMSN and motion onset or offset was measured. **Figure 33** shows an example of iMSN calcium activity from a single 3 min video. Each horizontal line represents the activity of one iMSN, each bright dot is a spike of calcium activity and the vertical green and red bars indicate the motion onset and offset events, respectively.

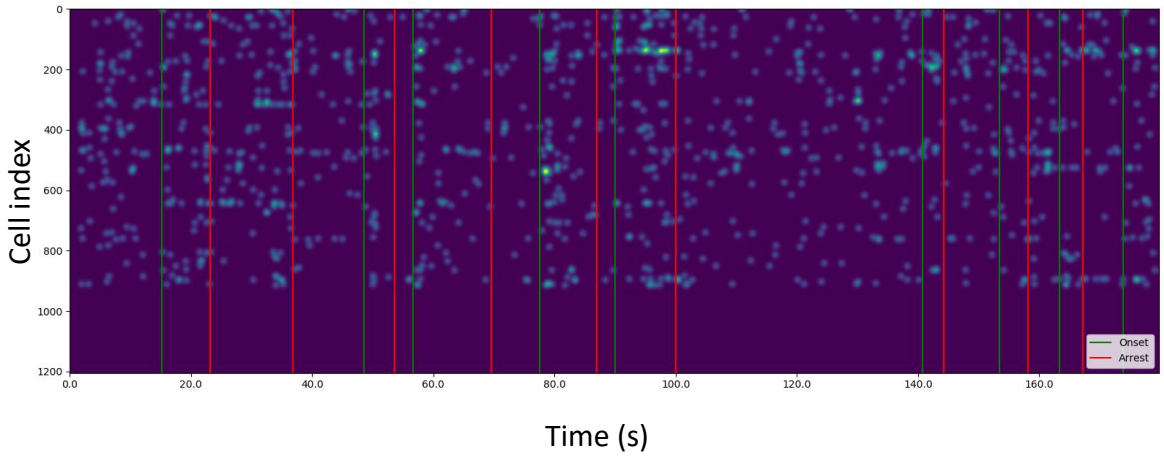

Figure 33. Pairing of behaviour and cell events. The image represents calcium activities in a single 3 min video. Each horizontal line represents the activity of a given neuron with a bright dot drawn at each spike of calcium activity. Motion onsets are reported as vertical green bars, motion offsets as vertical red bars.

Neurons are categorized based on the average delay of their firing compared to motion onset or offset in an interval time of 2 s before and after the motion event (onset or offset). In **Figure 34**, each horizontal line reports the activity of a given neuron during the 2 s before and 2 s after the motion event. Within this line each dot corresponds to a spike. The datasets are subdivided into pre-injection (first and third images of each experimental condition) and post-injection periods (second and fourth images of each experimental condition) and each set of four horizontal images represents a different experimental condition. The cells are ordered based on the average delay of calcium spikes compared to motion onsets and offsets in pre-injection condition. The order of neuron lines of the pre-injection period was kept to plot the activities of neurons in the post-injection period. If populations of neurons with constant activation delays exist, it is reasonable to expect that they would be ordered in the same manner in the post-injection plots as in the pre-injection plots. Instead, the order of post-injection activity delay seems to be randomly distributed with respect to pre-injection activity delay, leading to the conclusion that activity timing compared to motion onsets and offsets is not dependent on the activity of single neurons, but is rather

dependent on ensemble activity. It remains possible that a more accurate analysis with a wider sample would uncover subpopulations of neurons that have preferential firing time locked to specific animal behaviour (such as a specific movement) or clusters of neurons that constantly fire synchronously or in fixed sequences.

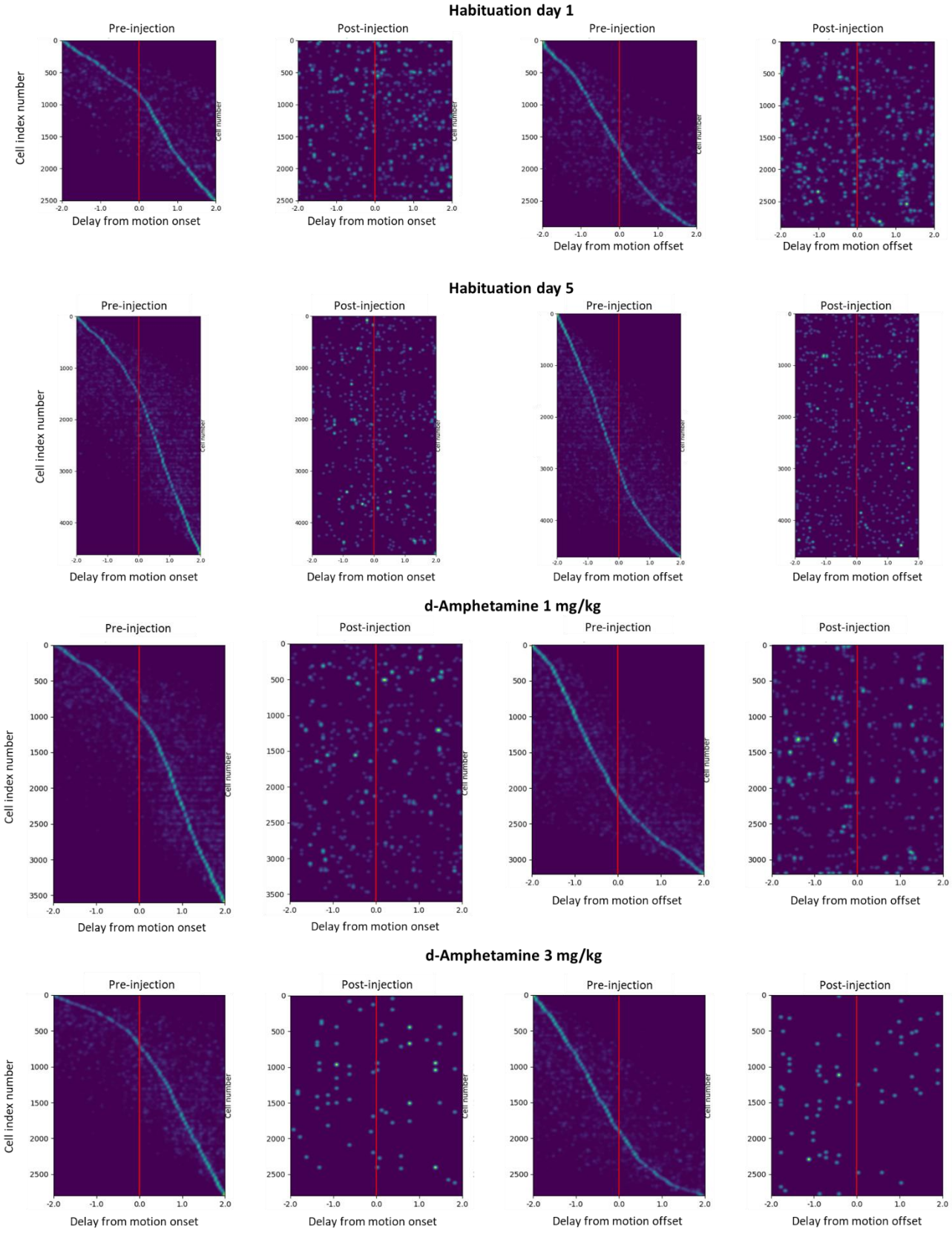

Figure 34. Activity of single iMSNs is not time-locked to motion events. The activity of each neuron is reported in a single horizontal line. Cells are ordered based on the average delay of their calcium spikes with respect to motion onsets and offsets (vertical red lines). The order of neuron lines of the pre-injection period is kept to plot the activities of neurons in the post-injection period.

Effects of d-Amphetamine treatments on iMSN parameters in moving and non-moving frames

The same analysis was performed on the other activity parameters of iMSNs (**Figures 35**). d-Amphetamine 3 mg/kg significantly decreases average spike frequency and increases average spike duration in both moving and non-moving frames (**Figure 35 a, b**), and a trend for a significant increase is detected for average spike amplitude during non-moving frames (**Figure 35c**). d-Amphetamine 1 mg/kg increases average spike duration in both moving and non-moving frames (**Figure 35b**), and shows a trend for a significant decrease in average spike frequency in non-moving frames (**Figure 35a**). For each histogram Repeated measure 2way ANOVA is performed, Dunnett post-hoc test VS. habituation day 1. For spike frequency: moving and not moving F (1, 8) = 0.4772, p=0.5092, post/pre experiment type F (3, 24) = 5.65, p=0.0045, Interaction: moving and not moving x post/pre experiment type F (3, 24) = 4.345, p=0.0140. For spike duration moving and not moving F (1, 8) = 10.67, p=0.0114, post/pre experiment type F (3, 24) = 16.64, p<0.0001, Interaction: moving and not moving x post/pre experiment type F (3, 24) = 4.16, p=0.0166. For spike amplitude: moving and not moving F (1, 8) = 0.4772, p=0.5124, post/pre experiment type F (3, 24) = 4.311, p=0.0144, Interaction: moving and not moving x post/pre experiment type F (3, 24) = 0.233, p=0.8725.

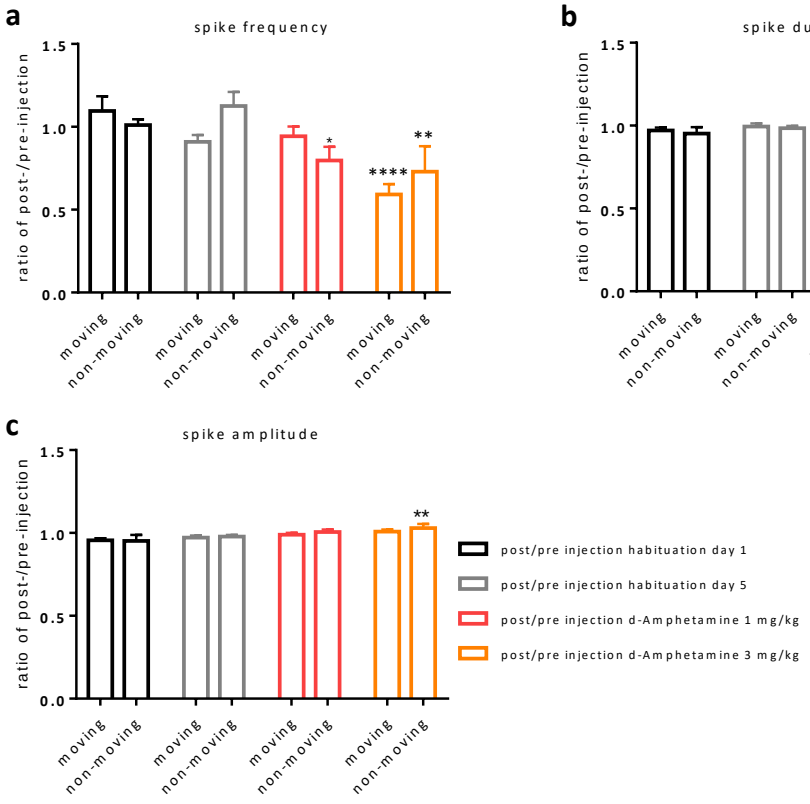

Figure 35. d-Amphetamine treatments have effects on spike parameters in moving and non-moving frames. The data are presented as ratio of treatment/baseline (i.e., post-injection/pre-injection) values. A ratio = 1 means that the treatment has no effect. Repeated measure 2way ANOVA (moving/non-moving*experiment type) has been performed. Error bars represent SEM. * p<0.05, ** p<0.01, *** p<0.001

Histological analysis

At the end of the last OFT session mice were sacrificed to confirm the endoscope position. **Figure 36** reports a representative image of the endoscope localization, area within dotted lines. Cells expressing GCaMP6s are stained in green, whereas Hoechst positive cells are stained in blue.

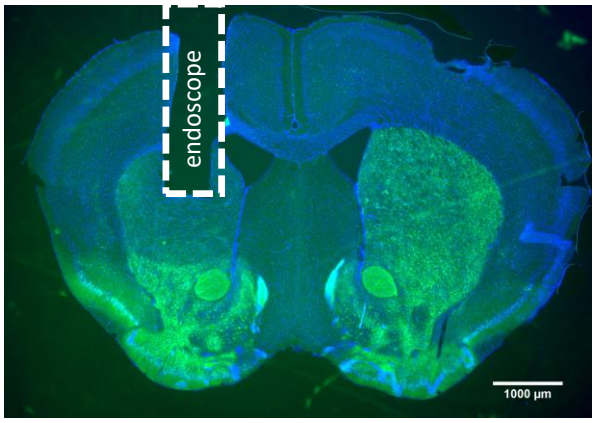

Figure 36. Endoscope localization. The image represents the histology from one A2A GCamp6s mouse. Cells expressing GCaMP6s are stained in green, whereas Hoechst positive cells are stained in blue. Scale bar is 1000 µm.

Discussion

Analysis of calcium events

Epifluorescence endoscopic imaging raw data consist of a huge amount of videos, in which neurons appear brightly with a specific frequency of activation. One problem that we successfully resolved was to convert this huge amount of image-related data into numerical data, in which the bright dots are converted into spikes with specific amplitude and duration and appearing at a specific frequency. To do so, calcium imaging data go through: motion correction, source extraction and deconvolution, as explained in the materials and methods. We decided to use the pipeline of CaImAn and CNMF-E to achieve this goal. However, by applying CNMF-E algorithm, we found the output problematic because, as reported in the **Figure 18** (Materials and Methods, Data Analysis for calcium imaging), the software fits a high amount of low peaks, that are in fact noise. In detail, CNMF-E considers as proper calcium peaks the traces fitted as a series of exponential calcium spikes, already denoised, indicated as estimates.C. On the other hand, from CNMF-E python documentation, the fitting residual is the noise not considered during the fitting and indicated as estimates.R. Therefore, the real calcium traces have to be considered as the sum of estimates.R and estimates.C. The wrong identification as a peak of noise leads to overestimation of iMSN calcium activity, which is the indirect measure of general neuronal activity, and the impossibility to identify safely activations with low intensity. To overcome this obstacle, we used a custom Python script to perform our own peak detection on the traces, selecting only spikes with a signal higher than 4 SD of the noise, and lasting at least a second. This method is in line with the work of Parker and colleagues (Parker et al 2018) who identified fluorescence traces by applying threshold-of ≥ 3 SD above the baseline signal for ≥1.4s.

Due to these limitations, while the usefulness of CaImAn pipeline and CNMF-E software remains evident, a pipeline supervised for each single step is warranted. Moreover, it would be desirable that customised scripts that often appear in the material and method of published paper on this subject become public.

iMSN involvement in action initiation and arrest

The BG are a group of subcortical nuclei involved in the control of voluntary movements. The classical model proposes that, from two distinct striatal neuronal populations (iMSNs and dMSNs) originate two different pathways (indirect and direct pathways) with opposite roles: MSNs of the direct pathway facilitate movement, while MSNs of the indirect pathway inhibit it. This model is supported by the notion that hypokinetic neurological disorders, such as Parkinson's disease, depend on the hyperactivity of the indirect pathway and hypoactivity of the direct pathway caused by DA depletion, whereas hyperkinetic disorders, such as Huntington's chorea, are produced by hyperactivity of the direct pathway (Albin et al 1989, DeLong 1990).

However, in order to understand the function of these two pathways it is necessary to monitor and compare their activity at cellular level in freely behaving mice. Recent studies, using transgenic mouse lines, have highlighted the role of both pathways in motor behaviour (Gerfen et al 2013, Gong et al 2007). Using this approach, the authors highlighted the concurrent activation of direct and indirect pathways during the initiation of actions (Cui et al 2013).

To study the relations between motion events and neuronal activity it is necessary to precisely identify onset and offset of single motion events with sub-second precision, since Ca^{2+} spikes have around 1 s duration. It seems evident that a reliable and automatized detection method is required to reach this goal when extended datasets are considered. Our approach is derived from previously reported methods, such as the method described in Parker and colleagues (Parker et al 2018) who considered the mean of Ca^{2+} event rates as a function of locomotor speed normalized with the mean of Ca^{2+} event rates while the mouse was at rest. Rest was defined as a speed lower than 0.5 cm/s. Moreover, they identified as a motion event all movement events that lasted ≥ 2 s and occurred ≥ 2 s after the previous movement event.

Once we paired MSN activity and motion events, we could show that increased firing of iMSNs contributes to the encoding of locomotion. In detail, as reported in **Figure 28** (Results, Analysis of longitudinal cell activity in relation to movement), the analysis of average cell spikes time locked to motion events demonstrates that iMSN activity rises around 0.5-0.3 s before the motion onset and falls around 0.5 s before the motion offset. This result challenges the idea that iMSNs are physiologically related to movement inhibition. The iMSN activity that we observed, precisely contributes to the encoding of locomotion and raised before its onset. While the activity of the indirect pathway could be different from that of the direct pathway in a more subtle way, present

and previous data contradict the oversimplified view of the classical theories on direct and indirect pathway function and dysfunction. However, in comparison with data shown by Parker and colleagues (Parker et al 2018), our data present some differences. Among them, in our case the average of cell spikes started to rise around 0.5-0.3 s before motion onset, while the data from Parker and colleagues showed an increase of calcium event rate around one second before the motion onset. Similarly, for the motion offset, our data report that the average cell spikes fall around 0.5 s before the motion offset, while for the authors is around 1 s before motion offset. This discrepancy in iMSN calcium event rate could be due to some different parameters applied during the extraction of velocity data or the timing identification of motion event (onset and offset).

Parker and colleagues (Parker et al 2018) demonstrated the encoding of movement by striatal MSNs using *in vivo* calcium imaging. In their work, Ca^{2+} event rates rose and fell in the direct and indirect MSN with similar kinetics with respect to locomotor activity onset and offset, respectively (**Figure 37**). Averaged overall movement events (motion onset and arrest), showed that MSN activity rose approximately 1 s before motion onset and fell around 1 s before the event of motion offset, as previously mentioned. Their data showed that iMSN and dMSN had indistinguishable kinetics.

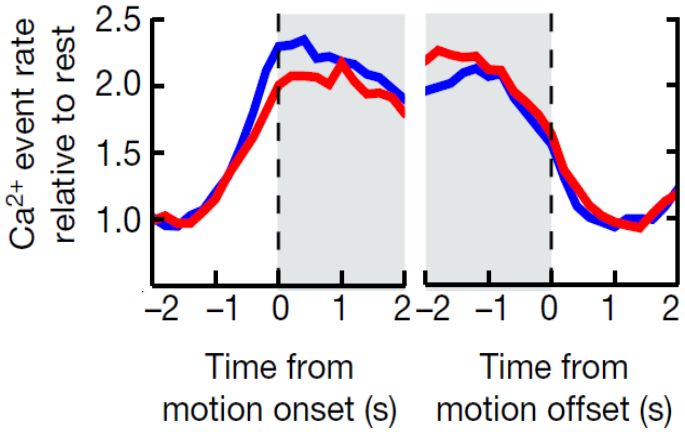

Figure 37. Direct and indirect MSNs encode movement. Grey shading indicates locomotion (velocity > 0.5 cm/s), whereas white area resting (<0.5 cm/s). The graph shows calcium event rate relative to motion onset and offset. Blue traces are the average of calcium events for dMSNs, while red traces for iMSNs (Parker et al 2018).

These results were also supported by previous experiments performed by Cui and colleagues (Cui et al 2013). In this latter study, the authors used fibre optics and time-correlated single-photon counting to demonstrate the concurrent activation of direct and indirect pathway when animals initiated the actions. Data collection was achieved by measuring GCaMP3 fluorescence during a lever pressing operant task. GCaMP3 fluorescence increased during action initiation with a similar kinetics for direct and indirect pathway. Both pathways were more active during movement than during inactive state, as reported in the figure below **(Figure 38)**.

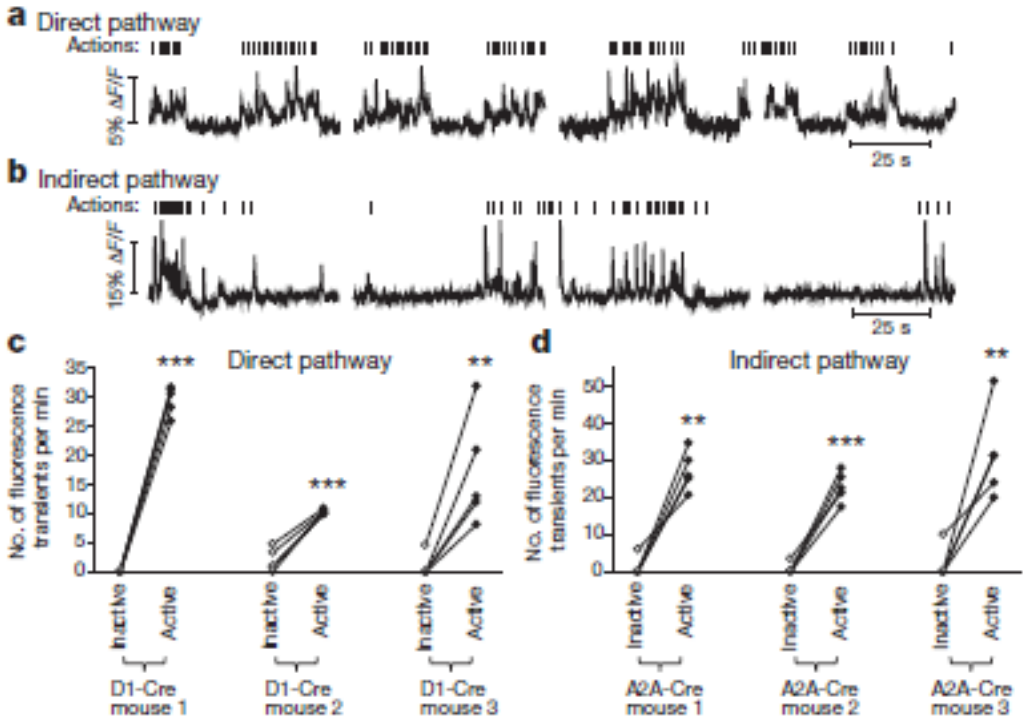

Figure 38. MSN of direct and indirect pathway are active during action initiation in a lever pressing task. a) fluorescence changing in direct pathway related to the operant actions (lever presses + magazine entries), indicated as vertical ticks. **b)** fluorescence changing in indirect pathway related to the operant actions. **c)** and **d)** comparison of changing in fluorescence of dMSNs and iMSN during activate and inactive state (Cui et al 2013).

Tecuapetla and colleagues, by using optogenetic inhibition or stimulation of direct or indirect pathway, confirmed the contribution of both pathways to action (Tecuapetla et al 2016). Before movement initiation, the latency for initiation was increased by manipulation of striatonigral (or direct) pathway or aborted by alteration of striatopallidal (or indirect) pathway. Moreover, ongoing action was impaired by inhibition of both pathways after action initiation.

Present and previous experiments can also shed a new light on the pathophysiology of movement disorders like Parkinson's disease. In a Parkinson's disease animal model, 14 days after the injection of 6-hydroxydopamine (6-OHDA) into the SNc, Parker and colleagues (Parker et al 2018), observed a marked alteration of Ca^{2+} event rates only in iMSNs but not in dMSNs. iMSN activity increased over baseline but with a significant reduction in the curve slope at the movement onset and the same was true in the opposite direction for movement offset. This probably indicates a reduction in the encoding of movement by iMSNs. This selective impairment of iMSNs in movement encoding in a Parkinson's disease model suggests that these neurons may be a specific target for more effective therapeutic approaches.

d-Amphetamine-elicited changes in global iMSN parameters

d-Amphetamine produces a dose-dependent alteration of locomotor activity. As reported in Results (Locomotor effects of d-Amphetamine treatment), acute i.p. injection of d-Amphetamine at 3 mg/kg dose markedly increased locomotor activity, whereas acute i.p. injection of d-Amphetamine at 1 mg/kg dose mildly (and non-significantly) decreased locomotor activity (**Figure 19**). In addition, d-Amphetamine 3 mg/kg dose did not change the proportion of time spent moving, suggesting that the animals increase their locomotor speed during the moving episodes. Instead, d-Amphetamine 1 mg/kg dose decreased the amount of time spent moving (**Figure 21**). The behavioural effect of d-Amphetamine at low doses have been poorly investigated: some authors reported a mild decrease of locomotor activity with 1 mg/kg (Ramos et al 2021), while others reported an increase of movement with 2 mg/kg (Yates et al 2007).

We further analysed the effect of d-Amphetamine at 1 mg/kg and 3 mg/kg dose on iMSN activity in freely moving mice. The iMSN parameters that we extract from peak analysis were: average number of active cells, average spike frequency (Hz), average spike amplitude and average spike duration (s). These parameters were analysed for each experiment type and were divided between pre- and post-injection. Our results highlight a dose-dependent significant effect of d-Amphetamine on iMSN activity. d-Amphetamine 3 mg/kg, in comparison with the control group (habituation day 1), reduced the number of active cell (cells that have at least one spike), and the average spike frequency, while it increased the average spike duration (**Figure 23**). Further analysis of these parameters in moving and non-moving periods, showed that the average spike frequency is reduced in both moving and non-moving frames, and the duration is increased in both moving and non-moving frames. Instead, spike amplitude is modestly increased only in non-moving periods (**Figure 35**). This change is not visible in the global analysis possibly because of the relatively minor proportion of non-moving periods and the modest intensity of the change. These results suggest that d-Amphetamine-induced hyperlocomotion is, at least in part, mediated by an inhibition of iMSN activity, and more specifically, by a silencing of a subpopulation of iMSNs unrelated to the moving state of the mouse.

Although d-Amphetamine at 1 mg/kg does not produce significant locomotor effects, and even reduces the moving time, its effects are similar to, though less intense than, those of the higher dose. The separated analysis of moving/non-moving periods, showed that the decrease in spike frequency is only significant in non-moving frames. A more accurate behavioural analysis (such as

the ongoing analysis with DeepLabCut and Simba) that refines the simple dichotomy “movement Vs. rest”, may shed further light on this apparent discrepancy between neuronal changes and behavioural changes at the two doses. In parallel, an analysis of the effects of d-Amphetamine 1 and 3 mg/kg on the other striatal neuronal populations, above all the dMSNs, is certainly warranted.

The effects of amphetamine and other psychostimulants on the activity of iMSNs and dMSNs have been extensively investigated through several approaches. The effects of the acute exposure to psychostimulant drugs on the expression of activity-related immediate early genes (IEGs), including c-Fos, Zif268 (Egr1) and FosB were intensely studied. Acute administration of amphetamine as well as cocaine, has differential effects on c-Fos expression in D1 and D2 MSNs depending on the site of drug administration, home cage or a new environment (Badiani et al 1999, Uslaner et al 2001) . In this latter case, both D1 and D2 MSNs express amphetamine-induced c-Fos (Ferguson et al 2004). Similarly, acute cocaine treatment activated the ERK cascade, exclusively in D1 MSNs but induced c-Fos and Zif268 in D1 MSNs and, to a lower extent, D2 MSNs (Bertran-Gonzalez et al 2008). Accordingly, a previous study using in situ hybridization in mice showed an induction of c-Fos in D1 and D2 MSNs by cocaine treatment (Ferguson et al 2006). Acute exposure to amphetamine or cocaine, induced FosB in D1 MSNs but not in D2 MSNs (Berretta et al 1992). Overall, as far as IEG expression is concerned, acute psychostimulant treatment appears to impact D1 MSN activity more intensely than D2 MSN activity.

An involvement of both striatal DMS populations in amphetamine effects was also demonstrated by experiments showing that ablation of D1 MSNs in dorsomedial striatum and D2 MSNs in dorsolateral striatum decreases and increases, respectively, locomotor effects of acute amphetamine administration (Durieux et al 2012).

Experiments on extracellular recordings of striatal activity show that amphetamine globally depresses MSN activity. Systemic amphetamine increased the firing rates of slower firing neurons but decreased the firing rates of faster firing neurons (Ma et al 2013). Accordingly, local amphetamine administration depressed population spike amplitude in dorsal striatum (Danielsson et al 2021).

As regards the cellular mechanisms of MSN activation by dopaminergic neurotransmission, which is activated by psychostimulant drugs and in general by all drugs of abuse, DA, through D1R, facilitates the transition from the down- to the up-state of D1 MSNs elicited by corticostriatal glutamatergic neurotransmission, and impedes, through D2Rs, the transition from the down- to the up-state of D2 MSNs (Gerfen & Surmeier 2011, Salery et al 2020, Surmeier et al 2007).

To this complex picture, the present work adds the simultaneous *in vivo* visualization over an extended period of time of an ample population of iMSNs, and the precise determination of iMSN activity changes in relation to movement onset or offset. As shown in **Figure 28**, both doses of d-Amphetamine do not show changes in iMSN movement encoding when compared to all other groups. However, a significant reduction in the baseline calcium spike frequency was detected with 3 mg/kg doses compared to all other groups (Results, **Figure 29**), confirming that one single injection of d-Amphetamine is associated with a significant change spike frequency. The second significant effect of d-Amphetamine at 3 mg/kg is a relative increase in peak number of spikes after motion onset (Results, **Figure 31**). A third effect is related to motion offset, where d-Amphetamine 3 mg/kg treatment is associated to a delay in the return to baseline spike frequency with respect to the other treatment groups (**Figure 30b**). The analysis of spike frequency kinetics of motion onset and offset confirmed that d-Amphetamine 3 mg/kg treatment does not alter the half-time of activity rise (**Figure 32**, Hal-time rise) but significantly delays the half-time of activity decay (**Figure 32,** Half-time decay). This detailed analysis of iMSN activity after d-Amphetamine at 3 mg/kg treatment in relation to motion onset and offset indicates that iMSN population activity is depressed by the treatment but increases proportionally more intensely at motion onset and remains active for a more prolonged period at motion offset.

Overall, the analysis of d-Amphetamine at 3 mg/kg treatment impact on iMSNs indicates that, similarly to what was observed after DA denervation (Parker et al. 2018), the pharmacological treatment with a psychostimulant breaks the physiological balance between striatal population activities. In fact, while iMSNs are co-activated with dMSNs in relation to the change in locomotion speed that occurs at motion onset (present data and Parker et al. 2018), increase in locomotion speed that occurs after amphetamine treatment is associated to a depression of the iMSNs at population level. This evidence fits well with the classical notion that activity of the indirect pathway inhibits movement, and therefore its depression would favour movement acceleration. It is therefore possible that the more recent proposal on the necessity of dMSN and iMSN population co-activation to initiate movement applies to physiological control of movement, whereas the classical notion of dMSN/iMSN antagonism applies to altered movement conditions such as those present after DA denervation and amphetamine treatment.

Bibliography

Aaron G, Yuste R. 2006. Reverse optical probing (ROPING) of neocortical circuits. *Synapse* 60: 437-40

Abudukeyoumu N, Hernandez-Flores T, Garcia-Munoz M, Arbuthnott GW. 2019. Cholinergic modulation of striatal microcircuits. *Eur J Neurosci* 49: 604-22

Adelsberger H, Garaschuk O, Konnerth A. 2005. Cortical calcium waves in resting newborn mice. *Nat Neurosci* 8: 988-90

Aggarwal S, Mortensen OV. 2017. Overview of Monoamine Transporters. *Curr Protoc Pharmacol* 79: 12 16 1-12 16 17

Albin RL, Young AB, Penney JB. 1989. The functional anatomy of basal ganglia disorders. *Trends Neurosci* 12: 366-75

Alexander GE, Crutcher MD. 1990. Functional architecture of basal ganglia circuits: neural substrates of parallel processing. *Trends Neurosci* 13: 266-71

Alexander GE, DeLong MR. 1985. Microstimulation of the primate neostriatum. II. Somatotopic organization of striatal microexcitable zones and their relation to neuronal response properties. *J Neurophysiol* 53: 1417-30

Alexander GE, DeLong MR, Strick PL. 1986. Parallel organization of functionally segregated circuits linking basal ganglia and cortex. *Annu Rev Neurosci* 9: 357-81

Amalric M, Koob GF. 1993. Functionally selective neurochemical afferents and efferents of the mesocorticolimbic and nigrostriatal dopamine system. *Prog Brain Res* 99: 209-26

Aosaki T, Kiuchi K, Kawaguchi Y. 1998. Dopamine D1-like receptor activation excites rat striatal large aspiny neurons in vitro. *J Neurosci* 18: 5180-90

Aosaki T, Tsubokawa H, Ishida A, Watanabe K, Graybiel AM, Kimura M. 1994. Responses of tonically active neurons in the primate's striatum undergo systematic changes during behavioral sensorimotor conditioning. *J Neurosci* 14: 3969-84

Artola A, Singer W. 1993. Long-term depression of excitatory synaptic transmission and its relationship to long-term potentiation. *Trends Neurosci* 16: 480-7

Axelrod J, Kopin IJ. 1969. The uptake, storage, release and metabolism of noradrenaline in sympathetic nerves. *Prog Brain Res* 31: 21-32

Badiani A, Oates MM, Day HE, Watson SJ, Akil H, Robinson TE. 1999. Environmental modulation of amphetamine-induced c-fos expression in D1 versus D2 striatal neurons. *Behav Brain Res* 103: 203-9

Bagur R, Hajnoczky G. 2017. Intracellular Ca(2+) Sensing: Its Role in Calcium Homeostasis and Signaling. *Mol Cell* 66: 780-88

Baker BJ, Kosmidis EK, Vucinic D, Falk CX, Cohen LB, et al. 2005. Imaging brain activity with voltage- and calcium-sensitive dyes. *Cell Mol Neurobiol* 25: 245-82

Baker DA, Specio SE, Tran-Nguyen LT, Neisewander JL. 1998. Amphetamine infused into the ventrolateral striatum produces oral stereotypies and conditioned place preference. *Pharmacol Biochem Behav* 61: 107-11

Baldo BA, Koob GF, Markou A. 1999. Role of adenosine A2 receptors in brain stimulation reward under baseline conditions and during cocaine withdrawal in rats. *J Neurosci* 19: 11017-26

Balkenius A, Johansson AJ, Balkenius C. 2015. Comparing Analysis Methods in Functional Calcium Imaging of the Insect Brain. *PLoS One* 10: e0129614

Balleine BW, Liljeholm M, Ostlund SB. 2009. The integrative function of the basal ganglia in instrumental conditioning. *Behav Brain Res* 199: 43-52

Barbera G, Liang B, Zhang L, Gerfen CR, Culurciello E, et al. 2016. Spatially Compact Neural Clusters in the Dorsal Striatum Encode Locomotion Relevant Information. *Neuron* 92: 202-13

Barondes SH, Cohen HD. 1968. Arousal and the conversion of "short-term" to "long-term" memory. *Proc Natl Acad Sci U S A* 61: 923-9

Bastia E, Xu YH, Scibelli AC, Day YJ, Linden J, et al. 2005. A crucial role for forebrain adenosine A(2A) receptors in amphetamine sensitization. *Neuropsychopharmacology* 30: 891-900

Bateup HS, Santini E, Shen W, Birnbaum S, Valjent E, et al. 2010. Distinct subclasses of medium spiny neurons differentially regulate striatal motor behaviors. *Proc Natl Acad Sci U S A* 107: 14845-50

Beier KT, Steinberg EE, DeLoach KE, Xie S, Miyamichi K, et al. 2015. Circuit Architecture of VTA Dopamine Neurons Revealed by Systematic Input-Output Mapping. *Cell* 162: 622-34

Bennett BD, Bolam JP. 1994. Synaptic input and output of parvalbumin-immunoreactive neurons in the neostriatum of the rat. *Neuroscience* 62: 707-19

Berendse HW, Galis-de Graaf Y, Groenewegen HJ. 1992. Topographical organization and relationship with ventral striatal compartments of prefrontal corticostriatal projections in the rat. *J Comp Neurol* 316: 314-47

Berendse HW, Groenewegen HJ. 1990. Organization of the thalamostriatal projections in the rat, with special emphasis on the ventral striatum. *J Comp Neurol* 299: 187-228

Bernard V, Laribi O, Levey AI, Bloch B. 1998. Subcellular redistribution of m2 muscarinic acetylcholine receptors in striatal interneurons in vivo after acute cholinergic stimulation. *J Neurosci* 18: 10207-18

Berretta S, Robertson HA, Graybiel AM. 1992. Dopamine and glutamate agonists stimulate neuron-specific expression of Fos-like protein in the striatum. *J Neurophysiol* 68: 767-77

Berridge MJ. 1993. Inositol trisphosphate and calcium signalling. *Nature* 361: 315-25

Berridge MJ. 1998. Neuronal calcium signaling. *Neuron* 21: 13-26

Berridge MJ, Bootman MD, Roderick HL. 2003. Calcium signalling: dynamics, homeostasis and remodelling. *Nat Rev Mol Cell Biol* 4: 517-29

Berridge MJ, Lipp P, Bootman MD. 2000. The versatility and universality of calcium signalling. *Nat Rev Mol Cell Biol* 1: 11-21

Bertran-Gonzalez J, Bosch C, Maroteaux M, Matamales M, Herve D, et al. 2008. Opposing patterns of signaling activation in dopamine D1 and D2 receptor-expressing striatal neurons in response to cocaine and haloperidol. *J Neurosci* 28: 5671-85

Bignami G. 1966. Pharmacologic influences on mating behavior in the male rat. Effects of d-amphetamine, LSD-25, strychnine, nicotine and various anticholinergic agents. *Psychopharmacologia* 10: 44-58

Bloodgood BL, Sabatini BL. 2007. Nonlinear regulation of unitary synaptic signals by CaV(2.3) voltage-sensitive calcium channels located in dendritic spines. *Neuron* 53: 249-60

Bohdanecky Z, Jarvik ME. 1967. The effect of D-amphetamine and physostigmine upon acquisition and retrieval in a single trial learning task. *Arch Int Pharmacodyn Ther* 170: 58-65

Bonifazi P, Goldin M, Picardo MA, Jorquera I, Cattani A, et al. 2009. GABAergic hub neurons orchestrate synchrony in developing hippocampal networks. *Science* 326: 1419-24

Bonnavion P, Fernandez EP, Varin C, de Kerchove d'Exaerde A. 2019. It takes two to tango: Dorsal direct and indirect pathways orchestration of motor learning and behavioral flexibility. *Neurochem Int* 124: 200-14

Bortolato M, Chen K, Shih JC. 2008. Monoamine oxidase inactivation: from pathophysiology to therapeutics. *Adv Drug Deliv Rev* 60: 1527-33

Brown JM, Hanson GR, Fleckenstein AE. 2000. Methamphetamine rapidly decreases vesicular dopamine uptake. *J Neurochem* 74: 2221-3

Brown JM, Riddle EL, Sandoval V, Weston RK, Hanson JE, et al. 2002. A single methamphetamine administration rapidly decreases vesicular dopamine uptake. *J Pharmacol Exp Ther* 302: 497-501

Brown JR, Arbuthnott GW. 1983. The electrophysiology of dopamine (D2) receptors: a study of the actions of dopamine on corticostriatal transmission. *Neuroscience* 10: 349-55

Brown P. 2007. Abnormal oscillatory synchronisation in the motor system leads to impaired movement. *Curr Opin Neurobiol* 17: 656-64

Bucci D, Busceti CL, Calierno MT, Di Pietro P, Madonna M, et al. 2017. Systematic Morphometry of Catecholamine Nuclei in the Brainstem. *Front Neuroanat* 11: 98

Burnashev N, Zhou Z, Neher E, Sakmann B. 1995. Fractional calcium currents through recombinant GluR channels of the NMDA, AMPA and kainate receptor subtypes. *J Physiol* 485 (Pt 2): 403-18

Cachope R, Mateo Y, Mathur BN, Irving J, Wang HL, et al. 2012. Selective activation of cholinergic interneurons enhances accumbal phasic dopamine release: setting the tone for reward processing. *Cell Rep* 2: 33-41

Calabresi P, Centonze D, Gubellini P, Bernardi G. 1999a. Activation of M1-like muscarinic receptors is required for the induction of corticostriatal LTP. *Neuropharmacology* 38: 323-6

Calabresi P, Centonze D, Gubellini P, Marfia GA, Bernardi G. 1999b. Glutamate-triggered events inducing corticostriatal long-term depression. *J Neurosci* 19: 6102-10

Calabresi P, Centonze D, Gubellini P, Marfia GA, Pisani A, et al. 2000a. Synaptic transmission in the striatum: from plasticity to neurodegeneration. *Prog Neurobiol* 61: 231-65

Calabresi P, Centonze D, Gubellini P, Pisani A, Bernardi G. 1998. Endogenous ACh enhances striatal NMDA-responses via M1-like muscarinic receptors and PKC activation. *Eur J Neurosci* 10: 2887-95

Calabresi P, Centonze D, Gubellini P, Pisani A, Bernardi G. 2000b. Acetylcholine-mediated modulation of striatal function. *Trends Neurosci* 23: 120-6

Calabresi P, Gubellini P, Centonze D, Picconi B, Bernardi G, et al. 2000c. Dopamine and cAMP-regulated phosphoprotein 32 kDa controls both striatal long-term depression and long-term potentiation, opposing forms of synaptic plasticity. *J Neurosci* 20: 8443-51

Calabresi P, Gubellini P, Centonze D, Sancesario G, Morello M, et al. 1999c. A critical role of the nitric oxide/cGMP pathway in corticostriatal long-term depression. *J Neurosci* 19: 2489-99

Calabresi P, Maj R, Pisani A, Mercuri NB, Bernardi G. 1992a. Long-term synaptic depression in the striatum: physiological and pharmacological characterization. *J Neurosci* 12: 4224-33

Calabresi P, Mercuri NB, Bernardi G. 1990a. Synaptic and intrinsic control of membrane excitability of neostriatal neurons. II. An in vitro analysis. *J Neurophysiol* 63: 663-75

Calabresi P, Mercuri NB, Stefani A, Bernardi G. 1990b. Synaptic and intrinsic control of membrane excitability of neostriatal neurons. I. An in vivo analysis. *J Neurophysiol* 63: 651-62

Calabresi P, Pisani A, Mercuri NB, Bernardi G. 1992b. Long-term Potentiation in the Striatum is Unmasked by Removing the Voltage-dependent Magnesium Block of NMDA Receptor Channels. *Eur J Neurosci* 4: 929-35

Calabresi P, Pisani A, Mercuri NB, Bernardi G. 1994. Post-receptor mechanisms underlying striatal long-term depression. *J Neurosci* 14: 4871-81

Calabresi P, Pisani A, Mercuri NB, Bernardi G. 1996. The corticostriatal projection: from synaptic plasticity to dysfunctions of the basal ganglia. *Trends Neurosci* 19: 19-24

Calabresi P, Saiardi A, Pisani A, Baik JH, Centonze D, et al. 1997. Abnormal synaptic plasticity in the striatum of mice lacking dopamine D2 receptors. *J Neurosci* 17: 4536-44

Cardinal RN, Parkinson JA, Hall J, Everitt BJ. 2002. Emotion and motivation: the role of the amygdala, ventral striatum, and prefrontal cortex. *Neurosci Biobehav Rev* 26: 321-52

Carlson GC, Coulter DA. 2008. In vitro functional imaging in brain slices using fast voltage-sensitive dye imaging combined with whole-cell patch recording. *Nat Protoc* 3: 249-55

Carr DB, Day M, Cantrell AR, Held J, Scheuer T, et al. 2003. Transmitter modulation of slow, activity-dependent alterations in sodium channel availability endows neurons with a novel form of cellular plasticity. *Neuron* 39: 793-806

Carr GD, White NM. 1984. The relationship between stereotypy and memory improvement produced by amphetamine. *Psychopharmacology (Berl)* 82: 203-9

Catterall WA. 2000. Structure and regulation of voltage-gated Ca2+ channels. *Annu Rev Cell Dev Biol* 16: 521-55

Caulfield MP. 1993. Muscarinic receptors--characterization, coupling and function. *Pharmacol Ther* 58: 319-79

Centonze D, Grande C, Usiello A, Gubellini P, Erbs E, et al. 2003a. Receptor subtypes involved in the presynaptic and postsynaptic actions of dopamine on striatal interneurons. *J Neurosci* 23: 6245-54

Centonze D, Gubellini P, Pisani A, Bernardi G, Calabresi P. 2003b. Dopamine, acetylcholine and nitric oxide systems interact to induce corticostriatal synaptic plasticity. *Rev Neurosci* 14: 207-16

Centonze D, Napolitano M, Saulle E, Gubellini P, Picconi B, et al. 2002. Tissue plasminogen activator is required for corticostriatal long-term potentiation. *Eur J Neurosci* 16: 713-21

Centonze D, Picconi B, Gubellini P, Bernardi G, Calabresi P. 2001a. Dopaminergic control of synaptic plasticity in the dorsal striatum. *Eur J Neurosci* 13: 1071-7

Centonze D, Pisani A, Bonsi P, Giacomini P, Bernardi G, Calabresi P. 2001b. Stimulation of nitric oxide-cGMP pathway excites striatal cholinergic interneurons via protein kinase G activation. *J Neurosci* 21: 1393-400

Cepeda C, Andre VM, Yamazaki I, Wu N, Kleiman-Weiner M, Levine MS. 2008. Differential electrophysiological properties of dopamine D1 and D2 receptor-containing striatal medium-sized spiny neurons. *Eur J Neurosci* 27: 671-82

Cepeda C, Buchwald NA, Levine MS. 1993. Neuromodulatory actions of dopamine in the neostriatum are dependent upon the excitatory amino acid receptor subtypes activated. *Proc Natl Acad Sci U S A* 90: 9576-80

Cepeda C, Walsh JP, Peacock W, Buchwald NA, Levine MS. 1994. Neurophysiological, pharmacological and morphological properties of human caudate neurons recorded in vitro. *Neuroscience* 59: 89-103

Cetin A, Komai S, Eliava M, Seeburg PH, Osten P. 2006. Stereotaxic gene delivery in the rodent brain. *Nat Protoc* 1: 3166-73

Chalasani SH, Chronis N, Tsunozaki M, Gray JM, Ramot D, et al. 2007. Dissecting a circuit for olfactory behaviour in Caenorhabditis elegans. *Nature* 450: 63-70

Chan CS, Surmeier DJ, Yung WH. 2005. Striatal information signaling and integration in globus pallidus: timing matters. *Neurosignals* 14: 281-9

Charara A, Grace AA. 2003. Dopamine receptor subtypes selectively modulate excitatory afferents from the hippocampus and amygdala to rat nucleus accumbens neurons. *Neuropsychopharmacology* 28: 1412-21

Charpier S, Deniau JM. 1997. In vivo activity-dependent plasticity at cortico-striatal connections: evidence for physiological long-term potentiation. *Proc Natl Acad Sci U S A* 94: 7036-40

Charpier S, Mahon S, Deniau JM. 1999. In vivo induction of striatal long-term potentiation by low-frequency stimulation of the cerebral cortex. *Neuroscience* 91: 1209-22

Chhatwal JP, Hammack SE, Jasnow AM, Rainnie DG, Ressler KJ. 2007. Identification of cell-type-specific promoters within the brain using lentiviral vectors. *Gene Ther* 14: 575-83

Chia TH, Levene MJ. 2009. In vivo imaging of deep cortical layers using a microprism. *J Vis Exp*

Chiamulera C, Epping-Jordan MP, Zocchi A, Marcon C, Cottiny C, et al. 2001. Reinforcing and locomotor stimulant effects of cocaine are absent in mGluR5 null mutant mice. *Nat Neurosci* 4: 873-4

Choi S, Lovinger DM. 1997. Decreased probability of neurotransmitter release underlies striatal long-term depression and postnatal development of corticostriatal synapses. *Proc Natl Acad Sci U S A* 94: 2665-70

Christakou A, Robbins TW, Everitt BJ. 2004. Prefrontal cortical-ventral striatal interactions involved in affective modulation of attentional performance: implications for corticostriatal circuit function. *J Neurosci* 24: 773-80

Chuhma N, Mingote S, Kalmbach A, Yetnikoff L, Rayport S. 2017. Heterogeneity in Dopamine Neuron Synaptic Actions Across the Striatum and Its Relevance for Schizophrenia. *Biol Psychiatry* 81: 43-51

Clapham DE. 1995. Calcium signaling. *Cell* 80: 259-68

Clark FC, Steele BJ. 1966. Effects of D-amphetamine on performance under a multiple schedule in the rat. *Psychopharmacologia* 9: 157-69

Connor JA, Razani-Boroujerdi S, Greenwood AC, Cormier RJ, Petrozzino JJ, Lin RC. 1999. Reduced voltage-dependent Ca2+ signaling in CA1 neurons after brief ischemia in gerbils. *J Neurophysiol* 81: 299-306

Conquet F, Bashir ZI, Davies CH, Daniel H, Ferraguti F, et al. 1994. Motor deficit and impairment of synaptic plasticity in mice lacking mGluR1. *Nature* 372: 237-43

Consolo S, Garattini S, Ghielmetti R, Valzelli L. 1965. Concentrations of amphetamine in the brain in normal or aggressive mice. *J Pharm Pharmacol* 17: 666

Cowan RL, Wilson CJ. 1994. Spontaneous firing patterns and axonal projections of single corticostriatal neurons in the rat medial agranular cortex. *J Neurophysiol* 71: 17-32

Cowan WM, Powell TP. 1956. A study of thalamo-striate relations in the monkey. *Brain* 79: 364-90

Cowan WM, Powell TP. 1966. Strio-pallidal projection in the monkey. *J Neurol Neurosurg Psychiatry* 29: 426-39

Cox DH, Carvajal JJ, Rigby PW. 2002. Enhanced efficiency of pSV1-RecA-based BAC recombineering. *Biotechniques* 33: 1206-8

Coyle JT, Axelrod J. 1971. Development of the uptake and storage of L-(3 H)norepinephrine in the rat brain. *J Neurochem* 18: 2061-75

Crutcher MD, DeLong MR. 1984. Single cell studies of the primate putamen. I. Functional organization. *Exp Brain Res* 53: 233-43

Cui G, Jun SB, Jin X, Pham MD, Vogel SS, et al. 2013. Concurrent activation of striatal direct and indirect pathways during action initiation. *Nature* 494: 238-42

Cunha RA. 2001. Adenosine as a neuromodulator and as a homeostatic regulator in the nervous system: different roles, different sources and different receptors. *Neurochem Int* 38: 107-25

Cunha RA, Vizi ES, Ribeiro JA, Sebastiao AM. 1996. Preferential release of ATP and its extracellular catabolism as a source of adenosine upon high- but not low-frequency stimulation of rat hippocampal slices. *J Neurochem* 67: 2180-7

Dahlstrom A, Fuxe K. 1964. Localization of monoamines in the lower brain stem. *Experientia* 20: 398-9

Daigle TL, Madisen L, Hage TA, Valley MT, Knoblich U, et al. 2018. A Suite of Transgenic Driver and Reporter Mouse Lines with Enhanced Brain-Cell-Type Targeting and Functionality. *Cell* 174: 465-80 e22

Danielsson K, Lagstrom O, Ericson M, Soderpalm B, Adermark L. 2021. Subregion-specific effects on striatal neurotransmission and dopamine-signaling by acute and repeated amphetamine exposure. *Neuropharmacology* 194: 108638

Dautan D, Huerta-Ocampo I, Witten IB, Deisseroth K, Bolam JP, et al. 2014. A major external source of cholinergic innervation of the striatum and nucleus accumbens originates in the brainstem. *J Neurosci* 34: 4509-18

De Vry J, Martinez-Martinez P, Losen M, Temel Y, Steckler T, et al. 2010. In vivo electroporation of the central nervous system: a non-viral approach for targeted gene delivery. *Prog Neurobiol* 92: 227-44

DeLong MR. 1990. Primate models of movement disorders of basal ganglia origin. *Trends Neurosci* 13: 281-5

Deng YP, Xie JP, Wang HB, Lei WL, Chen Q, Reiner A. 2007. Differential localization of the GluR1 and GluR2 subunits of the AMPA-type glutamate receptor among striatal neuron types in rats. *J Chem Neuroanat* 33: 167-92

Denk W, Strickler JH, Webb WW. 1990. Two-photon laser scanning fluorescence microscopy. *Science* 248: 73-6

Denk W, Svoboda K. 1997. Photon upmanship: why multiphoton imaging is more than a gimmick. *Neuron* 18: 351-7

Desban M, Gauchy C, Glowinski J, Kemel ML. 1995. Heterogeneous topographical distribution of the striatonigral and striatopallidal neurons in the matrix compartment of the cat caudate nucleus. *J Comp Neurol* 352: 117-33

Devan BD, White NM. 1999. Parallel information processing in the dorsal striatum: relation to hippocampal function. *J Neurosci* 19: 2789-98

DeVito JL, Anderson ME, Walsh KE. 1980. A horseradish peroxidase study of afferent connections of the globus pallidus in Macaca mulatta. *Exp Brain Res* 38: 65-73

Dickson PR, Lang CG, Hinton SC, Kelley AE. 1994. Oral stereotypy induced by amphetamine microinjection into striatum: an anatomical mapping study. *Neuroscience* 61: 81-91

Dittgen T, Nimmerjahn A, Komai S, Licznerski P, Waters J, et al. 2004. Lentivirus-based genetic manipulations of cortical neurons and their optical and electrophysiological monitoring in vivo. *Proc Natl Acad Sci U S A* 101: 18206-11

Dombeck DA, Harvey CD, Tian L, Looger LL, Tank DW. 2010. Functional imaging of hippocampal place cells at cellular resolution during virtual navigation. *Nat Neurosci* 13: 1433-40

Donoghue JP, Herkenham M. 1986. Neostriatal projections from individual cortical fields conform to histochemically distinct striatal compartments in the rat. *Brain Res* 365: 397-403

Dos Santos Villar F, Walsh JP. 1999. Modulation of long-term synaptic plasticity at excitatory striatal synapses. *Neuroscience* 90: 1031-41

Doty BA, Doty LA. 1966. Facilitative effects of amphetamine on avoidance conditioning in relation to age and problem difficulty. *Psychopharmacologia* 9: 234-41

Duchen MR. 1999. Contributions of mitochondria to animal physiology: from homeostatic sensor to calcium signalling and cell death. *J Physiol* 516 (Pt 1): 1-17

Durieux PF, Bearzatto B, Guiducci S, Buch T, Waisman A, et al. 2009. D2R striatopallidal neurons inhibit both locomotor and drug reward processes. *Nat Neurosci* 12: 393-5

Durieux PF, Schiffmann SN, de Kerchove d'Exaerde A. 2012. Differential regulation of motor control and response to dopaminergic drugs by D1R and D2R neurons in distinct dorsal striatum subregions. *EMBO J* 31: 640-53

Eagle DM, Robbins TW. 2003. Inhibitory control in rats performing a stop-signal reaction-time task: effects of lesions of the medial striatum and d-amphetamine. *Behav Neurosci* 117: 1302-17

Eglen RM. 2006. Muscarinic receptor subtypes in neuronal and non-neuronal cholinergic function. *Auton Autacoid Pharmacol* 26: 219-33

Eilers J, Konnerth A. 2009. Dye loading with patch pipettes. *Cold Spring Harb Protoc* 2009: pdb prot5201

Engelbrecht CJ, Johnston RS, Seibel EJ, Helmchen F. 2008. Ultra-compact fiber-optic two-photon microscope for functional fluorescence imaging in vivo. *Opt Express* 16: 5556-64

English DF, Ibanez-Sandoval O, Stark E, Tecuapetla F, Buzsaki G, et al. 2011. GABAergic circuits mediate the reinforcement-related signals of striatal cholinergic interneurons. *Nat Neurosci* 15: 123-30

Eskow Jaunarajs KL, Bonsi P, Chesselet MF, Standaert DG, Pisani A. 2015. Striatal cholinergic dysfunction as a unifying theme in the pathophysiology of dystonia. *Prog Neurobiol* 127-128: 91-107

Evangelista AM, Gattoni RC, Izquierdo I. 1970. Effect of amphetamine, nicotine and hexamethonium on performance of a conditioned response during acquisition and retention trials. *Pharmacology* 3: 91-6

Evans WO, Smith RP. 1964. Some effects of morphine and amphetamine on intellectual functions and mood. *Psychopharmacologia* 6: 49-56

Exley R, Cragg SJ. 2008. Presynaptic nicotinic receptors: a dynamic and diverse cholinergic filter of striatal dopamine neurotransmission. *Br J Pharmacol* 153 Suppl 1: S283-97

Fagni L, Chavis P, Ango F, Bockaert J. 2000. Complex interactions between mGluRs, intracellular Ca2+ stores and ion channels in neurons. *Trends Neurosci* 23: 80-8

Ferguson SM, Fasano S, Yang P, Brambilla R, Robinson TE. 2006. Knockout of ERK1 enhances cocaine-evoked immediate early gene expression and behavioral plasticity. *Neuropsychopharmacology* 31: 2660-8

Ferguson SM, Thomas MJ, Robinson TE. 2004. Morphine-induced c-fos mRNA expression in striatofugal circuits: modulation by dose, environmental context, and drug history. *Neuropsychopharmacology* 29: 1664-74

Ferrucci M, Limanaqi F, Ryskalin L, Biagioni F, Busceti CL, Fornai F. 2019. The Effects of Amphetamine and Methamphetamine on the Release of Norepinephrine, Dopamine and Acetylcholine From the Brainstem Reticular Formation. *Front Neuroanat* 13: 48

Fleckenstein AE, Volz TJ, Riddle EL, Gibb JW, Hanson GR. 2007. New insights into the mechanism of action of amphetamines. *Annu Rev Pharmacol Toxicol* 47: 681-98

Fletcher ML, Masurkar AV, Xing J, Imamura F, Xiong W, et al. 2009. Optical imaging of postsynaptic odor representation in the glomerular layer of the mouse olfactory bulb. *J Neurophysiol* 102: 817-30

Floresco SB. 2015. The nucleus accumbens: an interface between cognition, emotion, and action. *Annu Rev Psychol* 66: 25-52

Flusberg BA, Cocker ED, Piyawattanametha W, Jung JC, Cheung EL, Schnitzer MJ. 2005. Fiber-optic fluorescence imaging. *Nat Methods* 2: 941-50

Flusberg BA, Nimmerjahn A, Cocker ED, Mukamel EA, Barretto RP, et al. 2008. High-speed, miniaturized fluorescence microscopy in freely moving mice. *Nat Methods* 5: 935-8

Fredduzzi S, Moratalla R, Monopoli A, Cuellar B, Xu K, et al. 2002. Persistent behavioral sensitization to chronic L-DOPA requires A2A adenosine receptors. *J Neurosci* 22: 1054-62

Fredholm BB, AP IJ, Jacobson KA, Klotz KN, Linden J. 2001. International Union of Pharmacology. XXV. Nomenclature and classification of adenosine receptors. *Pharmacol Rev* 53: 527-52

Fucile S. 2004. Ca2+ permeability of nicotinic acetylcholine receptors. *Cell Calcium* 35: 1-8

Fuxe K, Marcellino D, Borroto-Escuela DO, Guescini M, Fernandez-Duenas V, et al. 2010. Adenosine-dopamine interactions in the pathophysiology and treatment of CNS disorders. *CNS Neurosci Ther* 16: e18-42

Gangarossa G, Espallergues J, Mailly P, De Bundel D, de Kerchove d'Exaerde A, et al. 2013. Spatial distribution of D1R- and D2R-expressing medium-sized spiny neurons differs along the rostro-caudal axis of the mouse dorsal striatum. *Front Neural Circuits* 7: 124

Garaschuk O, Milos RI, Konnerth A. 2006. Targeted bulk-loading of fluorescent indicators for two-photon brain imaging in vivo. *Nat Protoc* 1: 380-6

Garaschuk O, Schneggenburger R, Schirra C, Tempia F, Konnerth A. 1996. Fractional Ca2+ currents through somatic and dendritic glutamate receptor channels of rat hippocampal CA1 pyramidal neurones. *J Physiol* 491 (Pt 3): 757-72

Garcia-Munoz M, Patino P, Masliah E, Young SJ, Groves PM. 1996. Glutamate-dependent long-term presynaptic changes in corticostriatal excitability. *Neuroscience* 73: 109-19

Garcia-Munoz M, Young SJ, Groves PM. 1991. Terminal excitability of the corticostriatal pathway. I. Regulation by dopamine receptor stimulation. *Brain Res* 551: 195-206

Gelperin A, Flores J. 1997. Vital staining from dye-coated microprobes identifies new olfactory interneurons for optical and electrical recording. *J Neurosci Methods* 72: 97-108

Gerdeman G, Lovinger DM. 2001. CB1 cannabinoid receptor inhibits synaptic release of glutamate in rat dorsolateral striatum. *J Neurophysiol* 85: 468-71

Gerfen CR. 1984. The neostriatal mosaic: compartmentalization of corticostriatal input and striatonigral output systems. *Nature* 311: 461-4

Gerfen CR. 1985. The neostriatal mosaic. I. Compartmental organization of projections from the striatum to the substantia nigra in the rat. *J Comp Neurol* 236: 454-76

Gerfen CR. 1992a. The neostriatal mosaic: multiple levels of compartmental organization. *Trends Neurosci* 15: 133-9

Gerfen CR. 1992b. The neostriatal mosaic: multiple levels of compartmental organization. *J Neural Transm Suppl* 36: 43-59

Gerfen CR, Paletzki R, Heintz N. 2013. GENSAT BAC cre-recombinase driver lines to study the functional organization of cerebral cortical and basal ganglia circuits. *Neuron* 80: 1368-83

Gerfen CR, Surmeier DJ. 2011. Modulation of striatal projection systems by dopamine. *Annu Rev Neurosci* 34: 441-66

Gerfen CR, Wilson CJ. 1996. The basal ganglia In *Handbook of Chemical Neuroanatomy*, ed. LW Swanson, A BjÖrklund, T HÖkfelt, pp. 371-468: Elsevier

Gertler TS, Chan CS, Surmeier DJ. 2008. Dichotomous anatomical properties of adult striatal medium spiny neurons. *J Neurosci* 28: 10814-24

Gesi M, Santinami A, Ruffoli R, Conti G, Fornai F. 2001. Novel aspects of dopamine oxidative metabolism (confounding outcomes take place of certainties). *Pharmacol Toxicol* 89: 217-24

Gimenez-Amaya JM, McFarland NR, de las Heras S, Haber SN. 1995. Organization of thalamic projections to the ventral striatum in the primate. *J Comp Neurol* 354: 127-49

Giovannucci A, Friedrich J, Gunn P, Kalfon J, Brown BL, et al. 2019. CaImAn an open source tool for scalable calcium imaging data analysis. *Elife* 8

Gittis AH, Kreitzer AC. 2012. Striatal microcircuitry and movement disorders. *Trends Neurosci* 35: 557-64

Gittis AH, Nelson AB, Thwin MT, Palop JJ, Kreitzer AC. 2010. Distinct roles of GABAergic interneurons in the regulation of striatal output pathways. *J Neurosci* 30: 2223-34

Gong S, Doughty M, Harbaugh CR, Cummins A, Hatten ME, et al. 2007. Targeting Cre recombinase to specific neuron populations with bacterial artificial chromosome constructs. *J Neurosci* 27: 9817-23

Gotti C, Clementi F, Fornari A, Gaimarri A, Guiducci S, et al. 2009. Structural and functional diversity of native brain neuronal nicotinic receptors. *Biochem Pharmacol* 78: 703-11

Gotz T, Kraushaar U, Geiger J, Lubke J, Berger T, Jonas P. 1997. Functional properties of AMPA and NMDA receptors expressed in identified types of basal ganglia neurons. *J Neurosci* 17: 204-15

Graveland GA, DiFiglia M. 1985. The frequency and distribution of medium-sized neurons with indented nuclei in the primate and rodent neostriatum. *Brain Res* 327: 307-11

Graveland GA, Williams RS, DiFiglia M. 1985. A Golgi study of the human neostriatum: neurons and afferent fibers. *J Comp Neurol* 234: 317-33

Graybiel AM. 1998. The basal ganglia and chunking of action repertoires. *Neurobiol Learn Mem* 70: 119-36

Graybiel AM, Aosaki T, Flaherty AW, Kimura M. 1994. The basal ganglia and adaptive motor control. *Science* 265: 1826-31

Graybiel AM, Ragsdale CW, Jr. 1978. Histochemically distinct compartments in the striatum of human, monkeys, and cat demonstrated by acetylthiocholinesterase staining. *Proc Natl Acad Sci U S A* 75: 5723-6

Graybiel AM, Ragsdale CW, Jr., Yoneoka ES, Elde RP. 1981. An immunohistochemical study of enkephalins and other neuropeptides in the striatum of the cat with evidence that the opiate peptides are arranged to form mosaic patterns in register with the striosomal compartments visible by acetylcholinesterase staining. *Neuroscience* 6: 377-97

Graybiel AM, Rauch SL. 2000. Toward a neurobiology of obsessive-compulsive disorder. *Neuron* 28: 343-7

Greenberg DS, Houweling AR, Kerr JN. 2008. Population imaging of ongoing neuronal activity in the visual cortex of awake rats. *Nat Neurosci* 11: 749-51

Greif GJ, Lin YJ, Liu JC, Freedman JE. 1995. Dopamine-modulated potassium channels on rat striatal neurons: specific activation and cellular expression. *J Neurosci* 15: 4533-44

Grienberger C, Adelsberger H, Stroh A, Milos RI, Garaschuk O, et al. 2012. Sound-evoked network calcium transients in mouse auditory cortex in vivo. *J Physiol* 590: 899-918

Grienberger C, Konnerth A. 2012. Imaging calcium in neurons. *Neuron* 73: 862-85

Grinvald A, Cohen LB, Lesher S, Boyle MB. 1981. Simultaneous optical monitoring of activity of many neurons in invertebrate ganglia using a 124-element photodiode array. *J Neurophysiol* 45: 829-40

Groenewegen HJ. 2003. The basal ganglia and motor control. *Neural Plast* 10: 107-20

Groenewegen HJ, Berendse HW. 1994. The specificity of the 'nonspecific' midline and intralaminar thalamic nuclei. *Trends Neurosci* 17: 52-7

Groenewegen HJ, Berendse HW, Wolters JG, Lohman AH. 1990. The anatomical relationship of the prefrontal cortex with the striatopallidal system, the thalamus and the amygdala: evidence for a parallel organization. *Prog Brain Res* 85: 95-116; discussion 16-8

Grynkiewicz G, Poenie M, Tsien RY. 1985. A new generation of Ca2+ indicators with greatly improved fluorescence properties. *J Biol Chem* 260: 3440-50

Gubellini P, Pisani A, Centonze D, Bernardi G, Calabresi P. 2004. Metabotropic glutamate receptors and striatal synaptic plasticity: implications for neurological diseases. *Prog Neurobiol* 74: 271-300

Gubellini P, Saulle E, Centonze D, Bonsi P, Pisani A, et al. 2001. Selective involvement of mGlu1 receptors in corticostriatal LTD. *Neuropharmacology* 40: 839-46

Gubellini P, Saulle E, Centonze D, Costa C, Tropepi D, et al. 2003. Corticostriatal LTP requires combined mGluR1 and mGluR5 activation. *Neuropharmacology* 44: 8-16

Haber SN, McFarland NR. 1999. The concept of the ventral striatum in nonhuman primates. *Ann N Y Acad Sci* 877: 33-48

Haga T. 2013. Molecular properties of muscarinic acetylcholine receptors. *Proc Jpn Acad Ser B Phys Biol Sci* 89: 226-56

Hakansson K, Galdi S, Hendrick J, Snyder G, Greengard P, Fisone G. 2006. Regulation of phosphorylation of the GluR1 AMPA receptor by dopamine D2 receptors. *J Neurochem* 96: 482-8

Hartmann E. 1970. The D-state and norepinephrine-dependent systems. *Int Psychiatry Clin* 7: 308-28

Heal DJ, Smith SL, Gosden J, Nutt DJ. 2013. Amphetamine, past and present--a pharmacological and clinical perspective. *J Psychopharmacol* 27: 479-96

Hedreen JC, DeLong MR. 1991. Organization of striatopallidal, striatonigral, and nigrostriatal projections in the macaque. *J Comp Neurol* 304: 569-95

Heim N, Griesbeck O. 2004. Genetically encoded indicators of cellular calcium dynamics based on troponin C and green fluorescent protein. *J Biol Chem* 279: 14280-6

Heiman M, Schaefer A, Gong S, Peterson JD, Day M, et al. 2008. A translational profiling approach for the molecular characterization of CNS cell types. *Cell* 135: 738-48

Helmchen F, Fee MS, Tank DW, Denk W. 2001. A miniature head-mounted two-photon microscope. high-resolution brain imaging in freely moving animals. *Neuron* 31: 903-12

Helmchen F, Imoto K, Sakmann B. 1996. Ca2+ buffering and action potential-evoked Ca2+ signaling in dendrites of pyramidal neurons. *Biophys J* 70: 1069-81

Herkenham M, Pert CB. 1981. Mosaic distribution of opiate receptors, parafascicular projections and acetylcholinesterase in rat striatum. *Nature* 291: 415-8

Hernandez-Lopez S, Tkatch T, Perez-Garci E, Galarraga E, Bargas J, et al. 2000. D2 dopamine receptors in striatal medium spiny neurons reduce L-type Ca2+ currents and excitability via a novel PLC[beta]1-IP3-calcineurin-signaling cascade. *J Neurosci* 20: 8987-95

Herve D, Rogard M, Levi-Strauss M. 1995. Molecular analysis of the multiple Golf alpha subunit mRNAs in the rat brain. *Brain Res Mol Brain Res* 32: 125-34

Higley MJ, Sabatini BL. 2008. Calcium signaling in dendrites and spines: practical and functional considerations. *Neuron* 59: 902-13

Hikida T, Kaneko S, Isobe T, Kitabatake Y, Watanabe D, et al. 2001. Increased sensitivity to cocaine by cholinergic cell ablation in nucleus accumbens. *Proc Natl Acad Sci U S A* 98: 13351-4

Hilario M, Holloway T, Jin X, Costa RM. 2012. Different dorsal striatum circuits mediate action discrimination and action generalization. *Eur J Neurosci* 35: 1105-14

Hoebel BG. 1977. Pharmacologic control of feeding. *Annu Rev Pharmacol Toxicol* 17: 605-21

Holekamp TF, Turaga D, Holy TE. 2008. Fast three-dimensional fluorescence imaging of activity in neural populations by objective-coupled planar illumination microscopy. *Neuron* 57: 661-72

Holtzman SG, Jewett RE. 1971. The role of brain norepinephrine in the anorexic effects of dextroamphetamine and monoamine oxidase inhibitors in the rat. *Psychopharmacologia* 22: 151-61

Ibanez-Sandoval O, Tecuapetla F, Unal B, Shah F, Koos T, Tepper JM. 2010. Electrophysiological and morphological characteristics and synaptic connectivity of tyrosine hydroxylase-expressing neurons in adult mouse striatum. *J Neurosci* 30: 6999-7016

Ibanez-Sandoval O, Xenias HS, Tepper JM, Koos T. 2015. Dopaminergic and cholinergic modulation of striatal tyrosine hydroxylase interneurons. *Neuropharmacology* 95: 468-76

Ikemoto S. 2007. Dopamine reward circuitry: two projection systems from the ventral midbrain to the nucleus accumbens-olfactory tubercle complex. *Brain Res Rev* 56: 27-78

Inoue M. 2021. Genetically encoded calcium indicators to probe complex brain circuit dynamics in vivo. *Neurosci Res* 169: 2-8

Iversen LL, Glowinski J, Axelrod J. 1965. The uptake and storage of H3-norepinephrine in the reserpine-pretreated rat heart. *J Pharmacol Exp Ther* 150: 173-83

Jaffe DB, Johnston D, Lasser-Ross N, Lisman JE, Miyakawa H, Ross WN. 1992. The spread of Na+ spikes determines the pattern of dendritic Ca2+ entry into hippocampal neurons. *Nature* 357: 244-6

Jia H, Rochefort NL, Chen X, Konnerth A. 2011. In vivo two-photon imaging of sensory-evoked dendritic calcium signals in cortical neurons. *Nat Protoc* 6: 28-35

Jin X, Costa RM. 2015. Shaping action sequences in basal ganglia circuits. *Curr Opin Neurobiol* 33: 188-96

Jin X, Tecuapetla F, Costa RM. 2014. Basal ganglia subcircuits distinctively encode the parsing and concatenation of action sequences. *Nat Neurosci* 17: 423-30

Joel D, Weiner I. 2000. The connections of the dopaminergic system with the striatum in rats and primates: an analysis with respect to the functional and compartmental organization of the striatum. *Neuroscience* 96: 451-74

Johnson TN, Rosvold HE. 1971. Topographic projections on the globus pallidus and the substantia nigra of selectively placed lesions in the precommissural caudate nucleus and putamen in the monkey. *Exp Neurol* 33: 584-96

Judkewitz B, Rizzi M, Kitamura K, Hausser M. 2009. Targeted single-cell electroporation of mammalian neurons in vivo. *Nat Protoc* 4: 862-9

Jung JC, Mehta AD, Aksay E, Stepnoski R, Schnitzer MJ. 2004. In vivo mammalian brain imaging using one- and two-photon fluorescence microendoscopy. *J Neurophysiol* 92: 3121-33

Kahn L, Alonso G, Robbe D, Bockaert J, Manzoni OJ. 2001. Group 2 metabotropic glutamate receptors induced long term depression in mouse striatal slices. *Neurosci Lett* 316: 178-82

Kaneko S, Hikida T, Watanabe D, Ichinose H, Nagatsu T, et al. 2000. Synaptic integration mediated by striatal cholinergic interneurons in basal ganglia function. *Science* 289: 633-7

Kawaguchi Y. 1992. Large aspiny cells in the matrix of the rat neostriatum in vitro: physiological identification, relation to the compartments and excitatory postsynaptic currents. *J Neurophysiol* 67: 1669-82

Kelley AE, Delfs JM. 1991. Dopamine and conditioned reinforcement. I. Differential effects of amphetamine microinjections into striatal subregions. *Psychopharmacology (Berl)* 103: 187-96

Kelly RM, Strick PL. 2004. Macro-architecture of basal ganglia loops with the cerebral cortex: use of rabies virus to reveal multisynaptic circuits. *Prog Brain Res* 143: 449-59

Kerkerian L, Dusticier N, Nieoullon A. 1987. Modulatory effect of dopamine on high-affinity glutamate uptake in the rat striatum. *J Neurochem* 48: 1301-6

Kerr JN, Wickens JR. 2001. Dopamine D-1/D-5 receptor activation is required for long-term potentiation in the rat neostriatum in vitro. *J Neurophysiol* 85: 117-24

Kim P, Puoris'haag M, Cote D, Lin CP, Yun SH. 2008. In vivo confocal and multiphoton microendoscopy. *J Biomed Opt* 13: 010501

Kitai ST, Surmeier DJ. 1993. Cholinergic and dopaminergic modulation of potassium conductances in neostriatal neurons. *Adv Neurol* 60: 40-52

Kitamura K, Judkewitz B, Kano M, Denk W, Hausser M. 2008. Targeted patch-clamp recordings and single-cell electroporation of unlabeled neurons in vivo. *Nat Methods* 5: 61-7

Kitano K, Cateau H, Kaneda K, Nambu A, Takada M, Fukai T. 2002. Two-state membrane potential transitions of striatal spiny neurons as evidenced by numerical simulations and electrophysiological recordings in awake monkeys. *J Neurosci* 22: RC230

Klaus A, Martins GJ, Paixao VB, Zhou P, Paninski L, Costa RM. 2017. The Spatiotemporal Organization of the Striatum Encodes Action Space. *Neuron* 96: 949

Koester HJ, Sakmann B. 1998. Calcium dynamics in single spines during coincident pre- and postsynaptic activity depend on relative timing of back-propagating action potentials and subthreshold excitatory postsynaptic potentials. *Proc Natl Acad Sci U S A* 95: 9596-601

Kombian SB, Malenka RC. 1994. Simultaneous LTP of non-NMDA- and LTD of NMDA-receptor-mediated responses in the nucleus accumbens. *Nature* 368: 242-6

Kovalchuk Y, Eilers J, Lisman J, Konnerth A. 2000. NMDA receptor-mediated subthreshold Ca(2+) signals in spines of hippocampal neurons. *J Neurosci* 20: 1791-9

Kozloski J, Hamzei-Sichani F, Yuste R. 2001. Stereotyped position of local synaptic targets in neocortex. *Science* 293: 868-72

Krack P, Hariz MI, Baunez C, Guridi J, Obeso JA. 2010. Deep brain stimulation: from neurology to psychiatry? *Trends Neurosci* 33: 474-84

Kravitz AV, Freeze BS, Parker PR, Kay K, Thwin MT, et al. 2010. Regulation of parkinsonian motor behaviours by optogenetic control of basal ganglia circuitry. *Nature* 466: 622-6

Kreitzer AC. 2009. Physiology and pharmacology of striatal neurons. *Annu Rev Neurosci* 32: 127-47

Kreitzer AC, Malenka RC. 2008. Striatal plasticity and basal ganglia circuit function. *Neuron* 60: 543-54

Kulagina NV, Zigmond MJ, Michael AC. 2001. Glutamate regulates the spontaneous and evoked release of dopamine in the rat striatum. *Neuroscience* 102: 121-8

Kupchik YM, Brown RM, Heinsbroek JA, Lobo MK, Schwartz DJ, Kalivas PW. 2015. Coding the direct/indirect pathways by D1 and D2 receptors is not valid for accumbens projections. *Nat Neurosci* 18: 1230-2

Lanciego JL, Gonzalo N, Castle M, Sanchez-Escobar C, Aymerich MS, Obeso JA. 2004. Thalamic innervation of striatal and subthalamic neurons projecting to the rat entopeduncular nucleus. *Eur J Neurosci* 19: 1267-77

Lanciego JL, Luquin N, Obeso JA. 2012. Functional neuroanatomy of the basal ganglia. *Cold Spring Harb Perspect Med* 2: a009621

Lapper SR, Smith Y, Sadikot AF, Parent A, Bolam JP. 1992. Cortical input to parvalbumin-immunoreactive neurones in the putamen of the squirrel monkey. *Brain Res* 580: 215-24

Laties VG, Weiss B. 1966. Influence of drugs on behavior controlled by internal and external stimuli. *J Pharmacol Exp Ther* 152: 388-96

Lee SP, So CH, Rashid AJ, Varghese G, Cheng R, et al. 2004. Dopamine D1 and D2 receptor Co-activation generates a novel phospholipase C-mediated calcium signal. *J Biol Chem* 279: 35671-8

Lei W, Jiao Y, Del Mar N, Reiner A. 2004. Evidence for differential cortical input to direct pathway versus indirect pathway striatal projection neurons in rats. *J Neurosci* 24: 8289-99

Levene MJ, Dombeck DA, Kasischke KA, Molloy RP, Webb WW. 2004. In vivo multiphoton microscopy of deep brain tissue. *J Neurophysiol* 91: 1908-12

Lichtman JW, Conchello JA. 2005. Fluorescence microscopy. *Nat Methods* 2: 910-9

Liles SL. 1985. Activity of neurons in putamen during active and passive movements of wrist. *J Neurophysiol* 53: 217-36

Lilley CE, Branston RH, Coffin RS. 2001. Herpes simplex virus vectors for the nervous system. *Curr Gene Ther* 1: 339-58

Liu SJ, Zukin RS. 2007. Ca2+-permeable AMPA receptors in synaptic plasticity and neuronal death. *Trends Neurosci* 30: 126-34

Lobo MK, Karsten SL, Gray M, Geschwind DH, Yang XW. 2006. FACS-array profiling of striatal projection neuron subtypes in juvenile and adult mouse brains. *Nat Neurosci* 9: 443-52

Looger LL, Griesbeck O. 2012. Genetically encoded neural activity indicators. *Curr Opin Neurobiol* 22: 18-23

Lovinger DM, McCool BA. 1995. Metabotropic glutamate receptor-mediated presynaptic depression at corticostriatal synapses involves mGLuR2 or 3. *J Neurophysiol* 73: 1076-83

Lovinger DM, Partridge JG, Tang KC. 2003. Plastic control of striatal glutamatergic transmission by ensemble actions of several neurotransmitters and targets for drugs of abuse. *Ann N Y Acad Sci* 1003: 226-40

Lovinger DM, Tyler E. 1996. Synaptic transmission and modulation in the neostriatum. *Int Rev Neurobiol* 39: 77-111

Lovinger DM, Tyler EC, Merritt A. 1993. Short- and long-term synaptic depression in rat neostriatum. *J Neurophysiol* 70: 1937-49

Lu J, Li C, Singh-Alvarado J, Zhou ZC, Frohlich F, et al. 2018. MIN1PIPE: A Miniscope 1-Photon-Based Calcium Imaging Signal Extraction Pipeline. *Cell Rep* 23: 3673-84

Lu XY, Ghasemzadeh MB, Kalivas PW. 1998. Expression of D1 receptor, D2 receptor, substance P and enkephalin messenger RNAs in the neurons projecting from the nucleus accumbens. *Neuroscience* 82: 767-80

Ma S, Pawlak AP, Cho J, Root DH, Barker DJ, West MO. 2013. Amphetamine's dose-dependent effects on dorsolateral striatum sensorimotor neuron firing. *Behav Brain Res* 244: 152-61

Madisen L, Garner AR, Shimaoka D, Chuong AS, Klapoetke NC, et al. 2015. Transgenic mice for intersectional targeting of neural sensors and effectors with high specificity and performance. *Neuron* 85: 942-58

Mahon S, Deniau JM, Charpier S. 2004. Corticostriatal plasticity: life after the depression. *Trends Neurosci* 27: 460-7

Mank M, Santos AF, Direnberger S, Mrsic-Flogel TD, Hofer SB, et al. 2008. A genetically encoded calcium indicator for chronic in vivo two-photon imaging. *Nat Methods* 5: 805-11

Mao BQ, Hamzei-Sichani F, Aronov D, Froemke RC, Yuste R. 2001. Dynamics of spontaneous activity in neocortical slices. *Neuron* 32: 883-98

Margrie TW, Brecht M, Sakmann B. 2002. In vivo, low-resistance, whole-cell recordings from neurons in the anaesthetized and awake mammalian brain. *Pflugers Arch* 444: 491-8

Margrie TW, Meyer AH, Caputi A, Monyer H, Hasan MT, et al. 2003. Targeted whole-cell recordings in the mammalian brain in vivo. *Neuron* 39: 911-8

Markowitz JE, Gillis WF, Beron CC, Neufeld SQ, Robertson K, et al. 2018. The Striatum Organizes 3D Behavior via Moment-to-Moment Action Selection. *Cell* 174: 44-58 e17

Marsden CD, Obeso JA. 1994. The functions of the basal ganglia and the paradox of stereotaxic surgery in Parkinson's disease. *Brain* 117 (Pt 4): 877-97

Mathis A, Mamidanna P, Cury KM, Abe T, Murthy VN, et al. 2018. DeepLabCut: markerless pose estimation of user-defined body parts with deep learning. *Nat Neurosci* 21: 1281-89

Maurice N, Mercer J, Chan CS, Hernandez-Lopez S, Held J, et al. 2004. D2 dopamine receptor-mediated modulation of voltage-dependent Na+ channels reduces autonomous activity in striatal cholinergic interneurons. *J Neurosci* 24: 10289-301

McBride WJ, Murphy JM, Ikemoto S. 1999. Localization of brain reinforcement mechanisms: intracranial self-administration and intracranial place-conditioning studies. *Behav Brain Res* 101: 129-52

McFarland NR, Haber SN. 2000. Convergent inputs from thalamic motor nuclei and frontal cortical areas to the dorsal striatum in the primate. *J Neurosci* 20: 3798-813

Miczek KA, Gold LH. 1983. Ethological analysis of amphetamine action on social behavior in squirrel monkeys (Saimiri sciureus). *Prog Clin Biol Res* 131: 137-55

Mink JW. 2003. The Basal Ganglia and involuntary movements: impaired inhibition of competing motor patterns. *Arch Neurol* 60: 1365-8

Missale C, Nash SR, Robinson SW, Jaber M, Caron MG. 1998. Dopamine receptors: from structure to function. *Physiol Rev* 78: 189-225

Mitchell PR, Doggett NS. 1980. Modulation of striatal [3H]-glutamic acid release by dopaminergic drugs. *Life Sci* 26: 2073-81

Monahan PE, Samulski RJ. 2000. Adeno-associated virus vectors for gene therapy: more pros than cons? *Mol Med Today* 6: 433-40

Mori A, Takahashi T, Miyashita Y, Kasai H. 1994. Two distinct glutamatergic synaptic inputs to striatal medium spiny neurones of neonatal rats and paired-pulse depression. *J Physiol* 476: 217-28

Morishima M, Kawaguchi Y. 2006. Recurrent connection patterns of corticostriatal pyramidal cells in frontal cortex. *J Neurosci* 26: 4394-405

Morris G, Arkadir D, Nevet A, Vaadia E, Bergman H. 2004. Coincident but distinct messages of midbrain dopamine and striatal tonically active neurons. *Neuron* 43: 133-43

Mukamel EA, Nimmerjahn A, Schnitzer MJ. 2009. Automated analysis of cellular signals from large-scale calcium imaging data. *Neuron* 63: 747-60

Murayama M, Perez-Garci E, Luscher HR, Larkum ME. 2007. Fiberoptic system for recording dendritic calcium signals in layer 5 neocortical pyramidal cells in freely moving rats. *J Neurophysiol* 98: 1791-805

Nagai T, Yamada S, Tominaga T, Ichikawa M, Miyawaki A. 2004. Expanded dynamic range of fluorescent indicators for Ca(2+) by circularly permuted yellow fluorescent proteins. *Proc Natl Acad Sci U S A* 101: 10554-9

Nagayama S, Zeng S, Xiong W, Fletcher ML, Masurkar AV, et al. 2007. In vivo simultaneous tracing and Ca(2+) imaging of local neuronal circuits. *Neuron* 53: 789-803

Nakai J, Ohkura M, Imoto K. 2001. A high signal-to-noise Ca(2+) probe composed of a single green fluorescent protein. *Nat Biotechnol* 19: 137-41

Nathanson JL, Jappelli R, Scheeff ED, Manning G, Obata K, et al. 2009. Short Promoters in Viral Vectors Drive Selective Expression in Mammalian Inhibitory Neurons, but do not Restrict Activity to Specific Inhibitory Cell-Types. *Front Neural Circuits* 3: 19

Nathanson NM. 2000. A multiplicity of muscarinic mechanisms: enough signaling pathways to take your breath away. *Proc Natl Acad Sci U S A* 97: 6245-7

Nauta WJ, Mehler WR. 1966. Projections of the lentiform nucleus in the monkey. *Brain Res* 1: 3-42

Nevian T, Helmchen F. 2007. Calcium indicator loading of neurons using single-cell electroporation. *Pflugers Arch* 454: 675-88

Nevian T, Sakmann B. 2006. Spine Ca2+ signaling in spike-timing-dependent plasticity. *J Neurosci* 26: 11001-13

Nishi K, Atkins PT, Surmeier DJ, Kitai ST. 1990. Muscarinic regulation of cyclic AMP metabolism in rat neostriatal cultures. *Brain Res* 534: 111-6

Niswender CM, Conn PJ. 2010. Metabotropic glutamate receptors: physiology, pharmacology, and disease. *Annu Rev Pharmacol Toxicol* 50: 295-322

O'Donnell P, Grace AA. 1993. Dopaminergic modulation of dye coupling between neurons in the core and shell regions of the nucleus accumbens. *J Neurosci* 13: 3456-71

Obeso JA, Rodriguez-Oroz MC, Rodriguez M, Arbizu J, Gimenez-Amaya JM. 2002. The basal ganglia and disorders of movement: pathophysiological mechanisms. *News Physiol Sci* 17: 51-5

Obeso JA, Rodriguez-Oroz MC, Rodriguez M, Lanciego JL, Artieda J, et al. 2000. Pathophysiology of the basal ganglia in Parkinson's disease. *Trends Neurosci* 23: S8-19

Oh J, Lee C, Kaang BK. 2019. Imaging and analysis of genetically encoded calcium indicators linking neural circuits and behaviors. *Korean J Physiol Pharmacol* 23: 237-49

Oheim M, Beaurepaire E, Chaigneau E, Mertz J, Charpak S. 2001. Two-photon microscopy in brain tissue: parameters influencing the imaging depth. *J Neurosci Methods* 111: 29-37

Ohki K, Chung S, Ch'ng YH, Kara P, Reid RC. 2005. Functional imaging with cellular resolution reveals precise micro-architecture in visual cortex. *Nature* 433: 597-603

Oldenburg IA, Sabatini BL. 2015. Antagonistic but Not Symmetric Regulation of Primary Motor Cortex by Basal Ganglia Direct and Indirect Pathways. *Neuron* 86: 1174-81

Olson L, Seiger A, Fuxe K. 1972. Heterogeneity of striatal and limbic dopamine innervation: highly fluorescent islands in developing and adult rats. *Brain Res* 44: 283-8

Olson PA, Tkatch T, Hernandez-Lopez S, Ulrich S, Ilijic E, et al. 2005. G-protein-coupled receptor modulation of striatal CaV1.3 L-type Ca2+ channels is dependent on a Shank-binding domain. *J Neurosci* 25: 1050-62

Osakada F, Mori T, Cetin AH, Marshel JH, Virgen B, Callaway EM. 2011. New rabies virus variants for monitoring and manipulating activity and gene expression in defined neural circuits. *Neuron* 71: 617-31

Oswald I. 1968. Drugs and sleep. *Pharmacol Rev* 20: 273-303

Packard MG, Knowlton BJ. 2002. Learning and memory functions of the Basal Ganglia. *Annu Rev Neurosci* 25: 563-93

Paredes RM, Etzler JC, Watts LT, Zheng W, Lechleiter JD. 2008. Chemical calcium indicators. *Methods* 46: 143-51

Parent A. 1990. Extrinsic connections of the basal ganglia. *Trends Neurosci* 13: 254-8

Parent A, Bouchard C, Smith Y. 1984. The striatopallidal and striatonigral projections: two distinct fiber systems in primate. *Brain Res* 303: 385-90

Parent A, Hazrati LN. 1995. Functional anatomy of the basal ganglia. II. The place of subthalamic nucleus and external pallidum in basal ganglia circuitry. *Brain Res Brain Res Rev* 20: 128-54

Parker JG, Marshall JD, Ahanonu B, Wu YW, Kim TH, et al. 2018. Diametric neural ensemble dynamics in parkinsonian and dyskinetic states. *Nature* 557: 177-82

Partridge JG, Tang KC, Lovinger DM. 2000. Regional and postnatal heterogeneity of activity-dependent long-term changes in synaptic efficacy in the dorsal striatum. *J Neurophysiol* 84: 1422-9

Perreault ML, Hasbi A, Alijaniaram M, Fan T, Varghese G, et al. 2010. The dopamine D1-D2 receptor heteromer localizes in dynorphin/enkephalin neurons: increased high affinity state following amphetamine and in schizophrenia. *J Biol Chem* 285: 36625-34

Perreault ML, Hasbi A, O'Dowd BF, George SR. 2011. The dopamine d1-d2 receptor heteromer in striatal medium spiny neurons: evidence for a third distinct neuronal pathway in Basal Ganglia. *Front Neuroanat* 5: 31

Perreault ML, O'Dowd BF, George SR. 2014. Dopamine D(1)-D(2) receptor heteromer regulates signaling cascades involved in addiction: potential relevance to adolescent drug susceptibility. *Dev Neurosci* 36: 287-96

Pert CB, Kuhar MJ, Snyder SH. 1976. Opiate receptor: autoradiographic localization in rat brain. *Proc Natl Acad Sci U S A* 73: 3729-33

Pisani A, Bernardi G, Ding J, Surmeier DJ. 2007. Re-emergence of striatal cholinergic interneurons in movement disorders. *Trends Neurosci* 30: 545-53

Pisani A, Bonsi P, Centonze D, Calabresi P, Bernardi G. 2000. Activation of D2-like dopamine receptors reduces synaptic inputs to striatal cholinergic interneurons. *J Neurosci* 20: RC69

Planert H, Szydlowski SN, Hjorth JJ, Grillner S, Silberberg G. 2010. Dynamics of synaptic transmission between fast-spiking interneurons and striatal projection neurons of the direct and indirect pathways. *J Neurosci* 30: 3499-507

Pnevmatikakis EA, Soudry D, Gao Y, Machado TA, Merel J, et al. 2016. Simultaneous Denoising, Deconvolution, and Demixing of Calcium Imaging Data. *Neuron* 89: 285-99

Pologruto TA, Yasuda R, Svoboda K. 2004. Monitoring neural activity and [Ca2+] with genetically encoded Ca2+ indicators. *J Neurosci* 24: 9572-9

Popoli P, Pintor A, Domenici MR, Frank C, Tebano MT, et al. 2002. Blockade of striatal adenosine A2A receptor reduces, through a presynaptic mechanism, quinolinic acid-induced excitotoxicity: possible relevance to neuroprotective interventions in neurodegenerative diseases of the striatum. *J Neurosci* 22: 1967-75

Pothos EN, Larsen KE, Krantz DE, Liu Y, Haycock JW, et al. 2000. Synaptic vesicle transporter expression regulates vesicle phenotype and quantal size. *J Neurosci* 20: 7297-306

Prakriya M, Lewis RS. 2015. Store-Operated Calcium Channels. *Physiol Rev* 95: 1383-436

Prensa L, Gimenez-Amaya JM, Parent A. 1999. Chemical heterogeneity of the striosomal compartment in the human striatum. *J Comp Neurol* 413: 603-18

Ragozzino ME. 2007. The contribution of the medial prefrontal cortex, orbitofrontal cortex, and dorsomedial striatum to behavioral flexibility. *Ann N Y Acad Sci* 1121: 355-75

Ragsdale CW, Jr., Graybiel AM. 1988. Fibers from the basolateral nucleus of the amygdala selectively innervate striosomes in the caudate nucleus of the cat. *J Comp Neurol* 269: 506-22

Raju DV, Shah DJ, Wright TM, Hall RA, Smith Y. 2006. Differential synaptology of vGluT2-containing thalamostriatal afferents between the patch and matrix compartments in rats. *J Comp Neurol* 499: 231-43

Ramos C, Roberts JB, Jasso KR, Ten Eyck TW, Everett T, et al. 2021. Neuron-specific cilia loss differentially alters locomotor responses to amphetamine in mice. *J Neurosci Res* 99: 827-42

Ramsey IS, Delling M, Clapham DE. 2006. An introduction to TRP channels. *Annu Rev Physiol* 68: 619-47

Randrup A, Munkvad I. 1966. Role of catecholamines in the amphetamine excitatory response. *Nature* 211: 540

Rashid AJ, So CH, Kong MM, Furtak T, El-Ghundi M, et al. 2007. D1-D2 dopamine receptor heterooligomers with unique pharmacology are coupled to rapid activation of Gq/11 in the striatum. *Proc Natl Acad Sci U S A* 104: 654-9

Rech RH. 1966. Amphetamine effects on poor performance of rats in a shuttle-box. *Psychopharmacologia* 9: 110-7

Rechtschaffen A, Maron L. 1964. The Effect of Amphetamine on the Sleep Cycle. *Electroencephalogr Clin Neurophysiol* 16: 438-45

Reiner A, Hart NM, Lei W, Deng Y. 2010. Corticostriatal projection neurons - dichotomous types and dichotomous functions. *Front Neuroanat* 4: 142

Reiner A, Jiao Y, Del Mar N, Laverghetta AV, Lei WL. 2003. Differential morphology of pyramidal tract-type and intratelencephalically projecting-type corticostriatal neurons and their intrastriatal terminals in rats. *J Comp Neurol* 457: 420-40

Reynolds JN, Hyland BI, Wickens JR. 2001. A cellular mechanism of reward-related learning. *Nature* 413: 67-70

Reynolds JN, Wickens JR. 2000. Substantia nigra dopamine regulates synaptic plasticity and membrane potential fluctuations in the rat neostriatum, in vivo. *Neuroscience* 99: 199-203

Robinson DS, Sourkes TL, Nies A, Harris LS, Spector S, et al. 1977. Monoamine metabolism in human brain. *Arch Gen Psychiatry* 34: 89-92

Rogers M, Dani JA. 1995. Comparison of quantitative calcium flux through NMDA, ATP, and ACh receptor channels. *Biophys J* 68: 501-6

Ross WN, Werman R. 1987. Mapping calcium transients in the dendrites of Purkinje cells from the guinea-pig cerebellum in vitro. *J Physiol* 389: 319-36

Rothman RB, Baumann MH. 2003. Monoamine transporters and psychostimulant drugs. *Eur J Pharmacol* 479: 23-40

Rowlands GF, Roberts PJ. 1980. Activation of dopamine receptors inhibits calcium-dependent glutamate release from cortico--striatal terminals in vitro. *Eur J Pharmacol* 62: 241-2

Runyan CA, Schummers J, Van Wart A, Kuhlman SJ, Wilson NR, et al. 2010. Response features of parvalbumin-expressing interneurons suggest precise roles for subtypes of inhibition in visual cortex. *Neuron* 67: 847-57

Russo SJ, Nestler EJ. 2013. The brain reward circuitry in mood disorders. *Nat Rev Neurosci* 14: 609-25

Sabatini BL, Oertner TG, Svoboda K. 2002. The life cycle of Ca(2+) ions in dendritic spines. *Neuron* 33: 439-52

Salery M, Trifilieff P, Caboche J, Vanhoutte P. 2020. From Signaling Molecules to Circuits and Behaviors: Cell-Type-Specific Adaptations to Psychostimulant Exposure in the Striatum. *Biol Psychiatry* 87: 944-53

Sasaki T, Takahashi N, Matsuki N, Ikegaya Y. 2008. Fast and accurate detection of action potentials from somatic calcium fluctuations. *J Neurophysiol* 100: 1668-76

Saunter CD, Semprini S, Buckley C, Mullins J, Girkin JM. 2012. Micro-endoscope for in vivo widefield high spatial resolution fluorescent imaging. *Biomed Opt Express* 3: 1274-8

Sawinski J, Wallace DJ, Greenberg DS, Grossmann S, Denk W, Kerr JN. 2009. Visually evoked activity in cortical cells imaged in freely moving animals. *Proc Natl Acad Sci U S A* 106: 19557-62

Scheel-Kruger J. 1971. Comparative studies of various amphetamine analogues demonstrating different interactions with the metabolism of the catecholamines in the brain. *Eur J Pharmacol* 14: 47-59

Scheuer T, Catterall WA. 2006. Control of neuronal excitability by phosphorylation and dephosphorylation of sodium channels. *Biochem Soc Trans* 34: 1299-302

Schiffmann SN, Fisone G, Moresco R, Cunha RA, Ferre S. 2007. Adenosine A2A receptors and basal ganglia physiology. *Prog Neurobiol* 83: 277-92

Schneggenburger R, Zhou Z, Konnerth A, Neher E. 1993. Fractional contribution of calcium to the cation current through glutamate receptor channels. *Neuron* 11: 133-43

Schultz W. 2006. Behavioral theories and the neurophysiology of reward. *Annu Rev Psychol* 57: 87-115

Schwaller B. 2010. Cytosolic Ca2+ buffers. *Cold Spring Harb Perspect Biol* 2: a004051

Sheintuch L, Rubin A, Brande-Eilat N, Geva N, Sadeh N, et al. 2017. Tracking the Same Neurons across Multiple Days in Ca(2+) Imaging Data. *Cell Rep* 21: 1102-15

Shen W, Flajolet M, Greengard P, Surmeier DJ. 2008. Dichotomous dopaminergic control of striatal synaptic plasticity. *Science* 321: 848-51

Shen W, Tian X, Day M, Ulrich S, Tkatch T, et al. 2007. Cholinergic modulation of Kir2 channels selectively elevates dendritic excitability in striatopallidal neurons. *Nat Neurosci* 10: 1458-66

Shevtsova Z, Malik JM, Michel U, Bahr M, Kugler S. 2005. Promoters and serotypes: targeting of adeno-associated virus vectors for gene transfer in the rat central nervous system in vitro and in vivo. *Exp Physiol* 90: 53-9

Shin JH, Song M, Paik SB, Jung MW. 2020. Spatial organization of functional clusters representing reward and movement information in the striatal direct and indirect pathways. *Proc Natl Acad Sci U S A* 117: 27004-15

Sidibe M, Smith Y. 1999. Thalamic inputs to striatal interneurons in monkeys: synaptic organization and co-localization of calcium binding proteins. *Neuroscience* 89: 1189-208

Silva AJ. 2017. Miniaturized two-photon microscope: seeing clearer and deeper into the brain. *Light Sci Appl* 6: e17104

Sitte HH, Freissmuth M. 2015. Amphetamines, new psychoactive drugs and the monoamine transporter cycle. *Trends Pharmacol Sci* 36: 41-50

Skeberdis VA, Chevaleyre V, Lau CG, Goldberg JH, Pettit DL, et al. 2006. Protein kinase A regulates calcium permeability of NMDA receptors. *Nat Neurosci* 9: 501-10

Smith CB. 1963. Enhancement by Reserpine and Alpha-Methyl Dopa of the Effects of D-Amphetamine Upon the Locomotor Activity of Mice. *J Pharmacol Exp Ther* 142: 343-50

Smith SJ, Augustine GJ. 1988. Calcium ions, active zones and synaptic transmitter release. *Trends Neurosci* 11: 458-64

Smith Y, Raju DV, Pare JF, Sidibe M. 2004. The thalamostriatal system: a highly specific network of the basal ganglia circuitry. *Trends Neurosci* 27: 520-7

Soares-Cunha C, Coimbra B, Sousa N, Rodrigues AJ. 2016. Reappraising striatal D1- and D2-neurons in reward and aversion. *Neurosci Biobehav Rev* 68: 370-86

Sobczyk A, Svoboda K. 2007. Activity-dependent plasticity of the NMDA-receptor fractional Ca2+ current. *Neuron* 53: 17-24

Sohya K, Kameyama K, Yanagawa Y, Obata K, Tsumoto T. 2007. GABAergic neurons are less selective to stimulus orientation than excitatory neurons in layer II/III of visual cortex, as revealed by in vivo functional Ca2+ imaging in transgenic mice. *J Neurosci* 27: 2145-9

Soudais C, Skander N, Kremer EJ. 2004. Long-term in vivo transduction of neurons throughout the rat CNS using novel helper-dependent CAV-2 vectors. *FASEB J* 18: 391-3

Sourkes TL. 1983. Monoamine oxidase: synthesis, metabolism and function. *Mod Probl Pharmacopsychiatry* 19: 1-14

Stark P, Tooty CW. 1967. Effects of amphetamines on eating elicited by hypothalamic stimulation. *J Pharmacol Exp Ther* 158: 272-8

Stefani A, Pisani A, Mercuri NB, Calabresi P. 1996. The modulation of calcium currents by the activation of mGluRs. Functional implications. *Mol Neurobiol* 13: 81-95

Stern EA, Jaeger D, Wilson CJ. 1998. Membrane potential synchrony of simultaneously recorded striatal spiny neurons in vivo. *Nature* 394: 475-8

Stoof JC, Kebabian JW. 1984. Two dopamine receptors: biochemistry, physiology and pharmacology. *Life Sci* 35: 2281-96

Stosiek C, Garaschuk O, Holthoff K, Konnerth A. 2003. In vivo two-photon calcium imaging of neuronal networks. *Proc Natl Acad Sci U S A* 100: 7319-24

Sullivan MR, Nimmerjahn A, Sarkisov DV, Helmchen F, Wang SS. 2005. In vivo calcium imaging of circuit activity in cerebellar cortex. *J Neurophysiol* 94: 1636-44

Sulzer D, Chen TK, Lau YY, Kristensen H, Rayport S, Ewing A. 1995. Amphetamine redistributes dopamine from synaptic vesicles to the cytosol and promotes reverse transport. *J Neurosci* 15: 4102-8

Sulzer D, Maidment NT, Rayport S. 1993. Amphetamine and other weak bases act to promote reverse transport of dopamine in ventral midbrain neurons. *J Neurochem* 60: 527-35

Sulzer D, Rayport S. 1990. Amphetamine and other psychostimulants reduce pH gradients in midbrain dopaminergic neurons and chromaffin granules: a mechanism of action. *Neuron* 5: 797-808

Sulzer D, Sonders MS, Poulsen NW, Galli A. 2005. Mechanisms of neurotransmitter release by amphetamines: a review. *Prog Neurobiol* 75: 406-33

Sung KW, Choi S, Lovinger DM. 2001. Activation of group I mGluRs is necessary for induction of long-term depression at striatal synapses. *J Neurophysiol* 86: 2405-12

Surmeier DJ, Bargas J, Hemmings HC, Jr., Nairn AC, Greengard P. 1995. Modulation of calcium currents by a D1 dopaminergic protein kinase/phosphatase cascade in rat neostriatal neurons. *Neuron* 14: 385-97

Surmeier DJ, Ding J, Day M, Wang Z, Shen W. 2007. D1 and D2 dopamine-receptor modulation of striatal glutamatergic signaling in striatal medium spiny neurons. *Trends Neurosci* 30: 228-35

Surmeier DJ, Eberwine J, Wilson CJ, Cao Y, Stefani A, Kitai ST. 1992. Dopamine receptor subtypes colocalize in rat striatonigral neurons. *Proc Natl Acad Sci U S A* 89: 10178-82

Svenningsson P, Nishi A, Fisone G, Girault JA, Nairn AC, Greengard P. 2004. DARPP-32: an integrator of neurotransmission. *Annu Rev Pharmacol Toxicol* 44: 269-96

Svoboda K, Denk W, Kleinfeld D, Tank DW. 1997. In vivo dendritic calcium dynamics in neocortical pyramidal neurons. *Nature* 385: 161-5

Svoboda K, Yasuda R. 2006. Principles of two-photon excitation microscopy and its applications to neuroscience. *Neuron* 50: 823-39

Szabo J. 1967. The efferent projections of the putamen in the monkey. *Exp Neurol* 19: 463-76

Tamamaki N, Yanagawa Y, Tomioka R, Miyazaki J, Obata K, Kaneko T. 2003. Green fluorescent protein expression and colocalization with calretinin, parvalbumin, and somatostatin in the GAD67-GFP knock-in mouse. *J Comp Neurol* 467: 60-79

Tecuapetla F, Jin X, Lima SQ, Costa RM. 2016. Complementary Contributions of Striatal Projection Pathways to Action Initiation and Execution. *Cell* 166: 703-15

Tegtmeier J, Brosch M, Janitzky K, Heinze HJ, Ohl FW, Lippert MT. 2018. CAVE: An Open-Source Tool for Combined Analysis of Head-Mounted Calcium Imaging and Behavior in MATLAB. *Front Neurosci* 12: 958

Tepper JM, Tecuapetla F, Koos T, Ibanez-Sandoval O. 2010. Heterogeneity and diversity of striatal GABAergic interneurons. *Front Neuroanat* 4: 150

Thornburg JE, Moore KE. 1972. A comparison of the locomotor stimulant properties of amantadine and l- and d-amphetamine in mice. *Neuropharmacology* 11: 675-82

Threlfell S, Lalic T, Platt NJ, Jennings KA, Deisseroth K, Cragg SJ. 2012. Striatal dopamine release is triggered by synchronized activity in cholinergic interneurons. *Neuron* 75: 58-64

Tian L, Hires SA, Mao T, Huber D, Chiappe ME, et al. 2009. Imaging neural activity in worms, flies and mice with improved GCaMP calcium indicators. *Nat Methods* 6: 875-81

Toth K, McBain CJ. 1998. Afferent-specific innervation of two distinct AMPA receptor subtypes on single hippocampal interneurons. *Nat Neurosci* 1: 572-8

Tozzi A, de Iure A, Di Filippo M, Tantucci M, Costa C, et al. 2011. The distinct role of medium spiny neurons and cholinergic interneurons in the D(2)/A(2)A receptor interaction in the striatum: implications for Parkinson's disease. *J Neurosci* 31: 1850-62

Tritsch NX, Sabatini BL. 2012. Dopaminergic modulation of synaptic transmission in cortex and striatum. *Neuron* 76: 33-50

Tsai PS, Friedman B, Ifarraguerri AI, Thompson BD, Lev-Ram V, et al. 2003. All-optical histology using ultrashort laser pulses. *Neuron* 39: 27-41

Tsien RY. 1989. Fluorescent probes of cell signaling. *Annu Rev Neurosci* 12: 227-53

Uslaner J, Badiani A, Norton CS, Day HE, Watson SJ, et al. 2001. Amphetamine and cocaine induce different patterns of c-fos mRNA expression in the striatum and subthalamic nucleus depending on environmental context. *Eur J Neurosci* 13: 1977-83

Vilchis C, Bargas J, Ayala GX, Galvan E, Galarraga E. 2000. Ca2+ channels that activate Ca2+-dependent K+ currents in neostriatal neurons. *Neuroscience* 95: 745-52

Voorn P, Vanderschuren LJ, Groenewegen HJ, Robbins TW, Pennartz CM. 2004. Putting a spin on the dorsal-ventral divide of the striatum. *Trends Neurosci* 27: 468-74

Vuillet J, Kerkerian L, Salin P, Nieoullon A. 1989. Ultrastructural features of NPY-containing neurons in the rat striatum. *Brain Res* 477: 241-51

Walsh JP. 1993. Depression of excitatory synaptic input in rat striatal neurons. *Brain Res* 608: 123-8

Wang JW, Wong AM, Flores J, Vosshall LB, Axel R. 2003. Two-photon calcium imaging reveals an odor-evoked map of activity in the fly brain. *Cell* 112: 271-82

Welch BL, Welch AS. 1966. Graded effect of social stimulation upon d-amphetamine toxicity, aggressiveness and heart and adrenal weight. *J Pharmacol Exp Ther* 151: 331-8

White NM, McDonald RJ. 2002. Multiple parallel memory systems in the brain of the rat. *Neurobiol Learn Mem* 77: 125-84

Wickens JR, Begg AJ, Arbuthnott GW. 1996. Dopamine reverses the depression of rat corticostriatal synapses which normally follows high-frequency stimulation of cortex in vitro. *Neuroscience* 70: 1-5

Wieraszko A, Goldsmith G, Seyfried TN. 1989. Stimulation-dependent release of adenosine triphosphate from hippocampal slices. *Brain Res* 485: 244-50

Wilson CJ. 1993. The generation of natural firing patterns in neostriatal neurons. *Prog Brain Res* 99: 277-97

Wilson CJ, Groves PM. 1980. Fine structure and synaptic connections of the common spiny neuron of the rat neostriatum: a study employing intracellular inject of horseradish peroxidase. *J Comp Neurol* 194: 599-615

Wirth D, Gama-Norton L, Riemer P, Sandhu U, Schucht R, Hauser H. 2007. Road to precision: recombinase-based targeting technologies for genome engineering. *Curr Opin Biotechnol* 18: 411-9

Witten IB, Lin SC, Brodsky M, Prakash R, Diester I, et al. 2010. Cholinergic interneurons control local circuit activity and cocaine conditioning. *Science* 330: 1677-81

Witten IB, Steinberg EE, Lee SY, Davidson TJ, Zalocusky KA, et al. 2011. Recombinase-driver rat lines: tools, techniques, and optogenetic application to dopamine-mediated reinforcement. *Neuron* 72: 721-33

Yan Z, Flores-Hernandez J, Surmeier DJ. 2001. Coordinated expression of muscarinic receptor messenger RNAs in striatal medium spiny neurons. *Neuroscience* 103: 1017-24

Yan Z, Song WJ, Surmeier J. 1997. D2 dopamine receptors reduce N-type Ca2+ currents in rat neostriatal cholinergic interneurons through a membrane-delimited, protein-kinase-C-insensitive pathway. *J Neurophysiol* 77: 1003-15

Yates JW, Meij JT, Sullivan JR, Richtand NM, Yu L. 2007. Bimodal effect of amphetamine on motor behaviors in C57BL/6 mice. *Neurosci Lett* 427: 66-70

Yin HH, Knowlton BJ. 2006. The role of the basal ganglia in habit formation. *Nat Rev Neurosci* 7: 464-76

Youdim MB. 1980. Biochemical characterization of the active site of brain monoamine oxidase. *Monogr Neural Sci* 7: 176-92

Youdim MB, Edmondson D, Tipton KF. 2006. The therapeutic potential of monoamine oxidase inhibitors. *Nat Rev Neurosci* 7: 295-309

Yuste R, Majewska A, Cash SS, Denk W. 1999. Mechanisms of calcium influx into hippocampal spines: heterogeneity among spines, coincidence detection by NMDA receptors, and optical quantal analysis. *J Neurosci* 19: 1976-87

Zahm DS, Brog JS. 1992. On the significance of subterritories in the "accumbens" part of the rat ventral striatum. *Neuroscience* 50: 751-67

Zahm DS, Heimer L. 1990. Two transpallidal pathways originating in the rat nucleus accumbens. *J Comp Neurol* 302: 437-46

Zhang Q, Pan D, Ji N. 2020. High-resolution in vivo optical-sectioning widefield microendoscopy. *Optica* 7: 1287-90

Zhou P, Resendez SL, Rodriguez-Romaguera J, Jimenez JC, Neufeld SQ, et al. 2018. Efficient and accurate extraction of in vivo calcium signals from microendoscopic video data. *Elife* 7

Zimmermann H. 2000. Extracellular metabolism of ATP and other nucleotides. *Naunyn Schmiedebergs Arch Pharmacol* 362: 299-309

Zong W, Wu R, Li M, Hu Y, Li Y, et al. 2017. Fast high-resolution miniature two-photon microscopy for brain imaging in freely behaving mice. *Nat Methods* 14: 713-19

Zucker RS. 1999. Calcium- and activity-dependent synaptic plasticity. *Curr Opin Neurobiol* 9: 305-13

Acknowledgments

I would like to thank my tutor Prof. Michele Zoli (Università degli Studi di Modena e Reggio Emilia) for the continuous assistance during my PhD experience and for his knowledge that enlightened the course of my PhD. His presence helped me in all the time of research and writing this thesis. I would like also to thank prof. Michele team for the constant support.

As all experiments related to this work were performed at the ULB (Université Libre de Bruxelles), I would also like to thank the supervision of Prof. Alban de Kerchove D'Exaerd, who gave me the access to his laboratory and research facilities. Without him and his team, it would have not been possible to conduct this thesis.

At the end, but not least, I would like to thank Dr. Paolo Pozzi, for the immense contribution in the analysis of the data of this project. During these three years he became a good friend, not only my co-tutor. His patience, motivation and insightful comments helped me to finish this experience with serenity. He helped me to growth professionally and personally.

Per prima cosa vorrei dedicare questo lavoro a due persone per me molto speciali: i miei nonni, Marì e Fausto. Dal prima anno di università mi avete sostenuto con tutto l'affetto di cui avevo bisogno e per la terza volta vi dedico la tesi, perché nella carriera accademica è quanto di più emotivamente importante io possa fare. Vi sarò sempre grata per il bene con cui mi avete aiutato a superare i vari ostacoli della vita, siete per me una fonte di felicità costante.

Inoltre, dedico questo lavoro a Michele. Se penso che abbiamo iniziato l'università insieme e abbiamo finito il dottorato insieme mi viene da sorridere. Michi, sono dieci anni che mi sopporti, non so se passato tutto questo tempo ci sia una sorta di premio per la sopportazione, ad ogni modo, lo meriteresti. Siamo stati compagni di tantissime avventure e chissà quante altre ci attendono. Grazie